Performance of different proton exchange membrane water electrolyser components

Richard Daniel Sutherland (B.Eng)

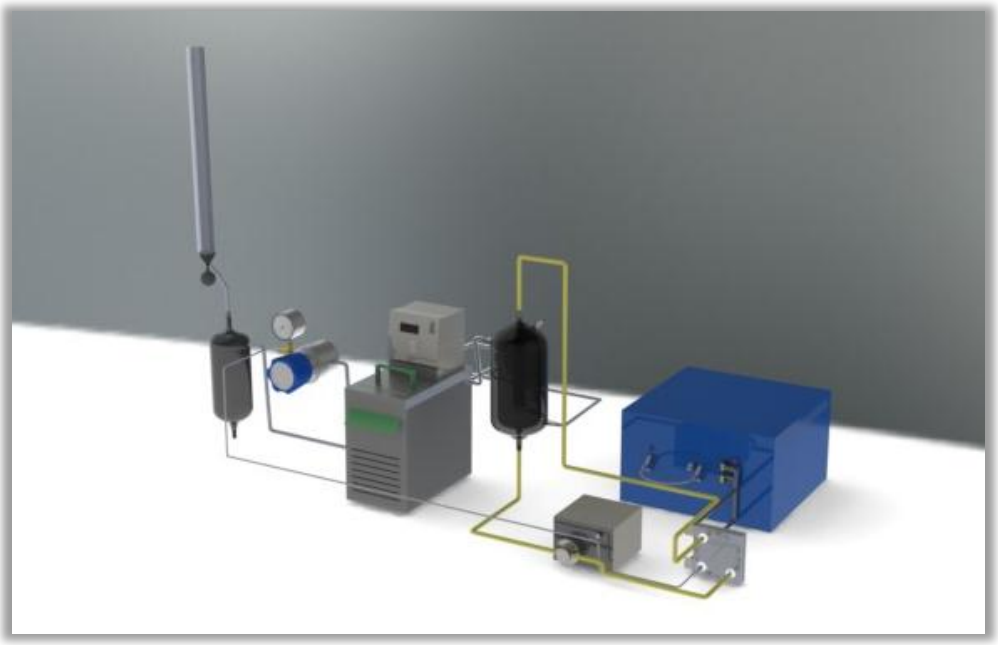

Dissertation submitted in fulfilment of the requirements for the degree of

MASTER of **ENGINEERING**

in CHEMICAL ENGINEERING

at the Potchefstroom Campus of the North-West University

Supervisor:	Dr. P. van der Gryp
Co-supervisor:	Prof. H.M. Krieg
	Dr. D. Bessarabov

Potchefstroom

November 2012

Abstract

Water electrolysis is one of the first methods used to generate hydrogen and is thus not considered to be a new technology. With advances in proton exchange membrane technology and the global tendency to implement renewable energy, the technology of water electrolysis by implementation of proton exchange membrane as solid electrolyte has developed into a major field of research over the last decade. To gain an understanding of different components of the electrolyser it is best to conduct a performance analysis based on hydrogen production rates and polarisation curves. The study aim was to compare the technologies of membrane electrode assembly with gas diffusion electrode and the proton exchange membranes of Nafion® and polybenzimidazole in a commercial water electrolyser. To determine which of the components are best suited for the process a laboratory scale electrolyser was to be used to replicate the commercially scaled performance. The effect of feed water contaminants on electrolyser performance was also investigated by introducing iron and magnesium salt solutions and aqueous methanol solutions in the feed reservoir. Components to be tested included different PEM types as well as the base component on which the electrocatalyst layer is applied. The proton exchange membranes compared were standard Nafion® N117 and polybenzimidazole meta-sulfone sulfonated polyphenyl sulfone (PBI-sPSU). A laboratory scale electrolyser from Giner Electrochemical Systems was utilised where different components were tested and compared with one another. Experimental results with commercial membrane electrode assemblies and gas diffusion electrodes demonstrated the influence of temperature on electrolyser performance for the proton exchange membranes, where energy efficiency increased with temperature. The effect of pressure was insignificant over the selected pressure range. Comparison of membrane electrode assembly and gas diffusion electrode technologies showed enhanced performance from MEA technology, this was most likely due to superior electrocatalyst contact with the PEM. Results of synthesised Nafion® N117 and PBI-sPSU MEA showed increased performance for PBI-sPSU, but it was found to be more susceptible to damage under severe conditions. The effect of metal cations in the supply reservoir exhibited reduced energy efficiencies and increased specific energy consumption for the test duration. Treatment with sulphuric acid was found to partially restore membrane electrode assembly performance, though it is believed that permanent damage was inflicted on the membrane electrode assembly electrocatalyst. Use of aqueous methanol solutions were found to increase electrolyser performance.

It was also found that aqueous methanol electrolysis occurs at lower current densities, whereas a combination of aqueous methanol and water electrolysis occurred at higher current densities depending on the concentration of methanol.

Keywords: PEM; water electrolysis; methanol electrolysis; MEA; GDE; contamination;

Acknowledgements

This study was inspired by a childhood dream, in which all I wanted to do was to manufacture hydrogen. I now know that it is easy to get hydrogen by simple electrolysis, but I have found that there is much to learn in research and that it is not as simple as it seems.

Completing the necessary experiments and chapters tests one's endurance. To endure one needs a good support network to keep a positive mind-set, to look forward and to just keep on walking. My support network is constructed of family, friends, supervisors and colleagues and I would like to thank them.

Saviour:	Jesus Christ
Supervision:	Dr. Percy van der Gryp Prof. Henning Krieg Dr. Dmitri Beserabov
Experimental construction assistance:	Mr. Adrian Brock
Experimental assistance:	Andries Kruger, Derik van der Westhuizen, Francois van Schalkwyk and Rolene Pascal.
Moral support:	Ralph Sutherland, Erna Sutherland, Suemaé Sutherland, Llewellyn Sutherland, Mariette Sutherland, Liza Shelton, Herman Barnard, Anita Barnard, Donnavan Kruger, Philip Ayres, Trevor Hallatt and Maricha Longland.

A special thank you to my father Ralph and mother Erna for motivating me from afar, my friends Donnavan, Philip and Trevor for moral support and my loving other half, Carolé, for all the motivation and time spent working with me.

Declaration

I, Richard Daniel Sutherland, hereby declare that this dissertation, “Performance of different proton exchange membrane water electrolyser components”, is my own work.

_____

Richard Sutherland

Potchefstroom

November 2012

Table of Contents

Nomenclature

Acronym	Description
BPR	Back pressure regulator
CCM	Catalyst-Coated Membrane
CCM-DS	Catalyst-Coated Membrane Direct wet-Spraying
CCM-DT	Catalyst-Coated Membrane Decal Transfer
CCS	Catalyst-Coated Substrate
EPDM	Ethylene-Propylene-Diene-Methylene
GDE	Gas Diffusion Electrode
GDL	Gas Diffusion Layer
GES	Giner Electrochemical Systems
HSA	High Surface Area
MEA	Membrane Electrode Assembly
OCV	Open Circuit Voltage
OER	Oxygen Evolution Reaction
PBI	Polybenzimidazole
PBI-SPSU	Polybenzimidazole meta-sulfone sulfonated polyphenyl sulfone
PEM	Proton Exchange Membrane
PFSA	Perflourosulfonic acid
PTFE	Polytetrafluoroethylene
SEM	Scanning Electron Microscope
SPE	Solid Polymer Electrolyte
SGEIS	Staircase Galvano Electrochemical Impedance Spectroscopy
TFE	Tetrafluoroethylene

Symbols

Symbol	Description	Unit
Ewe	PEM electrolyser cell voltage	V
F	Faraday constant	$C.mol^{-1}$
ΔH	Enthalpy	$kJ.mol^{-1}$
ΔG	Gibbs free energy	$kJ.mol^{-1}$
n	Number of electrons formed	-
p_{H2}	Partial pressure of hydrogen relative to atmospheric pressure	-
p_{O2}	Partial pressure of oxygen relative to atmospheric pressure	-
R	Ideal gas constant	$J.mol^{-1}.K^{-1}$
ΔS	Entropy	$J.mol^{-1}.K^{-1}$
V°	Standard cell voltage	V
$\varepsilon_{\Delta G}$	Energy efficiency	%

Introduction

Contents

1.1 Background and motivation

Global warming is a concern when considering sustainable development. Industrial plants and motor vehicles release both carbon dioxide and other greenhouse gases into the atmosphere. Coal and other fuel sources are combusted to create sufficient amounts of electricity and energy. The electricity and energy generated has to be viewed against the ever increasing global human population. The energy needs are thus increasing and the current means of energy generation has a negative impact on the environment, affecting present and future generations.

Considering fossil fuel reserves of oil, gas and coal, it is found that coal constitutes around 65% of fossil fuel reserves, and oil and gas make up the rest (Shafiee *et al.*, 2009:181.). It can be added that the estimation of fossil fuel reserves over the last few decades has not been reliable. Oil, gas and coal reserves will last approximately another 40, 70 and 200 years, respectively (Shafiee *et al.*, 2009:181.). Alternative sources of energy are thus needed to supply the increasing demand. Renewable energy is one answer to reduce the human impact on the environment, as well as to stem the depletion of fossil fuel reserves. Renewable energy sources that can be implemented include solar, wind, hydro (Barbir, 2005:661) and biomass.

An energy carrier is required to store the renewable energy, as some renewable energy sources, such as solar power, do not provide a continuous supply of power. Hydrogen could be used as an energy carrier in the future (Barbir, 2005:661). A series of technologies, such as reforming of natural gas, gasification of coal and biomass, water electrolysis, photo-catalytic splitting of water, thermolysis and thermo-chemical cycles can be used to generate hydrogen (Clarke *et al.*, 2010:928, Ni *et al.*, 2008:2748). Global hydrogen requirements include the production of ammonia, fertiliser and methanol, impurity removal in oil refineries and other chemical and metallurgical industries (Clarke *et al.*, 2010:928). Present hydrogen production needs are mostly being met with fossil fuel reforming (Smitkova *et al.*, 2011:7844), as saltwater electrolysis and water electrolysis produce only minor quantities of hydrogen. While fossil fuel reforming is presently a cheap and efficient means of generating hydrogen, hydrogen production with a renewable energy source has the best greenhouse gas reduction potential (Clarke *et al.*, 2010:928.).

Future hydrogen applications which include the motor vehicle and agricultural industries can also be implemented in remote areas to supply rural residents with electricity (Lagorse *et al.*, 2008:2871). Internal combustion systems that implement either spark-ignition or diesel configurations emit greenhouse gases and thermal NO_x which damage the ozone in the stratosphere. The implementation of a fuel-cell-powered electric vehicle seems to be one of the

best answers to the air quality problems on a longer-term basis (Gaffney *et al.*, 2009:32). Fuel cells create energy by converting gaseous fuels such as hydrogen or natural gas into electricity, based on electrochemical principles and can thus be regarded as batteries. However, since the oxidant and fuel are not a part of the fuel cell, they produce power on a continuous basis when supplied with fuel and oxidant, without requiring any recharging. When operating a fuel cell, the chemical conversion occurs at a much lower temperature than in an internal combustion engine. Furthermore, fuel cell operation does not result in thermal NO_x generation (Barbir, 2005:661) nor hydrocarbon or CO emissions, as there are no lubricating oils associated with fuel cells. Fuel cells can be used in vehicles without producing emissions. Hydrogen is seen as the most efficient fuel for use in fuel cells (Gaffney *et al.*, 2009:33) due to its applicability and high specific energy by mass (Ganley, 2009:3604). Some exclusive characteristics of hydrogen are that it is produced and converted into electricity at rather high efficiencies, its reagent (water) is available in abundance and hydrogen is considered to be a renewable fuel and environmentally compatible, as no pollutants and greenhouse gases are released into the environment (Sherif *et al.*, 2005:62).

Water electrolysis is just one of the many methods available to produce hydrogen with renewable energy sources and was discovered in the year 1800 (Kreuter *et al.*, 1998:539). Electrolysis has developed to a point where a Solid Polymer Electrolyte (SPE) loaded with platinum and iridium is used. The rate and efficiency of hydrogen production has increased drastically with technological advances in water electrolysis. Proton Exchange Membrane (PEM) water electrolysers are efficient but not viable as they are expensive to manufacture. Items contributing to the manufacturing cost of electrolysers include the generally used Nafion® polymer membrane, the platinum and iridium catalyst and the highly corrosion resistant current collector plates and flowfields. The field of water electrolysis, however, has potential as new technologies are being developed. One of the main components of a water electrolyser is the Membrane Electrode Assembly (MEA) where the reaction and the selective transport of hydrogen occur. Components of the MEA include the SPE, where usually a PEM is used, the cathode and the anode (Tang *et al.*, 2007:140). Gas Diffusion Electrodes (GDE) are similar to MEA and can also be implemented in a PEM water electrolyser. Catalyst development for both the anode and cathode is on-going. The anode receives the most attention due to its contribution to the overpotential, as well as its oxidative environment (Siracusano *et al.*, 2010:5558). PEM water electrolysis is a very promising method of generating hydrogen with a renewable energy source, as it is highly reliable and safe, with a high purity hydrogen being produced (Siracusano *et al.*, 2010:5558).

The high cost of PEM water electrolysers, however, makes the implementability thereof difficult in remote areas, for example of South Africa or other developing countries. Since commercial electrolyser manufacturers (Giner, Hamilton Sunstrand and Proton Energy Systems) are mostly located in developed countries, the import duties and exchange rates have a big influence on the price of an electrolyser. There is thus a need for the local development of PEM water electrolysers to increase our knowledge in the field in an attempt to reduce the final cost of the process. With the many different membranes developed for fuel cells, the testing of different PEM types in electrolysers will aid in the further development of PEM water electrolysis. The influence of additional reagents, such as ionic salts and alcohols, will aid in further implementation of water electrolysers.

1.2 Objectives

The aim of this study is to contribute to the research of PEM by evaluating both GDE and MEA in a PEM water electrolyser and monitoring the performance thereof. The aim of this study is also to evaluate the influence of cationic salts and methanol on MEA performance. The objectives can be divided into the performance and the degradation of components in a PEM water electrolyser.

Performance

- Comprehend the performance of different components for the production of hydrogen in a PEM water electrolyser.
- Assess the effect of temperature, pressure, catalyst and PEM type on the electrochemical performance.
- Explain the behaviour of the different components and conditions with regard to findings reported in the literature.

Degradation

- Investigate how the performance of electrolyser components can be affected by impurities.
- Assess the effect of regeneration and impurities at varying concentrations on electrolyser performance.
- Explain how the performance of the PEM water electrolyser is altered with regard to findings reported in the literature.

1.3 Scope of investigation

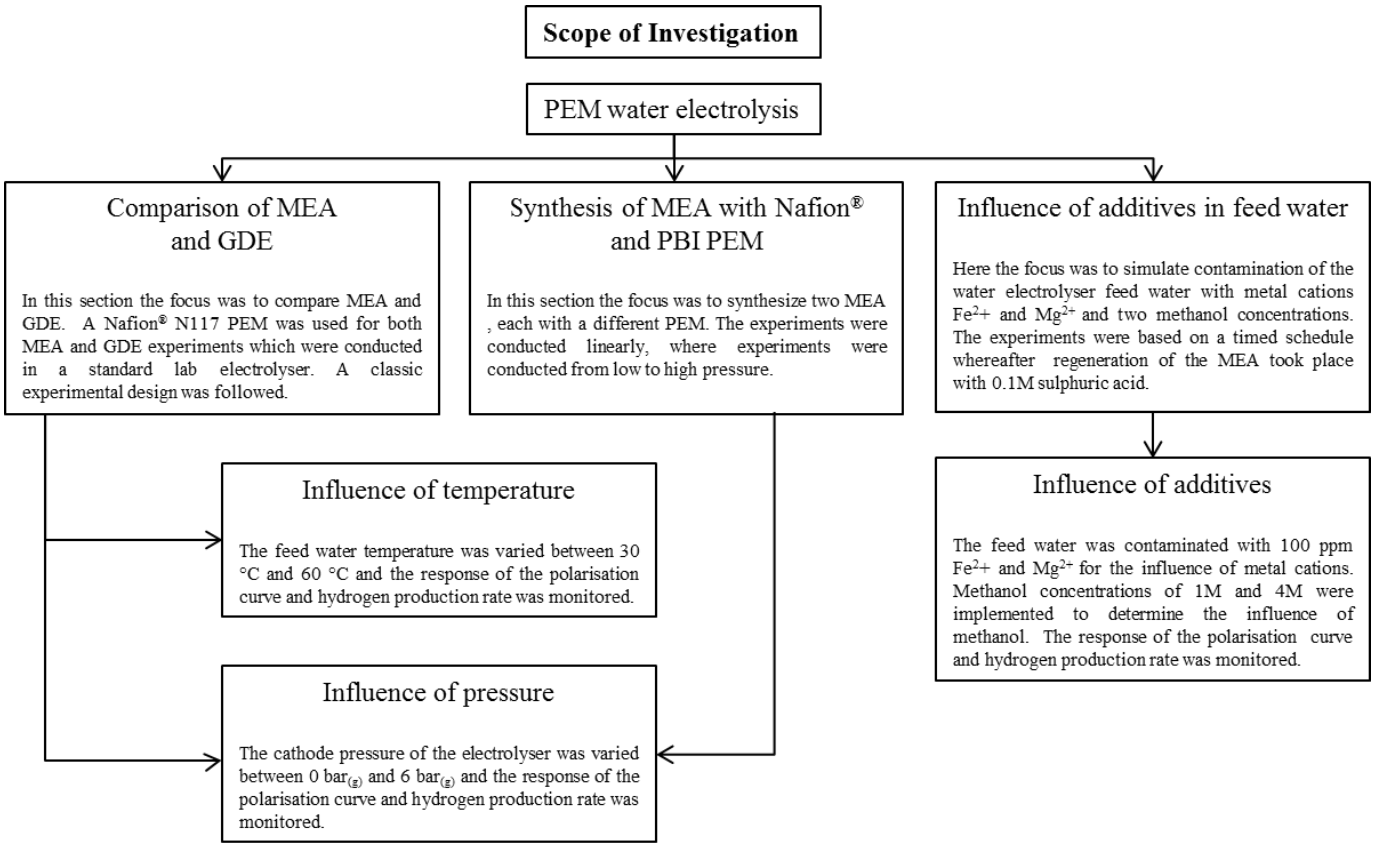

The dissertation consists of 5 chapters which are discussed in a stepwise manner. Chapter 1 gives a brief overview of why the investigation was conducted and provides information of what to expect in coming chapters.

Chapter 2 augments the literature described in the background and motivation of Chapter 1 giving an overview of a PEM water electrolyser and its components. The emphasis is placed on gaining further understanding of the field of electrolysis, electrolysers and its components. A thorough analysis of the PEM water electrolyser and all of its components is discussed. Subsequently, the performance of the PEM water electrolyser and how it is affected by degradation and varying process conditions will be discussed in detail.

Chapter 3 describes the experiments conducted. Here the materials, equipment and experimental setup are listed to present a picture of the experimental work.

In Chapter 4, the results generated from the experimental work are presented. The focal point of the results is the performance of the PEM water electrolyser. The performance evaluation sections are divided into three sections:

i. Nafion® MEA and GDE in a PEM water electrolyser at varying temperatures and pressures.
ii. Nafion® and PBI synthesised MEA at constant temperature and varying pressure.
iii. Nafion® MEA subjected to conditions of degradation and regeneration.

Chapter 5 concludes and evaluates the work described in this dissertation and gives suggestions for future work in this specific field.

1.4 References

BARBIR, F. 2005. PEM electrolysis for production of hydrogen from renewable energy sources. *Solar energy,* 78(5):661-669.

CLARKE, R.E., GIDDEY, S. & BADWAL, S.P.S. 2010. Stand-alone PEM water electrolysis system for fail safe operation with a renewable energy source. *International journal of hydrogen energy,* 35(3):928-935.

GAFFNEY, J.S. & MARLEY, N.A. 2009. The impacts of combustion emissions on air quality and climate – from coal to biofuels and beyond. *Atmospheric environment,* 43(1):23-36.

GANLEY, J.C. 2009. High temperature and pressure alkaline electrolysis. *International journal of hydrogen energy,* 34(9):3604-3611.

KREUTER, W. & HOFMANN, H. 1998. Electrolysis: The important energy transformer in a world of sustainable energy. *International journal of hydrogen energy,* 23(8):661-666.

LAGORSE, J., SIMÕES, M.G., MIRAOUI, A. & COSTERG, P. 2008. Energy cost analysis of a solar-hydrogen hybrid energy system for stand-alone applications. *International journal of hydrogen energy,* 33(12):2871-2879.

NI, M., LEUNG, M.K.H. & LEUNG, D.Y.C. 2008. Energy and exergy analysis of hydrogen production by a proton exchange membrane (PEM) electrolyzer plant. *Energy conversion and management,* 49(10):2748-2756.

SHAFIEE, S. & TOPAL, E. 2009. When will fossil fuel reserves be diminished? *Energy policy,* 37(1):181-189.

SHERIF, S.A., BARBIR, F. & VEZIROGLU, T.N. 2005. Towards a hydrogen economy. *The electricity journal,* 18(6):62-76.

SIRACUSANO, S., BAGLIO, V., DI BLASI, A., BRIGUGLIO, N., STASSI, A., ORNELAS, R., TRIFONI, E., ANTONUCCI, V. & ARICÒ, A.S. 2010. Electrochemical characterization of single cell and short stack PEM electrolyzers based on a nanosized IrO_2 anode electrocatalyst. *International journal of hydrogen energy,* 35(11):5558-5568.

SMITKOVA, M., JANÍČEK, F. & RICCARDI, J. 2011. Life cycle analysis of processes for hydrogen production. *International journal of hydrogen energy,* 36(13):7844-7851.

TANG, H., WANG, S., JIANG, S.P. & PAN, M. 2007. A comparative study of CCM and hot-pressed MEAs for PEM fuel cells. *Journal of power sources,* 170(1):140-144.

Literature Survey

Contents

2.1 History of electrolysis

Electrolytic water splitting was discovered by Nicholson and Carlisle in the year 1800, during the first industrial revolution. More than 400 industrial water electrolysers were in operation by 1902. The first large water electrolysis plant went into operation in 1939, and in 1948 the first pressurised industrial water electrolyser was built by Zdansky / Lonza (Kreuter *et al*., 1998:661). The development of the proton exchange membrane by Du Pont for use in water electrolysis, SO_2-depolarised electrolyser and fuel cells is the benchmark technology used today (Kreuter *et al*., 1998:661).

The categories for water electrolysis are alkaline and PEM, and the distinguishing factor is that alkaline water electrolysers implement a liquid electrolyte whereas PEM water electrolysers implement a SPE (Millet *et al*., 2010:5043).

2.1.1 Alkaline electrolysis

One of the most popular methods for hydrogen and oxygen production from water has been alkaline electrolysis of aqueous hydroxide solutions (Ganley, 2009:3604). In Figure 2-1 a schematic representation of such an electrolyser is shown.

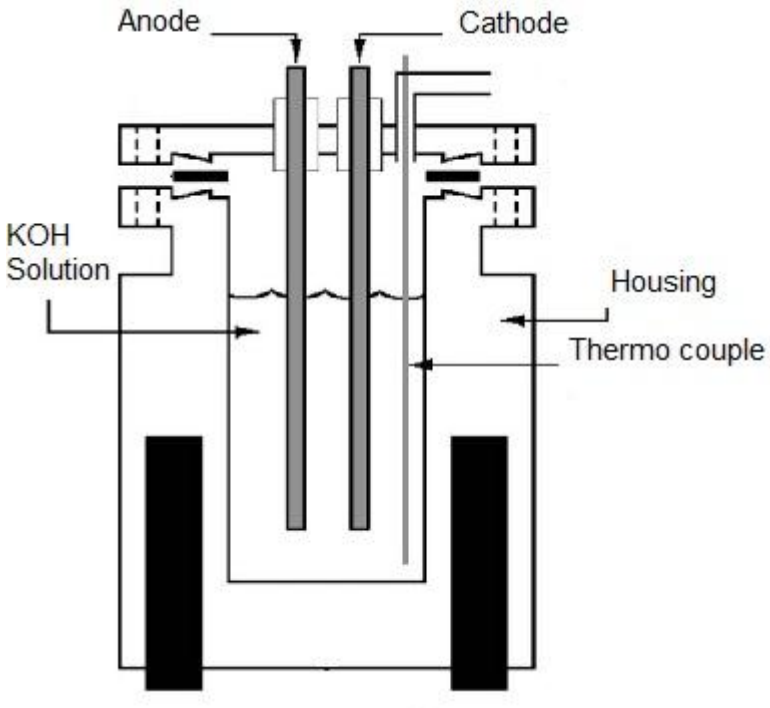

Figure 2-1 Alkaline electrolyser (Ganley, 2009:3604).

The alkaline electrolyser operates with a basic liquid electrolyte where gases of hydrogen and oxygen form at the respective electrodes.

2.1.2 PEM electrolysis

The electrolyser implementing a PEM is an attractive solution when compared with alkaline water electrolysers, due to the higher achievable current density, high purity hydrogen production and compactness of the electrolyser units. Advances in PEM technology include producing hydrogen at high pressures whilst keeping the process efficient, clean and safe. High pressure PEM water electrolysers are capable of operating with a high pressure gradient across the PEM, where the cathode side is operated at elevated pressures whilst the anode side is operated at nearly atmospheric pressure (Medina *et al*., 2010:5173).

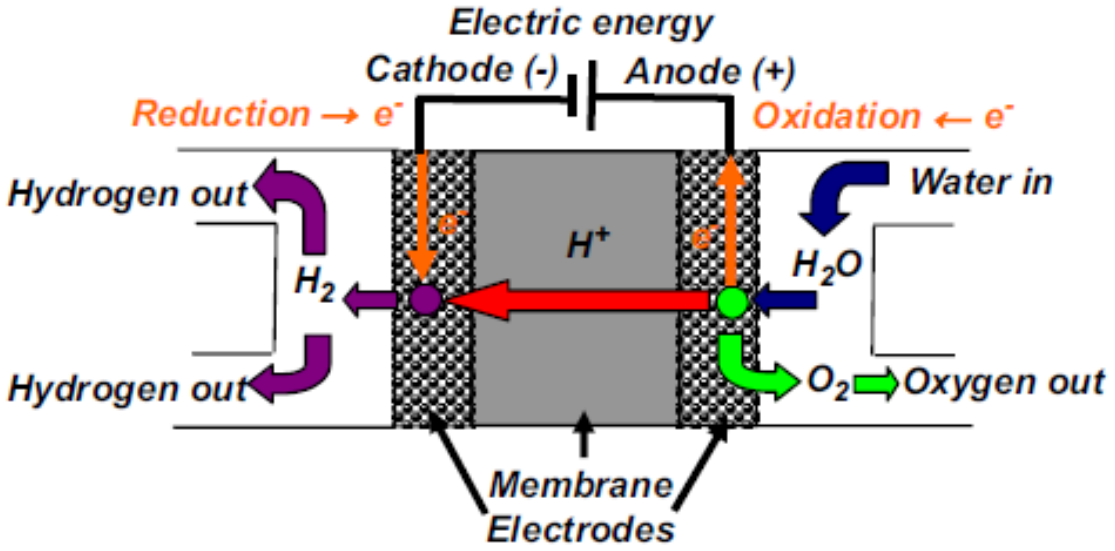

Figure 2-2 A graphical illustration of an operating PEM water electrolyser (Lebbal *et al.*, 2009:5992)

PEM water electrolysis applies an electric potential across the electrolyser terminals which split water molecules into oxygen, protons and electrons on the anode side of the cell (Nieminen *et al*., 2010). The protons move through the PEM to the cathode side of the electrolyser cell, where the protons and electrons combine to form hydrogen gas. A DC voltage higher than the thermoneutral voltage of the reaction (1.229 V) must be applied across the cathode and anode for the water electrolysis reaction to take place (Barbir, 2005:661).

According to Nieminen *et al.* (2010), a PEM electrolyser has two major drawbacks. Firstly, a deionised water supply is required to reduce membrane degradation since membrane degradation is accelerated when impurities are present in the water supply. Secondly, the operating temperature range is limited to 300-400K as the Nafion® PEM only operates efficiently in a highly hydrated state (Li *et al.*, 2009:449). The limited operating temperature range can however be an advantage in applications where little thermal energy is available, as the electrolyser will

still operate at a relatively high efficiency with little thermal energy. Subsequently, areas in which PEM water electrolysers are suitable include remote and rural areas (Nieminen *et al*., 2010).

When comparing PEM water electrolysis with the conventional alkaline process a number of advantages for electrolytic grade hydrogen are apparent:

- Higher reliability and safety.
- Higher hydrogen purity (>99.99%).
- Ecological cleanliness (Siracusano *et al.*, 2010:5558).
- Possibility of storing produced compressed gases (>200 bar) without additional compression costs (Grigoriev *et al.*, 2009:4968).

Some drawbacks are costs associated with components, as well as with the MEA preparation, including the use of noble metals and salts in the plating process (Millet *et al.*, 2009:4974). It is important to reduce catalyst costs by reducing electrocatalyst loading on the MEA whilst maintaining electrolyser performance.

2.2 PEM electrolyser components

PEM water electrolyser components differ according to the number of cells that make up the electrolyser stack. To improve its performance, the PEM has had numerous modifications to its physical and chemical structure since General Electric Corporation first introduced it in the late 1950s. Key components include the PEM and electrodes. Other electrolyser components are the GDL, flowfields and collector plates, which will be discussed in this section. The electrocatalysts developed to optimise the PEM performance (Biaku *et al.*, 2008:4247) also play a key role in the synthesis of the electrodes.

When dissembling a PEM water electrolyser, the key component required for operation is the MEA. The MEA consists of a PEM which is coated with electrocatalyst. An alternative to the use of a MEA is a GDE, which consists of an electrocatalyst-coated GDL. For water electrolysis implementing GDE, a GDE is placed on either side of the PEM and the electrolyser unit is closed up.

Figures 2-3 and 2-4 illustrate the difference between an electrolyser implementing a MEA and a GDE.

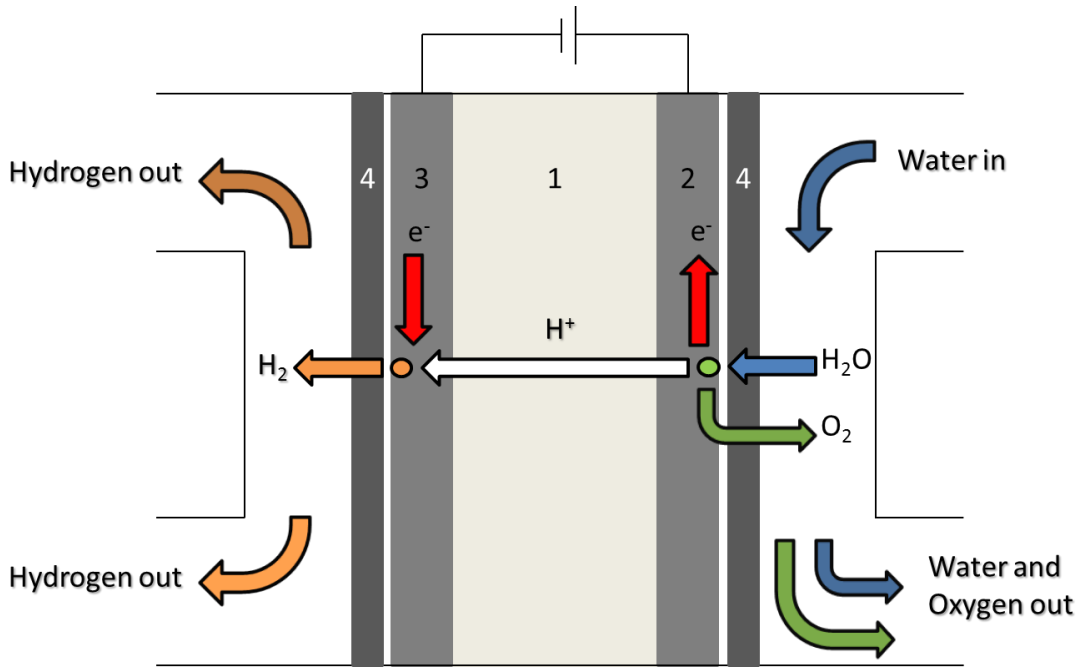

Figure 2-3 A graphical illustration of an operating PEM water electrolyser using a MEA (Lebbal *et al.*, 2009:5992)

The components illustrated in Figure 2-3 and 2-4 show the PEM (1) which forms the core of the MEA. The anode (2) and cathode (3) are situated next to the PEM. In the case of a MEA, the electrocatalyst layers are bonded directly onto the PEM as illustrated in Figure 2-3. In the case of

a GDE, the electrocatalyst is bonded to the GDL (4), in turn forming the GDE. Both MEA and GDE setups make water electrolysis possible, with conversion kits making it possible to convert an electrolyser unit to operate either with a MEA or a GDE.

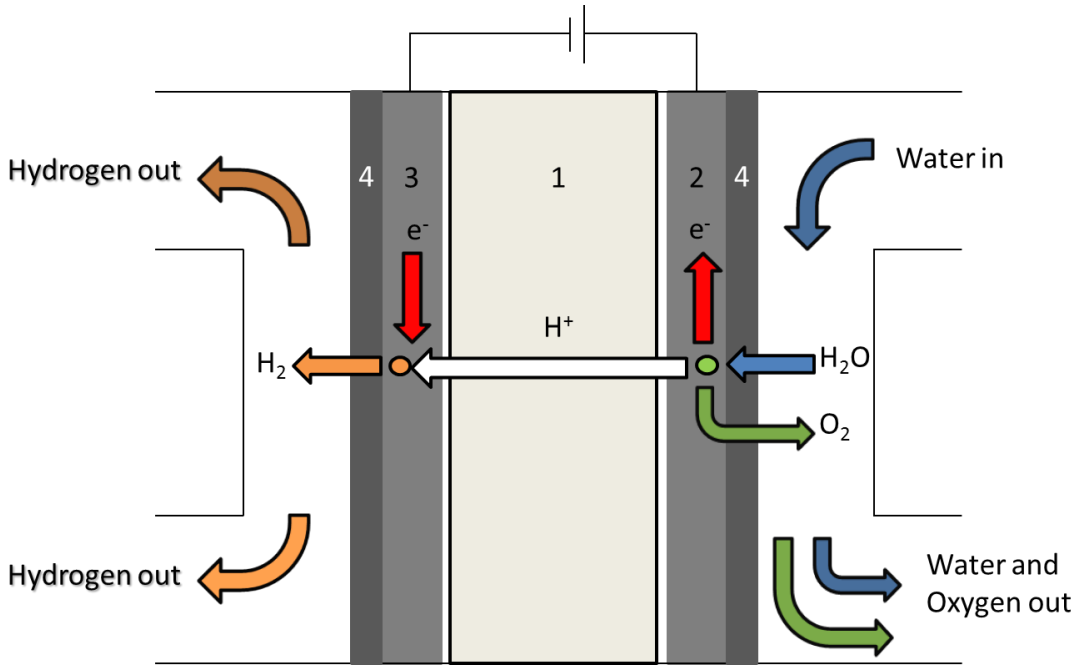

Figure 2-4 A graphical illustration of an operating PEM water electrolyser using a GDE (Lebbal *et al.*, 2009:5992)

2.2.1 Membrane Electrode Assembly

The MEA is a key component in PEM water electrolysis and fuel cell operation, as it forms the heart of the electrolyser/fuel cell. MEA are most commonly fabricated by either Catalyst-Coated Substrate (CCS) or Catalyst-Coated Membrane (CCM) techniques (Millet *et al*., 2009:4974,Sun *et al*., 2008:960,Tang *et al*., 2007:140).

Traditionally, the MEA is made by CCS, where the electrocatalyst is sprayed onto the current collector. During this process, the electrocatalyst is applied to either carbon cloth-support (Sun *et al*., 2008:960) or porous carbon paper (Tang *et al*., 2007:140) and sintered to form the electrodes. A PEM of choice is selected and the electrodes are placed on either side of the PEM and hot-pressed, forming the MEA (Millet *et al*., 2009:4974). This method is appropriate for production of MEAs on a large-scale. One shortcoming of this method is that a substantial amount of electrocatalyst may enter the carbon current collector. Once the current collectors and membrane are hot-pressed together the electrocatalyst is wasted (Thanasilp *et al*., 2010:3847).

The CCM method comprises two main fabrication techniques: direct wet-spraying onto the PEM (CCM-DS) or the Catalyst-Coated Membrane Decal Transfer technique (CCM-DT)

(Thanasilp *et al*., 2010:3847). For the CCM-DS technique a homogeneous ink of electrocatalyst, Nafion® and isopropanol is used. The electrocatalyst ink is then sprayed directly onto each side of the PEM and allowed to dry. Once dry, the PEM is inserted between the two carbon current collectors and the MEA is formed by hot-pressing (Song *et al*., 2008:4955). The application of the electrocatalyst ink by the CCM-DS method can result in extensive swelling of the membrane (Thanasilp *et al*., 2010:3847), which should be suppressed when making high quality CCM (Sun *et al*., 2008:960). When using the CCM-DT technique, the electrocatalyst ink is first applied to a Teflon support and then by means of hot-pressing transferred to the PEM (Tang *et al*., 2007a:140).

When comparing the different MEA fabrication methods, the CCM method stands out above the rest in terms of performance. When comparing the CCM-DT and CCM-DS techniques, the CCM-DT technique produces a MEA with a higher exchange current density, whilst the CCM-DS MEA has an exchange current density which lies between that of CCM-DT and the much lower values obtained for the more traditional CCS methods. Some advantages of CCM-DT, when compared to the conventional spraying method with the same Pt loading, are a considerably higher electrochemical performance, power density and electrochemical surface area. Lower charge transfer, mass transfer and ohmic resistance are also considered advantageous (Tang *et al*., 2007b:140,Thanasilp *et al*., 2010:3847). The improved power density of the CCM method is mainly due to improvement of catalyst utilisation and a comprehensive catalyst/ionomer interface (Tang *et al*., 2007a:140). MEA fabrication by the CCM-DT method exhibits smaller charge-transfer overpotential and a higher cell performance when compared with CCM-DS and CCS methods (Thanasilp *et al*., 2010:3847).

CCM-DT produces a MEA with the highest exchange current densities and outperforms MEA that are fabricated by other methods. One drawback of CCM-DT is that mass production by this method is difficult where simpler methods such as CCM-DS are considered for MEA fabrication.

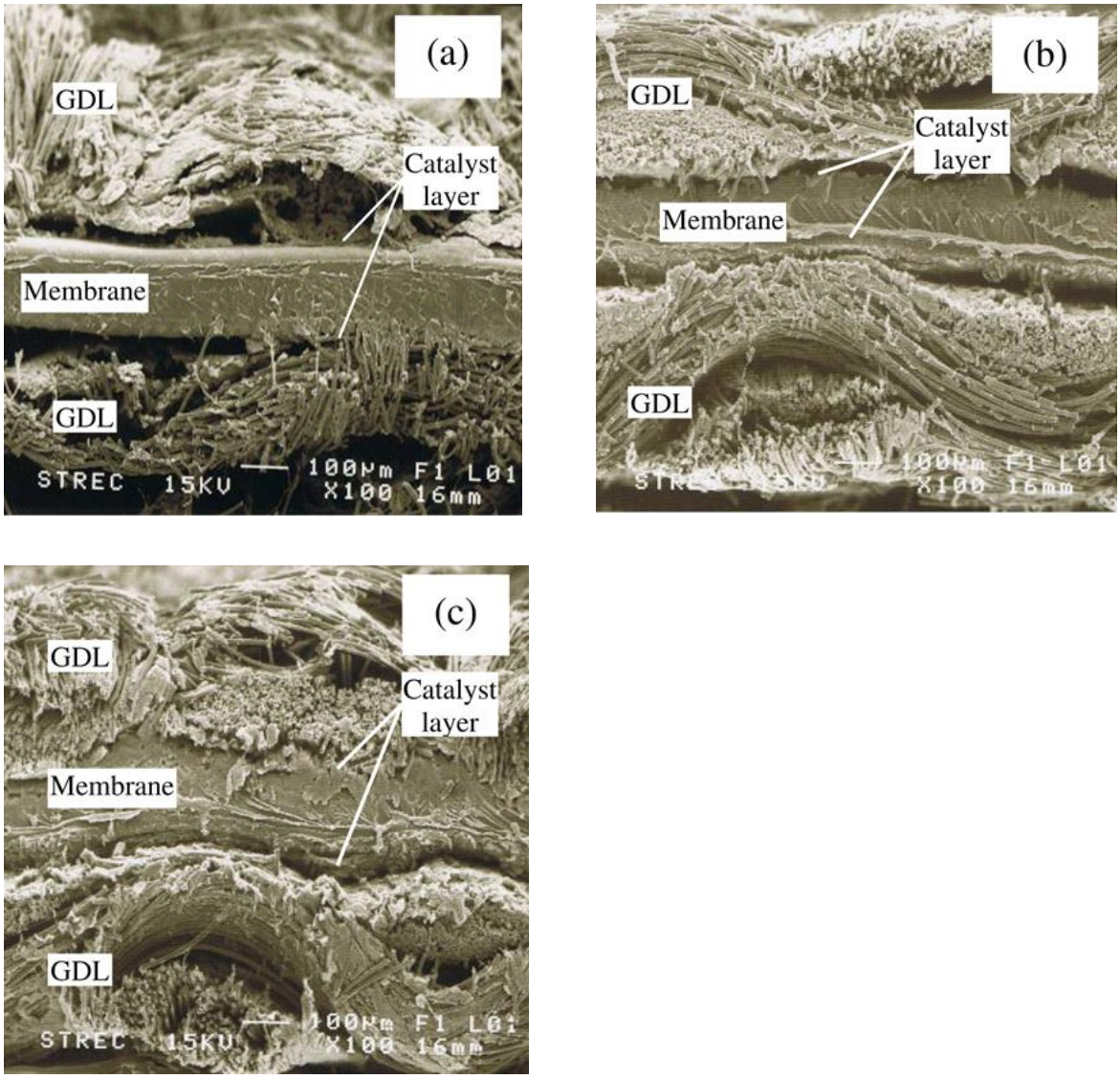

Figure 2-5 Representative SEM micrographs of cross-sectioned MEA prepared by CCS (a), CCM-DS (b) and CCM-DT (c) (Thanasilp *et al.*, 2010:3847).

Figure 2-5 illustrates how the catalyst layers are bonded to the membrane by the different fabrication methods mentioned. The electrocatalyst layers of (b) and (c) are visibly closer to the PEM (membrane) surface which usually implies an improved performance, confirming that the CCM-DS and CCM-DT techniques are superior to the other CCS techniques.

2.2.2 Proton Exchange Membrane

The PEM forms the core of the MEA and should thus be selected carefully. Numerous PEM are commercially available, which include a variety of Nafion® types, as well as other PEM materials, such as polybenzimidazoles (PBI) and its derivatives. Membranes used in PEM electrolysers must be stable, as conditions are both highly oxidative and reductive (Pan *et al.*, 2007:278). Other essential properties include high proton conductivity together with excellent

mechanical stability (Millet *et al*., 2009:4974). For the purpose of this study Nafion® and PBI PEM types will be discussed.

2.2.2.1 Nafion®

The company E. I. DuPont is responsible for both the development and production of Nafion® ionomers. Nafion® is made by copolymerising a perfluorinated vinyl ether comonomer and tetrafluoroethylene (TFE) (Mauritz *et al*., 2004:4535). The chemical structure of Nafion® is shown in Figure 2-6 (Collier *et al*., 2006:1838).

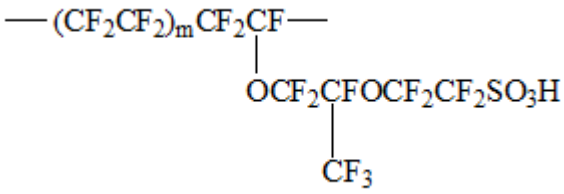

Figure 2-6 Nafion® structure : (Collier *et al*., 2006:1838).

The manufacture of Nafion® ionomers is generally based on the thermoplastic-SO_2F precursor form and can be extruded into sheets (Mauritz *et al.*, 2004:4535). Key properties of Nafion® PEM include high proton conductivity, mechanical, thermal (Collier *et al.*, 2006:1838) and oxidative stability (Li *et al.*, 2009:449, Mauritz *et al.*, 2004:4535, Millet *et al.*, 2010:5043). Other properties include good water management, high temperature hydration stability and high electro-osmotic drag (Mauritz *et al.*, 2004:4535,Millet *et al.*, 2010:5043).

Commercial applications of Nafion® are as polymer exchange membranes in fuel cells, PEM water electrolysers and electrochemical energy storage systems. Other Nafion® applications include chlor-alkali cells, Donnan dialysis cells, electrochromic devices, ion selective electrodes and implementing them as a strong acid catalyst (Mauritz *et al*., 2004:4535). Perfluorosulfonic acid (PFSA) polymer PEMs such as Nafion® are currently the benchmark materials of choice for PEM fuel cell and electrolyzer technology (Pan *et al*., 2007:278).

Catalytic agents, such as polymer films on metal surfaces, are most commonly produced using Nafion®. Currently, Nafion® is implemented in PEM water electrolysers as SPE. Large scale operations of PEM water electrolysis do, however, not use Nafion® as SPE due to its high price (Millet *et al.*, 2009:4974). A key factor influencing the efficiency of a PEM water electrolyser is the resistance of the PEM, which will be discussed in Section 2.4. Nafion® water uptake causes the swelling of ionic domains and the formation of proton conducting channels once critical water content has been reached. The conductivity of Nafion® increases with increasing water content

up to a point and then decreases due to a diminishing proton concentration (Collier *et al.*, 2006:1838). Other uses for Nafion® are as catalytic agents, such as polymer films on metal surfaces (Berezina *et al.*, 2002:509).

Disadvantages of Nafion® include cross-permeation of hydrogen when operated at high pressures and the limiting temperature range (Millet *et al.*, 2009:4974). The cross-permeation of hydrogen is a potential high risk. Hydrogen contaminates the generated oxygen on the anode side and can form explosive mixtures. Proper hydration is important as conductivity within the membrane is dependent on water to solvate protons from the sulfonic acid groups that form the backbone of the PEM (Pan *et al.*, 2007:278). PEM water electrolysis temperatures exceeding 100°C at atmospheric pressure limit the proper hydration of Nafion® (Millet *et al.*, 2009:4974). In addition, the low mechanical strength of Nafion® at high operational temperatures further limits the temperature to a value usually below 80°C (Li *et al.*, 2009:449).

2.2.2.2 PBI

PBI is a promising candidate for implementation in PEM fuel cell technology due to its outstanding mechanical properties (Ong *et al.*, 2010:7866) and thermal-chemical stability (Xing *et al.*, 2006:2011/05/17). High temperature PEM fuel cell operation is possible with PBI membranes (Pan *et al.*, 2007:278). An additional advantage is that a PBI-based PEM can be operated with little or no humidification.

Celazole® is the trademark of the most known commercial product of PBI. The chemical name of PBI is poly 2,2-*m*-(phenylene)-5,5-bibenzimidazole and the chemical structure of PBI is illustrated in Figure 2-7.

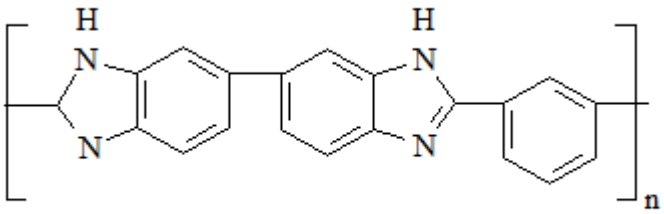

Figure 2-7 PBI (poly 2,2-*m*-(phenylene)-5,5-bibenzimidazole) structure (Li *et al.*, 2009:449)

As PBI can have many structures, the chemical structure shown in Figure 2-7 is also referred to as *m*PBI as the phenylene ring is meta-coordinated (Li *et al.*, 2009:449). The PBI polymer is basic by nature and can be complexed with strong acids or bases. In some cases the acidic and

basic polymers are mixed to produce a membrane with good mechanical and thermal properties (Xing *et al.*, 2006:2011/05/17). ABPBI (2,5-benzimidazole) is also part of the benzimidazole family. ABPBI has a low preparation cost, good mechanical strength and better water and phosphoric acid uptakes when compared to standard PBI (Ong *et al.*, 2010:7866).

Xing *et al*. (2006) found that a sulfonated polysulfone (sPSU)/PBI blend had increased thermal stability. The stability of the sPSU/PBI blend was due to the thermal stability of PBI, as well as the specific interactions between the acidic and basic components. Altogether the mechanical and chemical stability of the sPSU/PBI crosslinked blend PEM was better than pure PBI. Furthermore sPSU/PBI yielded adequate proton conductivity.

PBI membranes can absorb up to 15 – 19 wt% distilled water at room temperature (Li *et al.*, 2009:449) due to its high affinity for moisture, which is caused by intermolecular hydrogen bonding. The hydrogen bonding is caused by the phosphoric and phosphonic acids, which act as proton donors and proton acceptors. A hydrogen bond network is formed in which the breaking and forming of these bonds create a flow of protons through the membrane, also known as the proton conducting mechanism (Li *et al.*, 2009:449).

2.2.3 Electrocatalyst

Water electrolysis takes place at a lower energy requirement when using a suitable electrocatalyst for the specific reaction. The high costs associated with noble metal electrocatalysts have hampered the development of PEM water electrolysers. However, since non-noble metal electrocatalysts are not producing satisfactory activities when compared to noble metal electrocatalyst, further research into noble metal electrocatalyst development is thus an important focus area in PEM water electrolysis (Song *et al*., 2008:4955).

Catalysts for both the anode and the cathode reactions can be applied directly onto a PEM, current collectors or gas diffusion layers using a variety of techniques (Grigoriev *et al*., 2009:4968).

2.2.3.1 Anode

The anode side of PEM water electrolysers is considered corrosive. Oxygen is evolved at high electrode potential values, creating a highly oxidising environment (Millet *et al*., 2010:5043). According to extensive research and development on electrocatalysts for the oxygen evolution reaction (OER) the rare noble metals of Ir, Ru and platinum black and their oxides are the most suitable. IrO_2 is usually preferred over RuO_2 as it has a higher stability, but additional research is needed to further lower the anode electrical consumption (Song *et al*., 2008:4955). Similarly, Ir

has a higher efficiency than platinum black (Millet *et al*., 2009:4974). Metal platinum is also not used on the anode side of the water electrolyser due to oxide film formation on the catalyst, which lowers the surface conduction of the catalyst (Song *et al*., 2008:4955).

Non-noble metals such as Ni and Co cannot be used due to the acidic environment and high potential generated at the anode side of the water electrolyser (Song *et al*., 2008:4955).

2.2.3.2 Cathode

While iridium is often used as the anode catalyst, platinum is generally used on the cathode side of a water electrolyser, as it provides the best performance (Song *et al*., 2008:4955).

2.2.4 Gas diffusion layers and electrodes

The management of water and gas mixtures at the cathode and anode side of a PEM water electrolyser is essential to its performance. A Gas Diffusion Layer (GDL) in a PEM fuel cell regulates liquids and distributes gases to the MEA. The GDL also acts as a current collector in the PEM fuel cell (Sun *et al*., 2008:960). The key factor differentiating GDL from Gas Diffusion Electrodes (GDE) is the surface on which the electrocatalytic layer is deposited (Millet *et al*., 2009:4974). In the case of a GDE, the electrocatalytic layer is deposited onto the surface of the GDL and the GDL can be hot pressed onto the membrane. For a MEA, the electrocatalyst is directly deposited onto the PEM surface where after the GDL is placed or hot pressed onto the PEM.

2.2.4.1 Function of Gas diffusion layer/electrode

The inspection of a PEM water electrolyser reveals that the PEM does not possess a reinforced structure but is floppy by nature when wetted. A GDL is placed on the PEM active layer to reinforce the membrane (Escribano *et al*., 2006:8). GDLs are used in PEM fuel cells to improve water mass transport, gas storage and humidity distribution (Sun *et al*., 2008:960). In the case of PEM water electrolysers, the main functions of a GDL are to supply the active layers with reactants, to conduct current and to remove heat and oxygen from the MEA surface (Escribano *et al*., 2006:8).

2.2.4.2 Gas Diffusion Layer

The three main types of carbon substrates used as GDL are carbon cloth, carbon paper and carbon non-woven material. In some cases, expanded or sintered metals are used as GDL (Escribano *et al.*, 2006:8,Quick *et al.*, 2009:110).

A GDL typically possesses a double layered structure. The macro-porous layer, which is regarded as the core of the GDL is usually made from a carbon fibre substrate (Figure 2-8). A

micro-porous layer made from a carbon black mixture and a hydrophobic agent forms the second thinner layer (Quick *et al.*, 2009:110.). The hydrophobic agent used most commonly is polytetrafluoroethylene (PTFE), which is applied to the GDL to prevent flooding of the catalyst layer (Escribano *et al.*, 2006:8). Product water formed at the cathode during fuel cell operation can be removed from the electrocatalyst layer through the GDL to the flow field channels (Quick *et al.*, 2009:110). This concept can be applied to the cathode side of a PEM water electrolyser as water diffuses with the protons through the membrane by means of electro-osmotic drag (Mauritz *et al.*, 2004:4535,Millet *et al.*, 2010:5043). The hydrophobic treatment of the GDL creates hydrophilic and hydrophobic pores, which prevent water condensation in the GDL, ensuring a low water saturation level (Quick *et al.*, 2009:110).

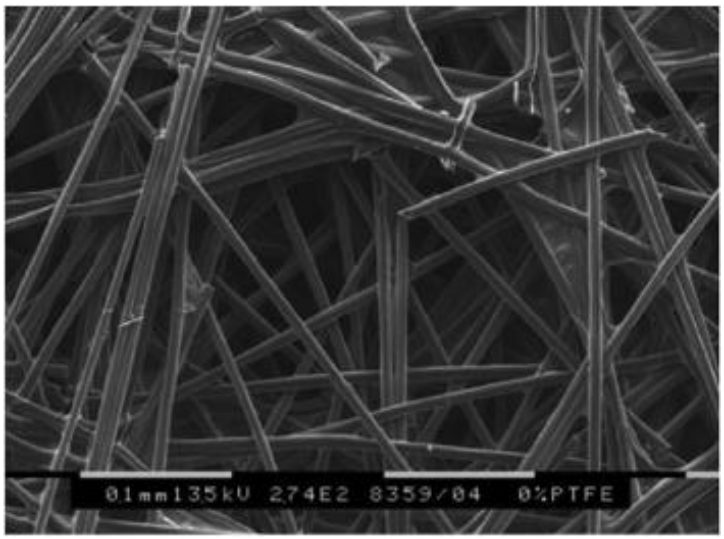

Figure 2-8 SEM pictures of carbon papers (Pan *et al.*, 2007:278)

Since the porosity, mechanical properties and electrical and thermal conductivities are influenced by the carbon fibre arrangement, hydrophobicity and thickness of the GDL, as shown in Figure 2-9 (Escribano *et al.*, 2006:8). The selection of GDL type is important to get optimum water flow and gas distribution on the anode side.

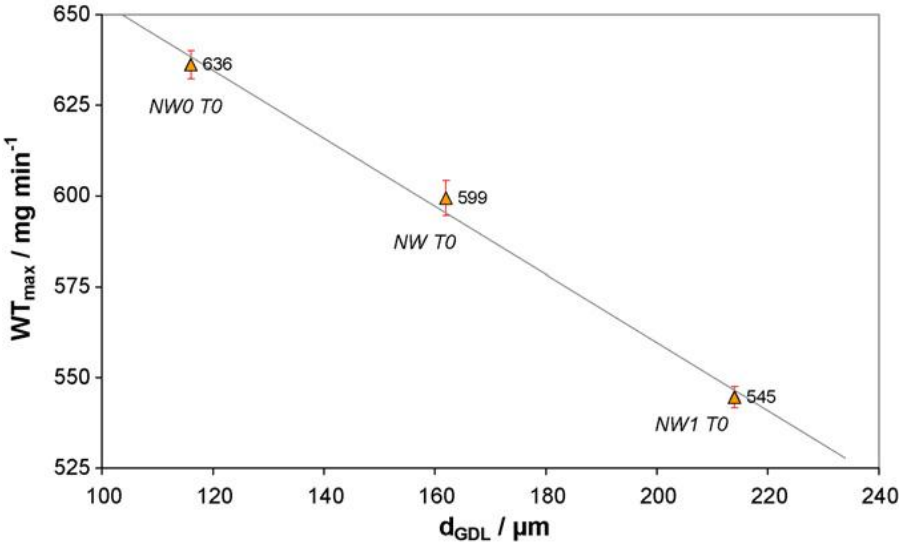

Figure 2-9 Water transport (WT) as function of the GDL thickness (Quick *et al.*, 2009:110).

Studies have shown that carbon cloth exhibits a higher performance under fully humidified conditions when compared to carbon paper. Carbon paper, on the other hand, exhibits a higher fuel cell performance under dry operating conditions. Carbon cloth has sufficient water removal capacity, whereas carbon paper has a better water retention (Quick *et al.*, 2009:110). These results originate from fuel cell testing where water removal on the anode side is important. Water electrolysis, contrariwise, needs sufficient anode water flow. The electrocatalytic layer on the anode side requires water for the commencement of PEM water electrolysis. Carbon paper GDL are thus best suited for the anode side and carbon cloth for the cathode side of a PEM water electrolyser.

2.2.4.3 Gas Diffusion Electrode (GDE)

The factor distinguishing GDLs and GDEs is the electrocatalytic layer that is deposited onto the GDL to form the GDE. GDE fabrication techniques include electrocatalytic spraying, slurry deposition or casting, dry rolling and GDL impregnation with an ionomer (Pan *et al.*, 2007:278). The GDE porosity (the electrocatalyst layer and carbon support) for fuel cells can be tailored by adding porogens such as ammonium oxalate, ammonium carbonate, ammonium acetate and zinc oxide (Pan *et al.*, 2007:278). The porogens should be volatile or soluble for effective removal after GDE fabrication.

A slight performance difference exists between MEAs and GDEs (Grigoriev *et al.*, 2009:4968). The surfaces on which the electrocatalyst is deposited, is physically different for MEA and GDE. MEAs have the electrocatalyst deposited directly onto the PEM and GDEs have the electrocatalyst deposited onto the GDL surface. Performance figures show that MEA are

marginally more efficient than GDE. The higher efficiency is most likely due to the amount of electrocatalyst in contact with and hence close proximity of the PEM.

2.2.5 Flowfields

The flow of reagents and products in a PEM water electrolyser is important as the PEM should be properly hydrated. Water flow in a PEM water electrolyser is as follows: De-ionised water enters the anode side, passes through a flowfield and diffuses through the porous GDL layer to the electrocatalyst layer. The anode product gas, oxygen, diffuses to the flowfield where the de-ionised water entrains the gas and exits the electrolyser (Ito *et al*., 2010:9550).

A variety of flowfields can be used in PEM water electrolysers, including serpentine-single, serpentine-dual, parallel flowfields (Ito *et al*., 2010:9550) and porous titanium sheets, which form part of the collector plates section (Millet *et al*., 2009:4974). Figure 2-10 clearly shows that parallel flowfields have superior efficiencies when compared to serpentine flowfields.

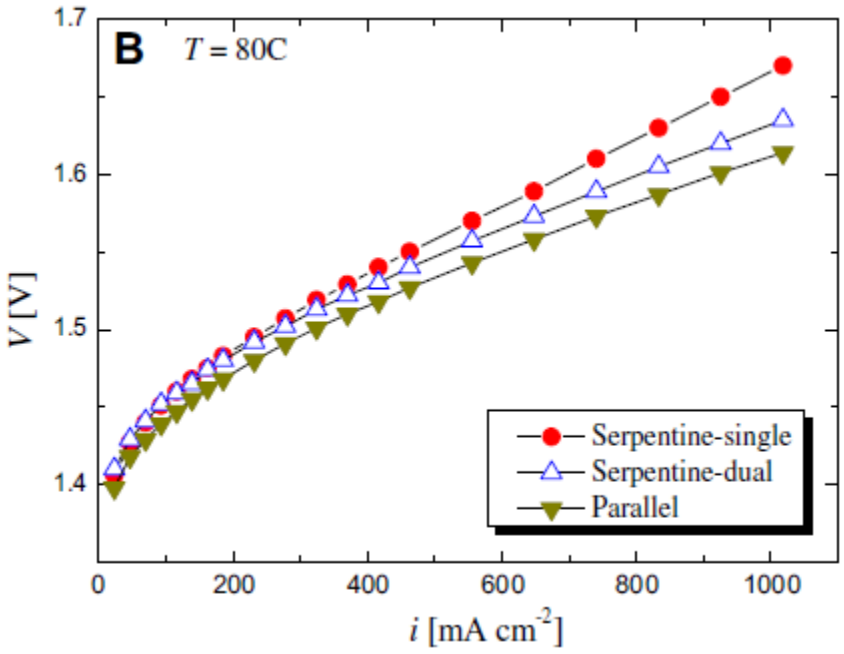

Figure 2-10 Effect of flowfield type on PEM water electrolyser polarisation curves (Ito *et al.*, 2010:9550.)

2.2.6 Collector plates

Collector plates are commonly referred to as current collectors. Collector plates are used as back plates in single cell PEM water electrolysers or as bipolar plates in a PEM electrolyser stack. Sintered titanium powder forms the porous current collectors within the PEM water electrolyser, while titanium bipolar plates of uniform porosity (Millet *et al*., 2009:4974) are used to separate the individual cells of a stack (Grigoriev *et al*., 2009:4968).

The porosity of current collectors influences gas removal and ohmic resistances of the collector plates. High porosities result in better gas removal, however, at the cost of increased ohmic resistance of the collector plates. The increased resistance will cause more losses at the current collector and catalytic contact points (Grigoriev *et al*., 2009:4968). Optimisation of porosity and pore size distribution is necessary for different operating current densities (Millet *et al*., 2009:4974) as high operating current densities (> 1A.cm^{-2}) for example yield more gas. The collector plates, therefore, have to be optimised to ensure that mass transport does not become a limiting factor (Grigoriev *et al*., 2009:4968). To allow for proper water and gas transport, the porosity of current collectors should lie in the range of 30-50% for water electrolysis (Grigoriev *et al*., 2009:4968). In addition, the even distribution of current through the current collector to the electrocatalytic layer and PEM is vital. Uneven distribution of current can cause hot spots to form on the PEM, which can lead to a shortened lifespan or permanent damage to the PEM (Millet *et al*., 2009:4974).

2.3 Electrolyser performance

The electrolyser performance section gives an electrochemical insight on how PEM water electrolysis works. Technical information on the overpotentials, temperature, pressure and degradation associated with operating the electrolyser is discussed.

2.3.1 Thermodynamics

PEM water electrolysis splits water molecules into oxygen, protons and electrons on the anode side of the cell. For water electrolysis to commence a DC potential difference higher than the thermo neutral voltage of the hydrolysis reaction (V° = 1.229V) is applied across the anode and cathode. The protons diffuse through the PEM to the cathode side of the cell. The protons and electrons then combine to form hydrogen gas (Barbir, 2005:661).

The enthalpy of reaction reaction is identical to the formation of liquid water at standard conditions (STP) $\Delta H_f°$= -285.83 kJ mol^{-1}. The change in Gibbs free energy (ΔG) represents the electricity required while the last term TΔS, represents absorbed heat from the environment at constant temperature. The reversible cell voltage for the splitting of water is also known as the standard cell voltage (V°), or the open circuit voltage representing the redox reaction (Lebbal *et al*., 2009:5992). Standard cell voltage (V°) is 1.229V at standard conditions of temperature and pressure (Rand *et al*., 2008:300).

2.3.1.1 Reactions

Half-reactions and the redox reaction associated with the electrolysis of water are portrayed by:

$$\boldsymbol{H_2O_{(l)} \rightarrow \frac{1}{2}\, O_{2(g)} + 2H^+ + 2e^-} \tag{2-1}$$

$$\boldsymbol{2H^+ + 2e^- \rightarrow H_{2(g)}} \tag{2-2}$$

$$\boldsymbol{H_2O_{(l)} \rightarrow H_{2(g)} + \frac{1}{2}\, O_{2(g)}} \tag{2-3}$$

The reaction of Equation 2-1 is known as the oxidation reaction, where the electrons are removed from the species. The reaction of Equation 2-2 is known as the reduction reaction, where electrons are added to a species. Equation 2-3 represents the reaction taking place within the cell and is known as the redox reaction (Millet *et al*., 2009:4975).

Gibbs free energy is defined by (Biaku *et al.*, 2008:4247):

$$\Delta G = \Delta H - T\Delta S \tag{2-4}$$

$$\Delta G = \Delta G° + RT ln\left(P_{H_2} P_{O_2}^{0.5}\right) \tag{2-5}$$

For the reaction associated with water electrolysis, the Gibbs free energy at constant temperature can be expressed in terms of the standard cell voltage (Millet *et al.*, 2009:4974):

$$V° = \frac{\Delta G}{nF} = \frac{\Delta G°}{nF} + \frac{RT}{nF} ln\left(P_{H_2} P_{O_2}^{0.5}\right) = E° + \frac{RT}{nF} ln\left(P_{H_2} P_{O_2}^{0.5}\right) \quad (2\text{-}6)$$

Where R, n, F, P_{H2} and P_{O2} represent the gas constant ($R=8.314 J.(mol.K)^{-1}$), the number of electrons generated per mole of water, the Faraday constant ($F=96487 C.mol^{-1}$) and the partial pressures of hydrogen and oxygen relative to atmospheric pressure (Lebbal *et al.*, 2009:5992).

According to Equation 2-6, the concentrations of reagents and products can have an effect on the reversible potential (Biaku *et al.*, 2008:4247). The partial pressures of reagents generated can vary depending on the design parameters of the electrolyser. The assumption is made that only hydrogen and water vapour exist in the gaseous phase on the cathode side of the electrolyser. It is also assumed that the anode side contains only oxygen and water vapour in the gaseous phase. For the case of low pressure PEM water electrolysis ideal behaviour of gases is assumed, making the law of Dalton valid (Biaku *et al.*, 2008:4247).

The specific energy consumption is a function of energy required per mass or volume of product. In the case of PEM water electrolysis the specific energy consumption (E_s) is a function of energy used per normal cubic meter (kWh/Nm^3). As the energy used, is a function of cell voltage and current density, it is also a function of operating temperature and pressure (Millet *et al.*, 2010:5043).

PEM water electrolyser efficiency is a function of temperature, pressure and current density and can be defined in two ways. Energy efficiency ($\varepsilon_{\Delta G}$) is calculated using the reversible potential, whereas enthalpy efficiency ($\varepsilon_{\Delta H}$) is calculated using the thermo-neutral voltage (assuming no net heat exchange to the surroundings). These definitions are related through entropy (ΔS).

$$\varepsilon_{\Delta G}(T, P, i) = \frac{V°(T,P)}{U^{cell}(T,P,i)} \quad (2\text{-}8)$$

where U^{cell} represents the measured cell voltage during operation. It should be noted that cell efficiencies are commonly expressed in terms of the energy efficiency (Millet *et al.*, 2009:4974).

2.3.2 Overpotential

The potential applied to an electrolyser must be high enough to overcome the reversible potential and overpotentials associated with a PEM water electrolyser. Overpotentials can be defined as irreversible resistances that must be overcome for any hydrogen to be generated (Barbir, 2005:661). Overpotentials present in PEM water electrolysis are caused by activation, ohmic and

concentration overpotentials, where the first two contribute the most to the overpotential. Overpotential losses mostly occur at the anode side of PEM water electrolysers (Song *et al*., 2008:4955).

2.3.2.1 Activation overpotential

The activation overpotential which occurs at both the anode and cathode of the electrolyser (Nieminen *et al.*, 2010) can be described as the resistance of the electrochemical reactions taking place and is, therefore, related to the activation energy (Nieminen *et al.*, 2010). For any conversion this overpotential must first be overcome (Biaku *et al*., 2008:4247). The activation overpotentials can be described as the difference between the observed voltage and the equivalent actual voltage needed for electron transfer to take place.

Both the anode and cathode contribute to the overall activation overpotential (Biaku *et al*., 2008:4247). The activation overpotential is considered the primary loss in low to medium temperature PEM water electrolysers. High exchange current density PEM water electrolyser operations generally require lower initial potential for the reaction to occur (Barbir, 2005:661).

2.3.2.2 Ohmic overpotential

The ohmic overpotential is a resistance that obeys Ohm's law and does not fluctuate with varying current densities of the PEM water electrolyser (Barbir, 2005:661). PEM resistance is the main source of ohmic overpotential (Lebbal *et al*., 2009:5992). Hydrogen diffusion through a Nafion® PEM, for example, offers minute resistance as the transport process is thermodynamically irreversible (Nieminen *et al.*, 2010). The overall ohmic overpotential depends on the PEM type, electrode and the contact between the PEM and electrode (Barbir, 2005:661).

Ohmic losses can be reduced by decreasing the PEM thickness (Nieminen *et al.*, 2010) and the distance between the current collector particles (Grigoriev *et al*., 2009:4968). Improved MEA manufacturing techniques have also contributed in reducing the ohmic overpotential (Barbir, 2005:661). While a thinner PEM will improve the efficiency of the PEM water electrolyser, it will also reduce the lifetime of the PEM used. Similarly, a reduced particle distance between the PEM and electrocatalyst introduces capillary effects (Grigoriev *et al*., 2009:4968), which lead to a reduced contact resistance at the price of mass transfer limitations.

2.3.2.3 Concentration overpotential

Concentration overpotentials in a PEM water electrolyser arise at high current densities. Large amounts of oxygen and hydrogen are then generated, creating partial pressures in the PEM water electrolyser, which are the major cause of concentration overpotentials in PEM water

electrolysers. The concentration overpotentials can be determined by subtracting the difference between the observed voltages at the higher partial pressures and the theoretical voltage required for the reaction to take place (Nieminen *et al*., 2010).

A simple description of concentration overpotentials is that the oxygen forming on the anode side of the PEM water electrolyser restricts the reagent water from reaching the electrocatalyst. The oxygen forms quickly enough to reduce the water contact on the catalyst surface, thus decreasing the PEM water electrolyser efficiency (Barbir, 2005:661). Concentration overpotential in the PEM water electrolyser can be defined as the ratio of partial pressures for the gases of hydrogen and oxygen versus that of water in the electrolyser. These partial pressures are important when determining concentration overpotentials (Nieminen *et al*., 2010).

The concentration overpotentials for PEM water electrolysis are usually not observed in moderate operating conditions (1.6 A.cm-2), but will occur at higher operating current densities (Barbir, 2005:661). This implies that current densities should be limited to achieve the highest possible efficiencies.

2.3.3 Operating conditions

The PEM water electrolyser can operate under varying conditions. Operating variables include current density, water temperature and flow rate and pressure within the anode and cathode compartments. Modern PEM water electrolysers operate efficiently at a current density of 0.5 $A.cm^{-2}$ (Millet *et al*., 2009:4974). New developments include PEM water electrolysers operating at current densities above 1 $A.cm^{-2}$.

2.3.3.1 Temperature

The temperature within a PEM water electrolyser has a significant influence on efficiency. A change in temperature brings a change in conductivity, implying that higher PEM water electrolyser operating temperatures result in increased electrode reactivity, since the PEM water electrolyser conductivity increases linearly with temperature. This in turn makes it possible to reach higher exchange current densities which lower the activation overpotential (Ni *et al*., 2008:2748). The conductivity will increase until the PEM is saturated with water (Barbir, 2005:661).

The improved performance at higher temperatures is related to improved performance both by the electrocatalyst and the PEM. Higher operating temperatures have a positive effect on overall PEM water electrolyser efficiency but the water temperature should not exceed 373 K at

atmospheric pressure as liquid water is a requirement to achieve such high conductivities (Ni *et al*., 2008:2748).

2.3.3.2 Pressure

PEM water electrolysers can operate at pressures higher than atmospheric pressure depending on design factors. According to thermodynamic principles, the pressurisation of the electrolyser cathode side will result in a slightly higher cell voltage. The higher cathode pressure is regarded as isothermal compression work (Barbir, 2005:661). The main purpose of high pressure operations is to save on compression costs and direct storage of hydrogen at high pressure. Additional losses of hydrogen may occur depending on the anode pressure, PEM type and thickness, as hydrogen permeation through the PEM can occur.

According to Grigoriev *et al*. (2009), the standard voltage of electrolysis follows the Nernst equation when the operating pressure is increased. In reality, high current densities (0.5-1.0 $A.cm^{-2}$) improve the kinetics of the electrolysis reaction, as higher pressures reduce the size of gaseous bubbles. Increasing operating pressure increases gas cross-permeation phenomena while decreasing faradaic efficiency. This negative effect counterbalances the improved kinetics at low operating current densities, but decreases as the current density is increased. Figure 2-11 clearly illustrates the effect of higher operating pressures.

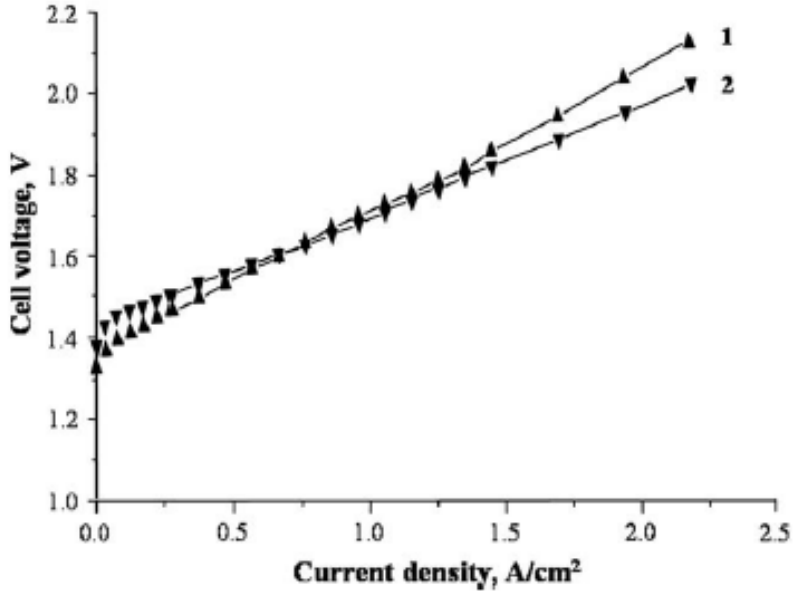

Figure 2-11 Effect of high pressure PEM water electrolysis at a temperature of 90°C and different operating pressures, 1 P = 1 bar, 2 P= 50 bar. Pt as cathodic electrocatalyst and Ir as anodic electrocatalyst on a Nafion® - 117 PEM. (Grigoriev *et* al. (2009)).

2.3.3.3 Methanol concentration

The addition of methanol to the reagent water of normal PEM water electrolysis is also known as electrochemical reforming or electrolysis. Figure 2-12 is a schematic presentation of such an electrolyser (Cloutier *et al.*, 2010:3967).

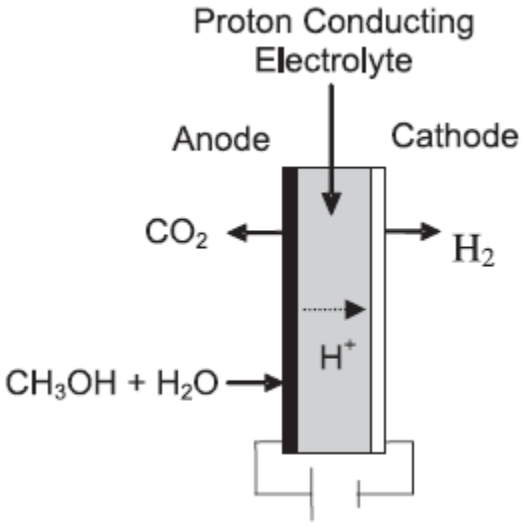

Figure 2-12 Schematic diagram of a methanol electrochemical electrolyser (Cloutier *et al.*, 2010:3967).

The anode, cathode and overall reactions are illustrated in Equations 2-9, 2-10 and 2-11. The anode reaction consists of dehydrogenation of the aqueous methanol feed and produces carbon dioxide, protons and electrons. The standard potential (V°) for the anode and overall reaction is 0.016 V, which is significantly lower than the standard potential of water electrolysis (1.229V) (Rand *et al.*, 2008:110). The estimated cost of hydrogen production for aqueous methanol electrolysis is approximately 50% less than that of PEM water electrolysis, including the price of methanol. The electrocatalysts typically used with aqueous methanol electrolysis are Pt/C or Pt-Ru/C for the anode and Pt/C for the cathode.

$$\boldsymbol{CH_3OH_{(l)} + H_2O_{(l)} \rightarrow CO_{2(g)} + 6H^+ + 6e^-} \quad (2\text{-}9)$$

$$\boldsymbol{6H^+ + 6e^- \rightarrow 3H_{2(g)}} \quad (2\text{-}10)$$

$$\boldsymbol{CH_3OH_{(l)} + H_2O_{(l)} \rightarrow 3H_{2(g)} + CO_{2(g)}} \quad (2\text{-}11)$$

Major disadvantages of aqueous methanol electrolysis are slow reaction kinetics of the anode with the oxidation of methanol and fuel losses, due to methanol and water crossover from the anode to the cathode.

Figure 2-13 illustrates how the different concentrations of aqueous methanol solutions affect the performance of the electrolyser. The IR corrected cell voltage represents the cell potential without ohmic losses and the voltages were determined with a Standard Hydrogen electrode (SHE) as reference electrode. Methanol concentration clearly influences the performance of the electrolyser. The 16M concentration of aqueous methanol reaches much higher current densities than the lower methanol concentrations of 1M and 4M.

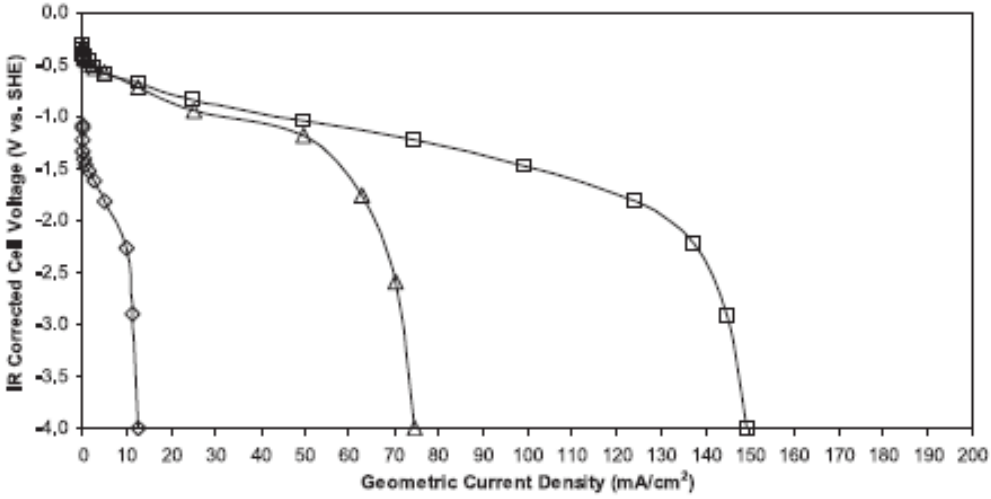

Figure 2-13 Effect of methanol concentration on cell voltage at increasing geometric current densities with 4 $mg.cm^{-2}$ Pt-Ru black anode electrocatalyst (Cloutier *et al.*, 2010:3967).
[◊ 0M CH_3OH; Δ 2M CH_3OH; □ 16M CH_3OH]

Aqueous methanol electrolysis is said to reach steady state at lower current densities, where the oxidation of methanol takes place at an acceptable efficiency. Electrolyser operation with aqueous methanol at high current density results in the starting of an unwanted side-reaction, where water electrolysis starts to occur at potentials lower than 1.23 V. High current densities deliver lower overpotentials with high concentrations of methanol, where low current densities do not influence cell potential radically. Aqueous methanol electrolysis depends on whether the system is active or static. In the active case, aqueous methanol electrolysis is not as sensitive to methanol concentration when compared to the sensitivity of static aqueous methanol electrolysis. Figure 2-13 is an of static aqueous methanol electrolysis (Cloutier *et al.*, 2010:3967).

2.3.4 Degradation

Component degradation within a PEM water electrolyser is an essential topic to study as it influences both the lifetime and the performance of the PEM water electrolyser. The identification of PEM water electrolyser components vulnerable to degradation is important.

2.3.4.1 PEM degradation

The degradation of proton exchange membranes can be divided into three classes: chemical/electrochemical, mechanical and thermal degradation (Collier *et al*., 2006:1838).

Chemical/electrochemical degradation of the PEM mainly occurs at the anode side. The oxidising environment of the PEM water electrolyser plays a significant role in PEM degradation, where metal contaminants and free radical formation are some of the major causes of PEM degradation. The formation of peroxy and hydroperoxy radicals in PEM cells is considered to be the main reason for chemical degradation. A mechanism for radical formation could be as follows:

$$H_2 \rightarrow 2H^{\cdot} \quad (2\text{-}12)$$

$$H^{\cdot} + O_2 \rightarrow HO_2^{\cdot} \quad (2\text{-}13)$$

$$HO_2^{\cdot} + H^{\cdot} \rightarrow H_2O_2 \quad (2\text{-}14)$$

$$H_2O_2 + M^{2+} \rightarrow M^{3+} + {}^{\cdot}OH + OH^- \quad (2\text{-}15)$$

$${}^{\cdot}OH + H_2O_2 \rightarrow H_2O + HO_2^{\cdot} \quad (2\text{-}16)$$

In the first step of the mechanism (Equation 2-12), the formed hydrogen gas is transformed into two hydrogen free radicals. Thereafter, the hydrogen free radical is free to bond with oxygen as illustrated in the equation 2-13. The product Equation 2-13 bonds with a hydrogen free radical to form what is known as hydrogen peroxide (Equation 2-14), which is then free to bond with trace metals (Equation 2-15) that are present in solution and can diffuse into the PEM. The fifth step of the mechanism (Equation 2-16) chemically illustrates how the hydrogen peroxide free radical forms and will be able to attack the PEM. Based on this principle Fenton's reagent, consisting of hydrogen peroxide-ferrous ion system, is commonly used for accelerated tests of PEM (Collier *et al.*, 2006:1838).

The presence of foreign cations is problematic for PEM. This is especially the case for PEMs with sulfonic groups like Nafion®. Most cations such as Ca^{2+}, Cu^{2+}, Na^{+}, K^{+} and Mg^{2+} have affinities for sulfonic acid that are higher than that of hydrogen. Membrane conductivity

decreases proportionally to the ionic charge of the cation. Cation exchange influences the water content, ionic conductivity and transference numbers of the PEM. The exchange will ultimately result in a cell voltage increase. Proton displacement by other cations decreases membrane water content and creates an environment with a higher hydrogen peroxide concentration. One exception for hydrogen displacement is Li^+ as it is not displaced (Collier *et al.*, 2006:1838).

Common mechanical degradation is physical damage to the PEM in the form of tears, pinhole blisters and punctures (Collier *et al.*, 2006:1838). Degradation of this kind is usually caused by human error in the manufacture, handling or installation of the PEM. Mechanical degradation can also occur if the PEM is very thin and not suited for the conditions within the PEM water electrolyser cell. Disadvantages of thinner PEMs are lower physical strength and higher permeability of gases. This will let more gas crossover take place, increasing the PEM degradation rate (Collier *et al.*, 2006:1838).

As mentioned previously, high temperature PEM water electrolyser operations have a number of benefits, including higher conductivity of components (Barbir, 2005:661), reduced cooling requirements and better electrochemical kinetics (Collier *et al.*, 2006:1838). However, the detriment of high temperature operation is that degradation of the membrane and other components increases with temperature.

2.3.4.2 GDL degradation

GDL degradation in fuel cells takes place due to changes in the GDL wetting behaviour and structural changes, including the decomposition of PTFE, causing wetting changes of the GDL. The coverage of PTFE influences the amount of water within the GDL (Seidenberger *et al.*, 2011:5317). As the PTFE is reduced a critical water content value is reached, resulting in larger clusters being formed that connect all GDL regions. The clusters in turn can increase the degradation rate of the GDL. Since the GDL is subject to a highly oxidising environment both PTFE and carbon can be depleted. Impurities and mechanical effects can also lead to wetting changes. Structural changes of GDL can occur with excess GDL compression or the oxidation of carbon particles. Degradation of the GDL will affect the heat and electrical conductivity of the GDL and will negatively impact the PEM water electrolyser efficiency (Seidenberger *et al.*, 2011:5317).

2.4 Conclusion

The literature survey of PEM water electrolysis has shown that there are several different components, designs and variables that influence the way and efficiency in which a PEM water electrolyser operates. The MEA and how it is synthesised has the largest influence on electrolyser performance. The activation overpotential of the MEA depends on the electrocatalyst used and the way the electrocatalyst is applied to the PEM. The implementation of GDE seems to be an adequate alternative to the MEA as only the PEM will have to be replaced once the lifetime of the PEM is reached. It has been shown that operating conditions affect the performance and degradation of each component. Increased operating temperature has a substantial influence on electrolyser performance, where increased cathode pressure on the other hand is applied to save on hydrogen compression costs. Additives to the electrolyser feed water, such as metal ions and methanol will also affect electrolyser performance greatly. By taking all the key literature findings in perspective, it is clear that care should be taken when selecting a PEM water electrolyser, its components and its operating conditions.

2.5 References

BARBIR, F. 2005. PEM electrolysis for production of hydrogen from renewable energy sources. *Solar energy,* 78(5):661-669.

BEREZINA, N.P., TIMOFEEV, S.V. & KONONENKO, N.A. 2002. Effect of conditioning techniques of perfluorinated sulphocationic membranes on their hydrophylic and electrotransport properties. *Journal of membrane science,* 209(2):509-518.

BIAKU, C.Y., DALE, N.V., MANN, M.D., SALEHFAR, H., PETERS, A.J. & HAN, T. 2008. A semiempirical study of the temperature dependence of the anode charge transfer coefficient of a 6 kW PEM electrolyzer. *International journal of hydrogen energy,* 33(16):4247-4254.

COLLIER, A., WANG, H., ZI YUAN, X., ZHANG, J. & WILKINSON, D.P. 2006. Degradation of polymer electrolyte membranes. *International journal of hydrogen energy,* 31(13):1838-1854.

CLOUTIER, C.R. & WILKINSON, D.P. 2010. Electrolytic production of hydrogen from aqueous acidic methanol solutions. *International journal of hydrogen energy,* 35(9):3967-3984.

ESCRIBANO, S., BLACHOT, J., ETHÈVE, J., MORIN, A. & MOSDALE, R. 2006. Characterization of PEMFCs gas diffusion layers properties. *Journal of power sources,* 156(1):8-13.

GANLEY, J.C. 2009. High temperature and pressure alkaline electrolysis. *International journal of hydrogen energy,* 34(9):3604-3611.

GRIGORIEV, S.A., MILLET, P., VOLOBUEV, S.A. & FATEEV, V.N. 2009. Optimization of porous current collectors for PEM water electrolysers. *International journal of hydrogen energy,* 34(11):4968-4973.

ITO, H., MAEDA, T., NAKANO, A., HASEGAWA, Y., YOKOI, N., HWANG, C.M., ISHIDA, M., KATO, A. & YOSHIDA, T. 2010. Effect of flow regime of circulating water on a proton exchange membrane electrolyzer. *International journal of hydrogen energy,* 35(18):9550-9560.

KREUTER, W. & HOFMANN, H. 1998. Electrolysis: The important energy transformer in a world of sustainable energy. *International journal of hydrogen energy,* 23(8):661-666.

LEBBAL, M.E. & LECŒUCHE, S. 2009. Identification and monitoring of a PEM electrolyser based on dynamical modelling. *International journal of hydrogen energy,* 34(14):5992-5999.

LI, Q., JENSEN, J.O., SAVINELL, R.F. & BJERRUM, N.J. 2009. High temperature proton exchange membranes based on polybenzimidazoles for fuel cells. *Progress in polymer science,* 34(5):449-477.

MAURITZ, K.A. & MOORE, R.B. 2004. State of understanding of nafion. *Chemical reviews,* 104(10):4535-4585.

MEDINA, P. & SANTARELLI, M. 2010. Analysis of water transport in a high pressure PEM electrolyzer. *International journal of hydrogen energy,* 35(11):5173-5186.

MILLET, P., NGAMENI, R., GRIGORIEV, S.A., MBEMBA, N., BRISSET, F., RANJBARI, A. & ETIÉVANT, C. 2010. PEM water electrolyzers: From electrocatalysis to stack development. *International journal of hydrogen energy,* 35(10):5043-5052.

MILLET, P., DRAGOE, D., GRIGORIEV, S., FATEEV, V. & ETIEVANT, C. 2009. GenHyPEM: A research program on PEM water electrolysis supported by the european commission. *International journal of hydrogen energy,* 34(11):4974-4982.

NI, M., LEUNG, M.K.H. & LEUNG, D.Y.C. 2008. Energy and exergy analysis of hydrogen production by a proton exchange membrane (PEM) electrolyzer plant. *Energy conversion and management,* 49(10):2748-2756.

NIEMINEN, J., DINCER, I. & NATERER, G. 2010. Comparative performance analysis of PEM and solid oxide steam electrolysers. *International journal of hydrogen energy,* In Press, Corrected Proof.

ONG, A., JUNG, G., WU, C. & YAN, W. 2010. Single-step fabrication of ABPBI-based GDE and study of its MEA characteristics for high-temperature PEM fuel cells. *International journal of hydrogen energy,* 35(15):7866-7873.

PAN, C., LI, Q., JENSEN, J.O., HE, R., CLEEMANN, L.N., NILSSON, M.S., BJERRUM, N.J. & ZENG, Q. 2007. Preparation and operation of gas diffusion electrodes for high-temperature proton exchange membrane fuel cells. *Journal of power sources,* 172(1):278-286.

QUICK, C., RITZINGER, D., LEHNERT, W. & HARTNIG, C. 2009. Characterization of water transport in gas diffusion media. *Journal of power sources,* 190(1):110-120.

RAND, D.A.J. & DELL, R.M. 2008. **Hydrogen energy challenges and prospects**. 1st ed. Cambridge, UK: The Royal Society of Chemistry. 300p.

SEIDENBERGER, K., WILHELM, F., SCHMITT, T., LEHNERT, W. & SCHOLTA, J. 2011. Estimation of water distribution and degradation mechanisms in polymer electrolyte membrane fuel cell gas diffusion layers using a 3D monte carlo model. *Journal of power sources,* 196(12):5317-5324.

SIRACUSANO, S., BAGLIO, V., DI BLASI, A., BRIGUGLIO, N., STASSI, A., ORNELAS, R., TRIFONI, E., ANTONUCCI, V. & ARICÒ, A.S. 2010. Electrochemical characterization of single cell and short stack PEM electrolyzers based on a nanosized IrO2 anode electrocatalyst. *International journal of hydrogen energy,* 35(11):5558-5568.

SONG, S., ZHANG, H., MA, X., SHAO, Z., BAKER, R.T. & YI, B. 2008. Electrochemical investigation of electrocatalysts for the oxygen evolution reaction in PEM water electrolyzers. *International journal of hydrogen energy,* 33(19):4955-4961.

SUN, L., RAN, R., WANG, G. & SHAO, Z. 2008. Fabrication and performance test of a catalyst-coated membrane from direct spray deposition. *Solid state ionics,* 179(21-26):960-965.

TANG, H., WANG, S., JIANG, S.P. & PAN, M. 2007. A comparative study of CCM and hot-pressed MEAs for PEM fuel cells. *Journal of power sources,* 170(1):140-144.

THANASILP, S. & HUNSOM, M. 2010. Effect of MEA fabrication techniques on the cell performance of Pt–Pd/C electrocatalyst for oxygen reduction in PEM fuel cell. *Fuel,* 89(12):3847-3852.

XING, D. & KERRES, J. 2006. Improved performance of sulfonated polyarylene ethers for proton exchange membrane fuel cells. *POLYMERS FOR ADVANCED TECHNOLOGIES,* 2011/05/17.

Experimental

Contents

3.1 Materials

3.1.1 PEM, MEA and GDE used

Two commercially available PEM were used in this study, namely Nafion® and PBI. Nafion® N 117 was purchased from Ion Power Inc. and PBI-sPSU was kindly supplied by Dr. Kerres, Stuttgart University. Summarised specification sheets of Nafion® N 117 and PBI-sPSU are given in Table 3-1 and Table 3-2.

Table 3-1 Nafion® N117 specification sheet (DuPont, 2009)

Membrane type	N 117
Typical thickness	183 μm
Basis weight	360 $g.m^{-2}$
Specific gravity	1.98
Conductivity (minimum)	0.10 $S.cm^{-1}$
Water content (25°C, 50% RH)	5% water
Water uptake (100°C)	38% water

Table 3-2 PBI-sPSU specification sheet

Membrane type	Low temperature sPSU-BP-50 + PBI-OO	
Typical thickness	34 μm	
Polymer ratio (sPSU:PBI)	3g sPSU	0.235g PBI-00
Equivalent weight (EW)	740$g.mol^{-1}$	
Conductivity	0.0338 $S.cm^{-1}$	

(Schoeman, 2011)

The MEA manufactured by Giner Electrochemical Systems have a 20-wt% of Nafion® 1100EW ionomer included in the catalyst layer and are summarised in Table 3-3..

Table 3-3 MEA specifications as by Giner Electrochemical Systems

	Anode	**Cathode**
Membrane type	Nafion® N117	Nafion® N117
Catalyst deposition	Painting	Painting
Catalyst type	PtIr	Pt
Catalyst loading	4 $mg.cm^{-2}$	4 $mg.cm^{-2}$
MEA heat-pressing	Yes	Yes

The GDE were purchased from Giner Electrochemical Systems, LLC together with flowfields and gaskets. These components were installed into the standard electrolyser. The basic specifications of the anode and cathode GDEs are given in Table 3-4.

Table 3-4 GDE specifications as by Giner Electrochemical Systems.

	Anode	Cathode
Current collector material	Porous titanium	Toray TGPH-090
Catalyst type	PtIr	Pt
Catalyst loading	4 $mg.cm^{-2}$	4 $mg.cm^{-2}$
Catalyst deposition	Painting	Painting
GDE heat-pressing	No	No

3.1.2 Catalyst used

Platinum black (Industrial Analytical (Pty) LTD.) was used for MEA fabrication and Table 3-5 gives the specifications as provided by Industrial Analytical (Pty) LTD.

Table 3-5 Catalyst specifications as by Alfa Aesar, A Johnson Matthey Company.

Product	Platinum Black – High Surface Area (HSA)
Batch Number	CS0323 conforms to product code specification: 183003
Nominal surface area	27.56 $m^2.g^{-1}$
Loss on drying	0.19%
Loss on reduction (mean)	2.60%
Chloride	0.05%

3.1.3 Chemicals used

The chemicals used for the synthesis of electrocatalyst ink are given in Table 3-6.

Table 3-6 Chemicals for electrocatalyst ink preparation

Chemical	Supplier	Grade
Deionised water	In-house	18 MΩ
Ethylene glycol	Merck (PTY) LTD	Reag. Ph Eur,Reag. USP
Isopropanol	Merck (PTY) LTD	ACS,ISO,Reag. Ph Eur
20 wt% Nafion® solution	Ion Power Inc	D2021 alcohol based
Iron(II) sulphate	LABCHEM	
Magnesium sulphate	Saarchem (Pty) Ltd.	

3.2 MEA synthesis

The in-house MEA synthesis procedure for both Nafion® and PBI PEM is basically a three step procedure. The first step is the preparation of the electrocatalyst ink. Secondly, the electrocatalyst ink is deposited onto the PEM by means of spray deposition and the final step entails heat pressing the PEM and electrocatalyst together to form the MEA.

3.2.1 Electrocatalyst ink preparation

Platinum black was selected as electrocatalyst of choice. Platinum black demonstrates satisfactory results for shorter periods of PEM water electrolyser performance evaluation (Bessarabov, 2011). The compounds required for electrocatalyst ink preparation are summarised in Table 3-7.

Table 3-7 Chemicals and reagents for electrocatalyst ink preparation

Chemical/Reagent	Amount
Platinum black	0.125 g
Deionised water	2 g
Ethylene glycol	4 g
Isopropanol	12 g
20 wt% Nafion® solution	2 ml

The first step in preparing the electrocatalyst ink was to weigh the required amount of electrocatalyst in a light weight plastic mould. Once the correct amount of electrocatalyst was weighed the contents were transferred into the mixing bottle.

A mixing pellet that came with the electromagnetic stirrer (BOECO) was added to the mixing bottle. Next, 2 grams of deionised water and 2 grams of Nafion® solution were added to the mixing bottle. The cap was tightened onto the mixing bottle, ensuring that the bottle was sealed properly. The mixing bottle was then placed on the electromagnetic stirrer. The stirring intensity was set to level 4 and the contents of the mixing bottle stirred for a period of 5 minutes.

Next, the mixing bottle was placed in the ultrasonic bath (Eumax, UD200SH-6L) and the bottle contents were sonicated for a period of 2 hours. After sonication the mixing bottle was removed and opened. Thereafter, 12 ml of isopropanol and 4 ml of ethylene glycol was added to the mixing bottle in that order. Lastly, the cap was tightened onto the mixing bottle, which was then placed onto the electromagnetic stirrer. The contents was stirred for 1 hour and the mixing bottle was removed from the electromagnetic stirrer and placed back into the ultrasonic bath for 2 hours. Once the sonication period was completed the mixing bottle was removed from the ultrasonic bath. The mixing bottle solution was then inspected to see whether the solution was

homogeneous. In the case where the mixing bottle solution was non-homogeneous, the last step of sonication was repeated until a homogeneous solution was formed.

The electrocatalyst ink was then ready and the mixing bottle was kept on the electromagnetic stirrer to ensure homogeneity of the electrocatalyst ink solution.

3.2.2 Electrocatalyst spray deposition

The coating of the PEM with electrocatalyst ink can be accomplished by CCS or CCM techniques (Millet *et al*., 2009:4974,Sun *et al*., 2008:960,Tang *et al*., 2007:140). CCM-DS was selected for the coating of both the Nafion® N117 and PBI-sPSU PEMs as this technique is widely used and delivers satisfactory MEA quality.

A PEM spray frame was designed and manufactured to keep the PEM stationary whilst spraying it with the electrocatalyst ink. The selected PEM was placed over the extruding stainless steel bits of the one Perspex sheet. The other perspex sheet was then placed on the PEM and tightened evenly with wingnuts and bolts. This ensured that the PEM was properly secured, as illustrated in Figure 3-1

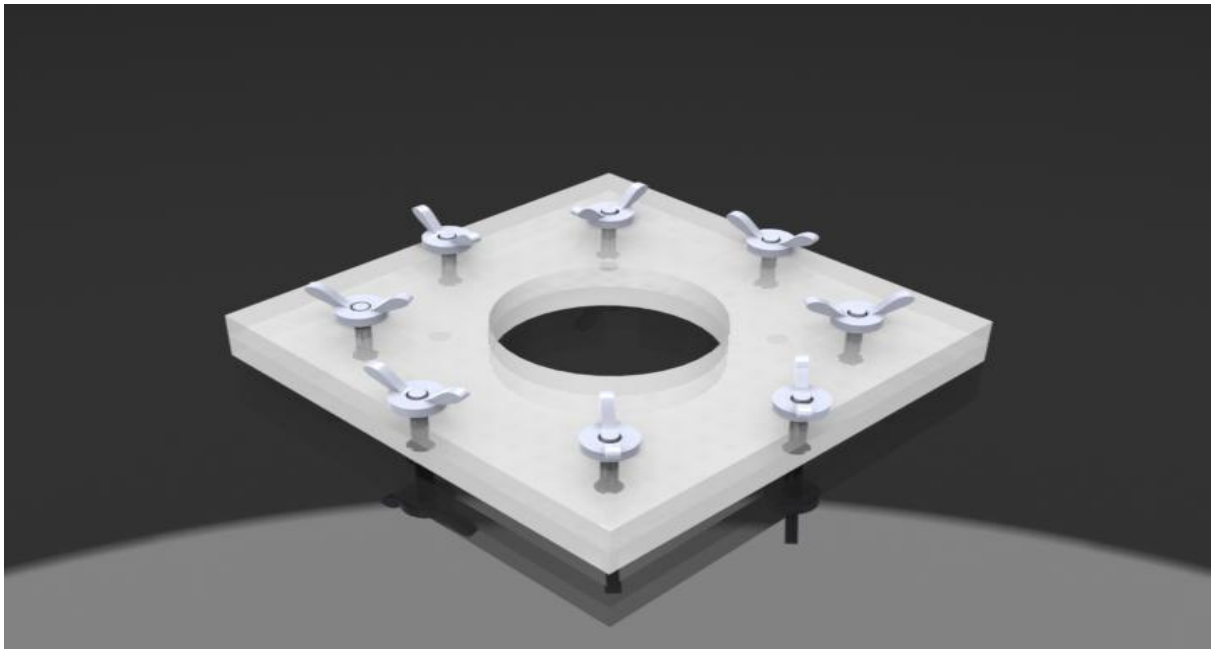

Figure 3-1 PEM spray frame

Different preparation methods for both PEM types were used before spraying commenced. Fully hydrated Nafion® PEM shrank once exposed to conditions of low humidity and heat. The shrunken Nafion® PEM expanded once exposed to water or humid conditions. Although the PBI also expanded once hydrated and shrank once exposed to heat and low humidity, the PBI PEM did not shrink to the extent Nafion® did.

The Nafion® PEM was fully hydrated by soaking it in deionised water and then tightened in the PEM spray frame. The PEM spray frame with the Nafion® N117 PEM was then placed in a convection oven (Labotec, ecotherm) at 40°C to dry the Nafion® PEM for 5 hours. As PBI is less prone to expand, the PEM was dried and cut into the correct MEA shape with a laser cutter. The PBI was then tightened in the PEM spray frame and was ready for spraying.

Once the PEM of choice was ready for spraying, the spraying equipment was set up. The spray gun (Iwata revolution) was coupled to the compressor (Puma) which was set to a pressure of 2 $bar_{(g)}$. The already prepared electrocatalyst ink was then poured into the reservoir of the spray gun. One layer of platinum black electrocatalyst was applied to one side of the membrane in circular motions of spraying. After an electrocatalyst layer was sprayed onto the PEM, a hairdryer was used to dry the catalyst layer and PEM. Layers of electrocatalyst were applied and weighed until the correct amount of electrocatalyst was present on the one PEM surface. The PEM spray frame with PEM was then placed in a convection oven for 5 hours at 40°C to ensure the removal of all the moisture in the PEM and catalyst layer. Once the MEA was dry, the precise electrocatalyst weight was measured to ensure that the PEM had the correct amount of platinum electrocatalyst. If the necessary amount of electrocatalyst was not attained, the spraying procedure of the PEM was repeated until the correct amount of platinum electrocatalyst (0.5 mg) was on the PEM. Once the required amount of electrocatalyst had been applied to the one side of the PEM, the exact same steps were followed to coat the other side of the PEM with the same amount of platinum electrocatalyst.

3.2.3 MEA heat pressing

Heat pressing is used to bond the electrocatalyst layer to the PEM to prevent the breaking off of the electrocatalyst layers once the MEA is rehydrated (Hoek, 2011). The coated PEM were removed from the PEM spray frame and placed between two Teflon platens, which were then placed on the heat press (CARVER, 12-12H). Heat pressing of the coated PEM took place at the Nafion® glass transition temperature of ±120°C for a period of 5 minutes at a pressure of $20kg.cm^{-2}$ of active area. The platens were placed in the centre of the heat press. Next the hydraulic lever of the heat press was pumped until the heat press pressure gauge showed a value of 1000kg. The heating elements of the heat press were then switched on and set to a temperature of 120°C. Heating of the Teflon platens to 120°C took approximately 25 minutes. The MEA was left in the heat press for a total time of 30 min where after the pressure of the heat press was relieved by turning the pressure relief valve in a counter-clockwise manner. The heating elements were switched off and the Teflon platens were removed from the heat press to cool down at 25°C. The MEA was then hydrated and stored in deionised water until the time that it was required.

3.3 MEA/GDE performance evaluation

The performance evaluation of a PEM water electrolyser with varying components requires a custom test bench, which ensures that the electrolyser operations are conducted at the desired operational conditions to produce accurate and repeatable results.

3.3.1 Experimental setup

The test bench used for PEM water electrolyser performance evaluation is illustrated in Figure 3-2. Key parameters measured by the test bench were cell voltage, hydrogen generation rate, cathode pressure and the anode outlet temperature. The potentiostat (1) (Bio-logic Science instruments) and computer supplied and monitored the necessary voltage and current to the PEM water electrolyser (3) (Giner Electrochemical Systems, LLC (GES)). The water reservoir (4) was a double walled cylinder. The feed water was kept in the inner cylinder of the water reservoir and was circulated through the PEM water electrolyser with a gear pump drive (2) (Cole-Parmer Instrument Company). The water bath (6) (Grant Instruments (Cambridge) Ltd) supplied heated water to the outer cylinder of the water reservoir which heats the feed water for the PEM water electrolyser. A thermometer was situated at the PEM water electrolyser outlet to ensure that the experiments were conducted at the desired temperature. The generated hydrogen gas exited the PEM water electrolyser where a back pressure regulator was used to ensure the desired cathode side backpressure. The hydrogen gas exited through a bubble flowmeter (7) where the rate and temperature of the generated hydrogen was obtained.

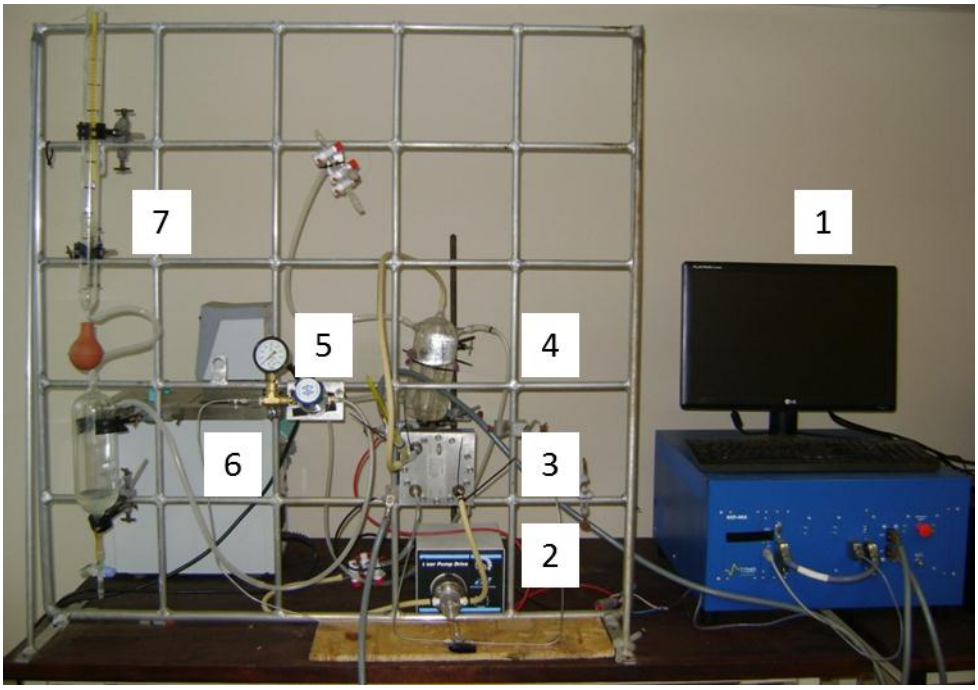

Figure 3-2 Electrolyser test bench

The PEM water electrolyser components of a laboratory scale electrolyser as supplied by Giner Electrochemical Systems, LLC (GES) are illustrated in Figure 3-3. The cathode side consists of the titanium collector plate (1), a black rubber seal (2) and on it an expanded titanium mesh (3), which acts as the flowfield. Next is the Ethylene-Propylene-Diene-Methylene (EPDM) gasket (4) which creates a space for the carbon cloth GDL (5). The MEA (6) then separates the cathode from the anode side. Next is the anode flowfield (7), which fits onto the black rubber seal (8). A titanium collector plate (9) is situated at the end of the anode side.

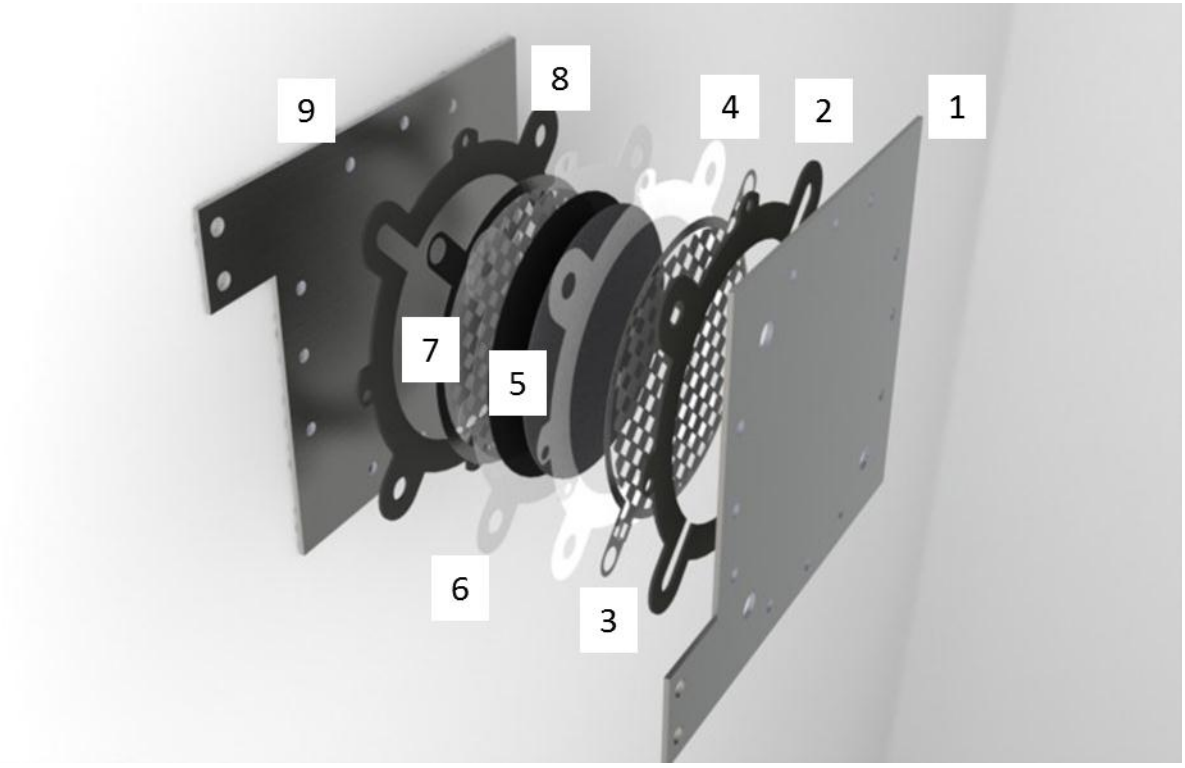

Figure 3-3 PEM water electrolyser components

3.3.2 Experimental design

The experimental design for all the experiments conducted, is illustrated in Figure 3-4. The experimental design is divided into four parts: Evaluation of MEA and GDE, evaluation of metal contaminant feed solutions, evaluation of aqueous methanol feed solutions and sulphuric acid regeneration. The MEA used, were termed according to the experiment type. N-MEA and N-GDE refer to experiments with Nafion® N117, where N-MEA is a commercial MEA and N-GDE implements commercial GDE. NS-MEA and PS-MEA are the synthesised MEA with Nafion® and PBI PEM. $FeSO_4$-MEA and $MgSO_4$-MEA are both commercial Nafion® MEA that were used for the Fe^{2+} and Mg^{2+} experiments. 1MeOH-MEA and 4MeOH-MEA are both commercial Nafion® MEA that were used for the 1M and 4M aqueous methanol experiments.

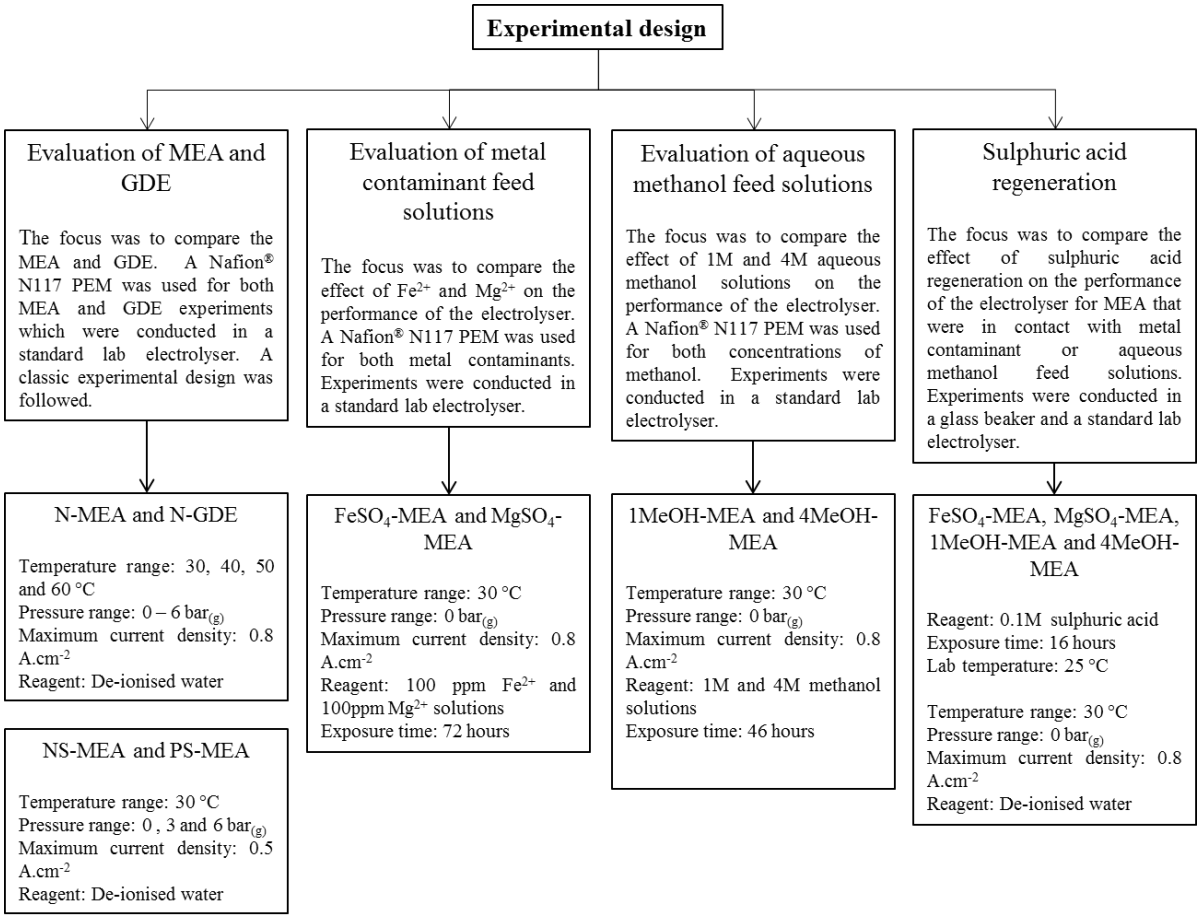

Figure 3-4 Experimental design

3.3.3 Experimental procedure: MEA/GDE performance evaluation

The experimental procedure for PEM devices is important as conditions and techniques applied in all the experiments should be reliable to ensure accurate results and discussion thereof. The testing of a MEA or GDE is basically a three step procedure. The first step was to inspect the experimental equipment to ensure that the experiments were conducted properly. Secondly, the experiment was carried out and lastly a post experimental procedure was performed. The experiments were conducted with the electrolyser test bench and PEM water electrolyser as illustrated in Figures 3-2 and 3-3.

3.3.3.1 Equipment inspection

Before experimentation on any PEM water electrolyser was started, the following checks were completed on the electrolyser test bench. Firstly, the water circulation systems were checked to ensure that the flow rate of water through the PEM water electrolyser was correct. The valve to the gear pump drive (Cole-Parmer Instrument Company) was opened to provide the gear pump with a consistent flow of deionised water. Next, the T-piece pressure selector (Swagelok) was set to the PEM water electrolyser that was to be used. The power and monitoring cables were connected to the PEM water electrolyser. Power cables of CA+ and GND were connected to the

positive (cathode) and negative (anode) terminals of the PEM water electrolyser with nuts and bolts. The computer and potentiostat were connected and the link between the two devices was established. Next the back pressure regulator (BPR) was set to 0 $bar_{(g)}$ by turning the valve in a counter-clockwise direction until turning by hand became impossible. The bubble flowmeter was cleaned and its soap reservoir was filled with liquid soap by removing the squeeze from the flowmeter and filling it to approximately 80% and then sliding the squeeze back onto the flowmeter.

3.3.3.2 Experimental protocol

The experiments were started by firstly switching on the water bath and selecting the required water temperature. The water was then circulated to heat the feed water to the desired feed water temperature for a period of 15 minutes. Next, the heated process water was circulated through the electrolyser for a period of 10 minutes to ensure that the desired temperature of the electrolyser was reached before the experiment was started. The EC-lab software was initialised on the computer and the Staircase Galvano Electrochemical Impedance Spectroscopy (SGEIS) experiment was selected. The EC-lab experiment specifications for purchased MEA/GDE and manufactured MEA are found in Tables 3-8 and 3-9.

Table 3-8 EC-lab experiment specifications: Purchased MEA/GDE

Variable	Value
Initial current value I_i	0 A
Final current value I_f	40 A
Current steps N	16
Period per step t_s	4 min
Recording interval dt	1 s
Amplitude I_a	10 mA
I Range	80 A

Table 3-9 EC-lab experiment specifications: Manufactured MEA

Variable	Value
Initial current value I_i	0 A
Final current value I_f	20 A
Current steps N	8
Period per step t_s	4 min
Recording interval dt	1 s
Amplitude I_a	10 mA
I Range	80 A

The fume hood was switched on before experimentation to remove all the generated hydrogen and oxygen. The experiment was carried out by clicking the "go" button on the EC-lab software. The graphs of voltage vs. current and time elapsed were monitored to ensure results with low noise and accurate results. As the current increased automatically, the hydrogen production rate was measured 1 minute after every step of current change. The rubber bulb of the bubble flowmeter was squeezed gently until a soap bubble was formed in the bubble flowmeter. The time for the bubble to travel 25 mL was then measured and recorded on the data sheet. Once the SGEIS experiment for the specific temperature and pressure was completed the generation of hydrogen ceased and the EC-lab software indicated that the experiment was completed.

On the completion of the MEA and GDE experiments, the data was processed with Excel and the required outputs of polarisation curves, hydrogen production rate and efficiencies were calculated.

3.3.3.3 Post-experimental protocol

After experimentation, the Open Circuit Voltage experiment was selected on the EC-lab software and operated for 2 minutes. The feed water temperature was changed to the desired value by adjusting the temperature on the water bath. When the desired feed water temperature had been reached, the water was circulated through the electrolysis cell for at least 10 minutes before a new experiment was started. The system back pressure was changed by turning the BPR in a clockwise direction to the desired pressure of the new experiment by switching the EC-lab software into manual mode. The current was increased to a value of 10A over a period of 30 seconds. When the current value was reached the backpressure regulator was turned in a clockwise manner until the desired pressure was reached. The manual experiment was stopped once the desired backpressure was reached and another Open Circuit Voltage experiment was executed for a period of 2 minutes.

3.3.4 Experimental procedure: $FeSO_4$ and $MgSO_4$ performance evaluation

The performance evaluation for both $FeSO_4$-MEA and $MgSO_4$-MEA were executed in a way very similar to that of Section 3.3.2. Key differences were that of the feed solution to the PEM water electrolyser and the exposure time of the MEA to the water solution.

The metal contaminants selected for performance evaluation were Fe^{2+} and Mg^{2+}. The first step in preparing the solutions was to weigh the required amounts of metal salts. Two volumetric flasks were then cleaned and the salts of iron (II) sulphate and magnesium sulphate were added, each metal salt in its separate volumetric flask. The next step was to add deionised water to each flask until the solution meniscus was parallel to the 1000 mL mark on the volumetric flask. The plugs were then placed on the volumetric flasks to prevent contamination of the 100ppm solutions. The volumetric flasks were then shaken for approximately one minute to ensure that all the metal salt had dissolved. Subsequently the water supply reservoir of the electrolyser was cleaned and dried, and the required metal ion solution was introduced into the water supply.

The experimental protocol differed slightly from the protocol in Section 3.3.3.2. The PEM water electrolyser was first operated with only deionised water according to the protocol of Section 3.3.3.2. Thereafter, the water supply reservoir was drained and cleaned and left to dry. Once dry, the water supply reservoir was filled with the metal solution of either Fe^{2+} or Mg^{2+}. The aqueous metal solution was circulated for one hour, followed by one hour of electrolyser operation, as described in Section 3.3.3.2. Once the electrolyser operation had been completed, the circulation of aqueous metal solution and electrolyser operation was repeated. As soon as the repetition had been completed, the circulation step was increased to 3 hours followed by 1 hour of electrolyser operation. The 3 hour circulation step was then repeated and followed by 1 hour of operation. The circulating period was ultimately increased in intervals of 1, 3, 6, 9 and 12 hours, and after every circulation period the electrolyser was operated for one hour. All the circulation periods and electrolyser operations were, therefore, repeated once. The total contact time of the MEA with the aqueous metal solution was a period of 72 hours.

On the completion of the metal ion solution experiments, the data was processed with Excel and the required outputs of polarisation curves, hydrogen production rates and efficiencies were calculated.

3.3.5 Experimental procedure: 1MeOH- and 4MeOH-MEA performance evaluation

The performance evaluation for both 1MeOH-MEA and 4MeOH-MEA were executed in a way very similar to that of Section 3.3.2. Key differences were that of the feed solution to the PEM water electrolyser and the exposure time of the MEA to the methanol solution.

The concentration of methanol selected, based on the work of Take *et al*. (2007), was 1M and 4M methanol concentrations. Firstly, the required volumes of methanol to prepare the solutions were calculated and measured using a burette. Two volumetric flasks were thoroughly cleaned and left to dry. Thereafter, the methanol for both 1M and 4M solutions was added to the separate volumetric flasks. The volumetric flasks were filled with deionised water and shaken for approximately one minute. Subsequently, the water supply reservoir was cleaned and dried, and the specific solution of either 1M or 4M methanol was introduced into the water supply reservoir.

The experimental protocol differed slightly from the previous protocol in Section 3.3.4. The PEM water electrolyser was firstly operated with only deionised water according to the protocol of Section 3.3.4. Thereafter, the water supply reservoir was drained and cleaned and left to dry. Once dry, the water supply reservoir was filled with methanol solutions of either 1M or 4M. The methanol solution was circulated for one hour followed by one hour of electrolyser operation, as described in Section 3.3.4. Once the electrolyser operation had been completed the circulation of aqueous methanol solution and electrolyser operation were repeated. As soon as the repetition had been completed, the circulation step was increased to 3 hours followed by 1 hour of electrolyser operation. The 3 hour circulation step was then repeated and followed by 1 hour of operation. The circulating period was ultimately increased in intervals of 1, 3, 6 and 9 hours, and after every circulation period the electrolyser was operated for one hour. All the circulation periods and electrolyser operations were therefore repeated once. The total contact time of the MEA with the aqueous methanol solution was a period of 46 hours.

On the completion of the aqueous methanol experiments, the data was processed with Excel and the required outputs of polarisation curves, hydrogen production rate and efficiencies were calculated.

3.3.6 Experimental procedure: Sulphuric acid regeneration

The regeneration of $FeSO_4$-MEA, $MgSO_4$-MEA, 1MeOH-MEA and 4MeOH-MEA were excecuted on the evidence of Collier *et al.* (2006), that pure sulphuric acid may reverse the degradation of a PEM.

After the MEA of $FeSO_4$-MEA, $MgSO_4$-MEA, 1MeOH-MEA and 4MeOH-MEA had been exposed to either metal contaminant or methanol aqueous solutions, the MEA was cautiously removed from the PEM water electrolyser unit and placed in a 2000 mL glass beaker. The beaker was filled with 250 mL of 0.1M sulphuric acid beforehand, and the magnetic pellet was placed in the beaker. The beaker with sulphuric acid and the MEA was then placed on the magnetic stirrer, which was then set to a stirring level of 3 for a total time of 16 hours. After the 16 hour duration, the MEA was removed from the beaker and rinsed three times with deionised water in a clean beaker (Bessarabov, 2011).

The effectiveness of MEA regeneration was lastly tested by inserting the regenerated MEA at hand into the PEM water electrolyser unit, and operating the electrolyser at 30°C at a pressure of 0 $bar_{(g)}$. This step was repeated twice.

On the completion of the sulphuric acid regeneration experiments, the data was processed with Excel and the required outputs of polarisation curves, hydrogen production rate and efficiencies were calculated.

3.4 References

BESSARABOV, D. 2011. Verbal communication with author. North-West University Potchefstroom.

COLLIER, A., WANG, H., ZI YUAN, X., ZHANG, J. & WILKINSON, D.P. 2006. Degradation of polymer electrolyte membranes. *International journal of hydrogen energy,* 31(13):1838-1854.

DUPONT. 2009. N 115, N117, N1110. http://www.ion-power.com/res/Nafion%20&%20XL%20MEA/NAFION_N115_N117_N1110.pdf.

HOEK, H. 2011. Verbal communication with author. North-West University Potchefstroom.

MILLET, P., DRAGOE, D., GRIGORIEV, S., FATEEV, V. & ETIEVANT, C. 2009. GenHyPEM: A research program on PEM water electrolysis supported by the european commission. *International journal of hydrogen energy,* 34(11):4974-4982.

SCHOEMAN, H. 2011. Verbal communication with author. North-West University Potchefstroom.

SUN, L., RAN, R., WANG, G. & SHAO, Z. 2008. Fabrication and performance test of a catalyst-coated membrane from direct spray deposition. *Solid state ionics,* 179(21-26):960-965.

TAKE, T., TSURUTANI, K., UMEDA, M. 2006. Hydrogen production by methanol-water solution electrolysis. *Journal of power sources,* 164(1):9-16.

TANG, H., WANG, S., JIANG, S.P. & PAN, M. 2007. A comparative study of CCM and hot-pressed MEAs for PEM fuel cells. *Journal of power sources,* 170(1):140-144.

Results and Discussion

Contents

4.1 General considerations

4.1.1 Basic PEM water electrolysis operation

The electrochemical reaction of PEM water electrolysis produces hydrogen and oxygen gas, which is illustrated in Equations 2-1 to 2-3 (Millet *et al*., 2009:4975) of Section 2.3 and forms the basis of the experiments conducted. A Standard cell voltage of 1.229V is required for the overall reaction to commence. An increase of current to the PEM water electrolyser has a direct influence on the cell voltage and hydrogen production rate. Cell voltage, current density and hydrogen production rate were therefore selected as primary process parameters to characterise the performance of the different MEA and GDE in PEM water electrolysis, based on studies of Millet *et al.* (2009).

4.1.2 Working definitions

The methods of Millet *et al*. (2010) were used to compare and evaluate the efficiency of the selected PEM water electrolyser components. For this study electrolyser performance is expressed in terms of cell voltage, energy efficiency ($\varepsilon_{\Delta G}$) and specific energy consumption (E_S).

Energy efficiency is defined as a comparison of the standard cell potential and the measured cell voltage of the PEM water electrolyser (Millet *et al.*, 2010:5043) as given in Equation 4-1.

$$\varepsilon_{\Delta G}(T,P,i) = \frac{V°(T,P)}{U^{cell}(T,P,i)} \qquad (4\text{-}1)$$

Standard cell potentials are calculated for the selected process temperatures and pressures thus ensuring the accuracy of the calculated energy efficiencies. Detail calculations of standard cell potentials are given in Appendix D.

Specific energy consumption is defined as the power required to produce a particular quantity of hydrogen as given in Equation 4-2. Specific energy consumption is a function of current density and is expressed in units of kWh.Nm^{-3} for the purpose of this study (Millet *et al.*, 2010:5043).

$$E_S(T,P,i) = \frac{U_{cell}(T,P,i)\times I}{\dot{m}_{H_2}} \qquad (4\text{-}2)$$

Specific energy consumption makes it possible to compare the different process conditions with a single variable and may be used for implementation purposes in future studies.

4.2 Synthesis of NS-MEA and PS-MEA

4.2.1 Introduction

The results of the in-house synthesised MEA for both Nafion® N117 (NS-MEA) and PBI-sPSU (PS-MEA) are discussed in this section. The MEA synthesis procedure of Section 3.2 was used in synthesising the selected MEA, after which they were evaluated in the PEM water electrolyser. The reproducibility of MEA performance was tested with the electrolyser test bench and SEM analysis was completed to show how the electrocatalyst layers were deposited onto the PEM surface. Detailed performance figures of the synthesised MEAs are discussed in Section 4.4.

4.2.2 Synthesis results and discussion

MEA synthesis with Nafion® N117 and PBI-sPSU membranes took place according to the procedure as described in Section 3.2. A typical MEA synthesis with CCM-DS is illustrated in Figure 4-1.

(a) (b)

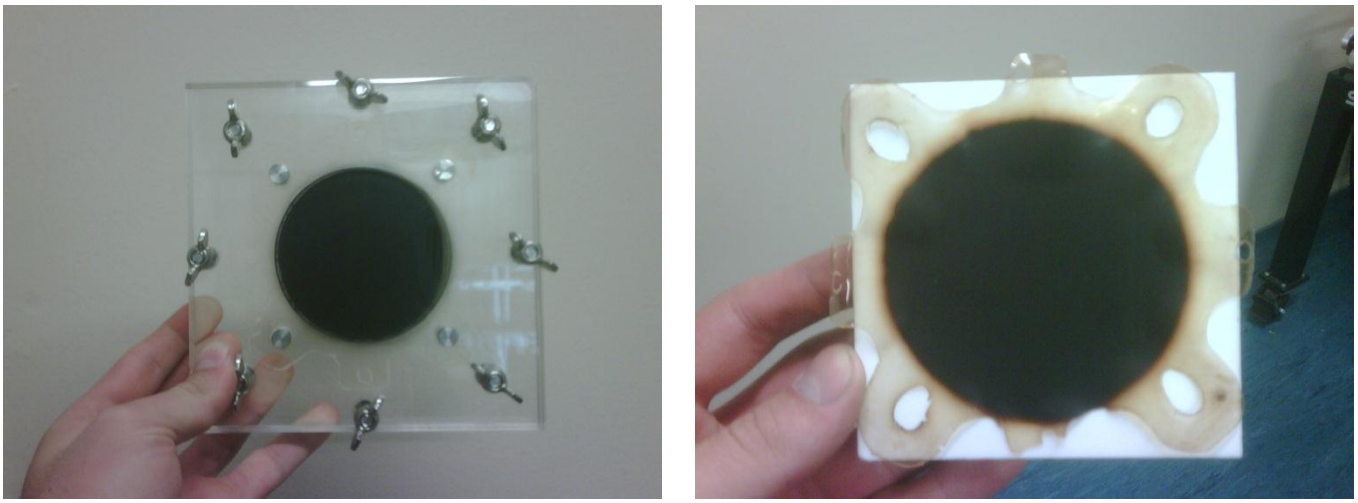

Figure 4-1 NS-MEA synthesis, a) NS-MEA after spray coating, b) NS-MEA after heat pressing.

Figure 4-1 illustrates the synthesis of NS-MEA, where (a) shows the MEA as it was spray coated and (b) the heat pressed MEA. From Figure 4-1 (b) it is evident that heat pressing bonded the electrocatalyst to the PEM as the electrocatalyst layer is not distinguishable from the PEM.

The evaluation of the synthesised MEA was performed by inserting the MEA in the standard laboratory electrolyser and completing four experiments at each selected pressure at a temperature of 30°C. The polarisation curves of the selected pressures are illustrated in Figure 4-2.

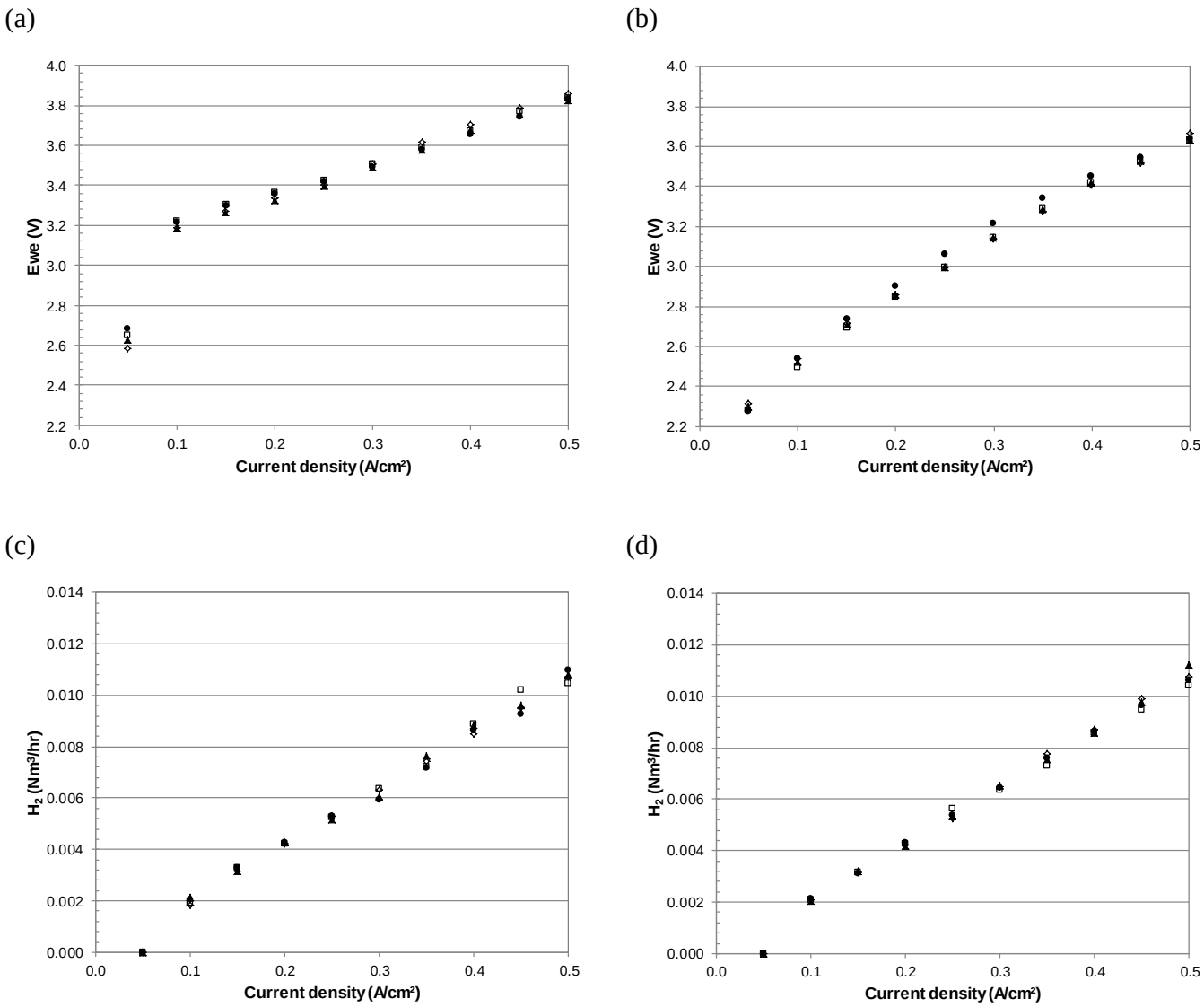

Figure 4-2 PEM water electrolysis with synthesized MEA and deionised water at a temperature of 30 °C, a) Polarisation curve: NS-MEA [6 $bar_{(g)}$], b) Polarisation curve: PS-MEA [0 $bar_{(g)}$], c) Hydrogen production rate: NS-MEA [6 $bar_{(g)}$] and d) Hydrogen production rate: PS-MEA [0 $bar_{(g)}$].
[● Run 1; □ Run 2; ▲ Run 3; ◊ Run 4]

The polarisation curves of NS-MEA and PS-MEA are depicted in Figures 4-2 (a) and (b), and graphically illustrate the repeatability of the synthesised MEA. Figure 4-2 (a) shows a sudden increase of cell voltage with increasing current density which increased linearly thereafter. The cell voltage of Figure 4-2 (b) increased at a declining rate as the current density increased. The hydrogen production curves of Figures 4-2 (c) and (d) illustrate the repeatability of hydrogen production with increasing current density for the synthesised MEA. A detailed description of the synthesised MEA performance figures is provided in Section 4.4.

The reproducibility data of the synthesised MEA is given in Table 4-1, where the standard deviation, mean values of cell voltage and hydrogen production rate at a current density of 0.5A.cm^{-2} are given.

Table 4-1 Experimental errors of NS-MEA and PS-MEA experiments

Reproducible experiment	**Ewe (V)**	**$\dot{H}_2$ (Nm^3/hr)**	**Ewe (V)**	**$\dot{H}_2$ (Nm^3/hr)**	**Ewe (V)**	**$\dot{H}_2$ (Nm^3/hr)**
NS-MEA	30°C, 0 bar$_{(g)}$		30°C, 3 bar$_{(g)}$		30°C, 6 bar$_{(g)}$	
Mean value (0.5A.cm^{-2})	3.806	0.01095	3.820	0.01084	3.838	0.01074
Standard deviation (σ)	0.0811	0.00029	0.0355	0.00040	0.0151	0.00021
PS-MEA	30°C, 0 bar$_{(g)}$		30°C, 3 bar$_{(g)}$		30°C, 6 bar$_{(g)}$	
Mean value (0.5A.cm^{-2})	3.642	0.0108	3.656	0.0113	3.647	0.0110
Standard deviation (σ)	0.0174	0.00032	0.0115	0.00034	0.0199	0.00009

The average standard deviation of the polarisation curves for the synthesised MEA of NS-MEA and PS-MEA were 0.0439 and 0.01627 respectively. The hydrogen production data of NS-MEA and PS-MEA showed a standard deviation of 0.0003 and 0.00026 respectively. Ito *et al.* (2012) found a reproducibility of ±3mV at temperatures of 70 and 80°C and a current density at 1A.cm^{-2}. The standard deviation of NS-MEA (±44mV) and PS-MEA (±16mV) is much higher than that of Ito *et al.* (2012). The difference in standard deviation is most likely due to the difference in experimental equipment and PEM water electrolyser internals. The experimental results of NS-MEA and PS-MEA were thus found to be constant and repeatable for PEM water electrolysis.

On opening the electrolyser after the evaluation of PS-MEA it was found that the anode electrocatalyst layer of PS-MEA was situated on the anode GDL of the electrolyser, as illustrated in Figure 4-3 (a). The cathode electrocatalyst layer was still situated on the PEM. From Figure 4-3 (b) it is evident that heat pressing of PS-MEA joined both the anode and cathode electrocatalyst layers on the surface of the PEM, but the electrocatalyst layers were distinguishable from the PEM.

(a) (b)

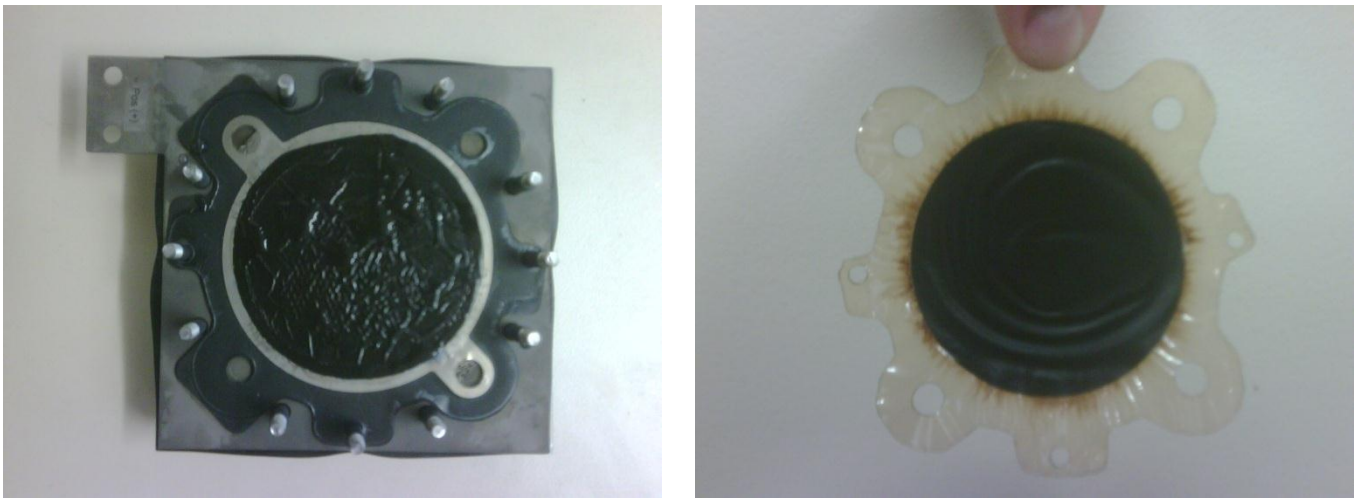

Figure 4-3 PS-MEA experiments, a) PS-MEA Cathode electrocatalyst layer on GDL and b) PS-MEA after heat pressing.

It is clear from Figure 4-3, that the electrocatalyst layer did not bind with the PEM. The poor bonding of the electrocatalyst layers may be due to the difference in glass transition temperatures of Nafion® and PBI-sPSU. The PBI-sPSU blend has a glass transition temperature higher than that of Nafion®. The heat pressing of the PS-MEA allowed the electrocatalyst layer to melt and bond the Nafion® solution and platinum catalyst together, but supposedly not to the PBI-sPSU PEM. The improper bonding may have also caused an additional ohmic overpotential due to poor contact of electrocatalyst with the PEM.

The structure of the MEA and how the electrocatalyst layers had bonded to the PEM were examined with a Scanning Electron Microscope (SEM). Figure 4-4 illustrates cross sectional views and cathode surfaces for NS-MEA and PS-MEA.

(a) (b)

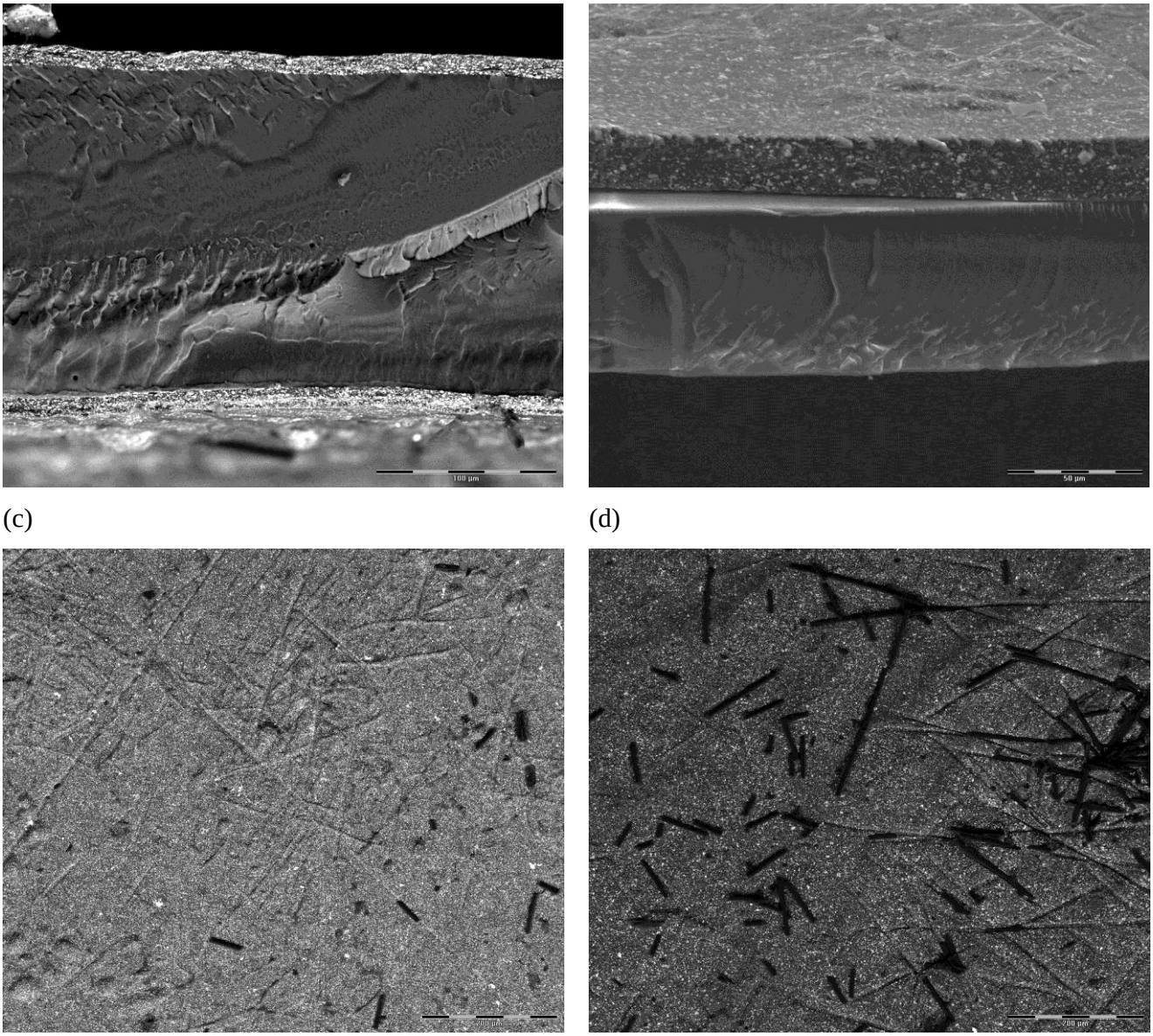

(c) (d)

Figure 4-4 SEM results, a) NS-MEA cross sectional view, b) PS-MEA cross sectional view, c) NS-MEA cathode surface, d) PS-MEA cathode surface.

The cross sectional view of Figure 4-4 (a) shows the anode as the top layer, the PEM as middle layer and cathode as bottom layer for NS-MEA. The cross sectional view of Figure 4-4 (b) clearly shows that no anode electrocatalyst layer was present for PS-MEA. This was due to the poor bonding of the electrocatalyst layer to the PBI PEM. The cross sectional and cathode surface images of Figure 4-4 exemplify the uniform distribution of electrocatalyst on the PEM , which also had small amounts of GDL residue on the cathode electrocatalyst layer.

The SEM also produced thicknesses and elemental analysis for both MEA and is given in Table 4-2.

Table 4-2 SEM elemental analysis results for NS-MEA and PS-MEA

Elemental analysis	NS-MEA		PS-MEA	
	Anode	Cathode	Anode	Cathode
C	15.9	16.87	84.86	15.5
O	4.91	4.96	5.44	5.29
F	63.04	62.17	6.53	60.06
S	1.86	1.77	-	1.78
Pt	14.3	14.24	3.17	17.37
Total	100	100	100	100

Table 4-3 SEM measurements of synthesised MEA

MEA SEM results	Anode	Cathode	PEM
NS-MEA			
Average thickness (μm)	10.47	11.04	178.99
Minimum thickness (μm)	9.93	10.11	177.86
Maximum thickness (μm)	10.82	11.89	179.70
Standard deviation	0.35	0.65	0.68
PS-MEA			
Average thickness (μm)	-	22.35	61.19
Minimum thickness (μm)	-	19.95	61.22
Maximum thickness (μm)	-	24.01	61.86
Standard deviation	-	1.14	0.8

Tables 4-2 and 4-3 portray the SEM elemental analysis results and measurements for the synthesised MEAs of NS-MEA and PS-MEA. The SEM elemental analysis results of Table 4-2 indicate that the electrocatalyst distribution on each side of the PEM was approximately the same for NS-MEA. The elemental analysis of PS-MEA showed low values of platinum for the anode due to the anode electrocatalyst layer coming off. Anode and cathode thickness values of Table 4-3 show that electrocatalyst layers of NS-MEA had very similar thicknesses. It is clear that the electrocatalyst had bonded properly to the Nafion® PEM when comparing the results to that of Thanasilp *et al.* (2010) in Figure 2-5.

The SEM elemental results of Table 4-2 indicate that the electrocatalyst distribution on each side of the PEM are approximately the same for NS-MEA, demonstrating that the experimental technique used, is adequate for creating Nafion® MEA. The elemental analysis of PS-MEA

shows low values of platinum for the anode due to the anode electrocatalyst layer coming off as a result of poor bonding of the electrocatalyst to the PEM. The polarisation curves of PS-MEA are most likely from the torque that was applied across the electrolyser, wedging the electrolcatalyst layer between the anode GDL and the MEA and keeping the electrocatalyst layer pressed to the PEM.

4.2.3 Concluding remarks

The results of synthesised MEA, NS-MEA and PS-MEA were presented in this section. Findings from polarisation curves and SEM analysis for NS-MEA showed that the electrocatalyst had bonded to the PEM and produced consistent performance results. PS-MEA, on the other hand, did not show adequate bonding of the electrocatalyst layer to the PEM, but did produce consistent performance results. The performance results of PS-MEA were most likely due to the torque applied over the electrolyser, which kept the anode electrocatalyst layer pressed firmly to the PEM. Further development of MEA with a PBI PEM is suggested, where a PBI based solution might be used for electrocatalyst ink preparation. The glass transition temperature of the selected PBI, should also be determined to establish the best temperature at which the PBI MEA should be heat pressed.

4.3 PEM water electrolysis with N-MEA and N-GDE

4.3.1 Introduction

In this section the performance of commercial N-MEA and N-GDE in a PEM water electrolyser were evaluated. The main difference between the components evaluated is the location of the electrocatalyst, as described in Section 2.2. The effects of temperature and cathode pressure range in the PEM water electrolyser were evaluated with respect to hydrogen production rates, energy efficiency and specific energy consumption. Experimental error calculations were done and the results of N-MEA and N-GDE were compared to ensure that the best technology was selected for future implementation.

4.3.2 Experimental error

The influence of water temperature and cathode pressure on the performance of the PEM water electrolyser were evaluated between 30°C and 60°C, and 0 $bar_{(g)}$ and 6 $bar_{(g)}$. The experimental error is an important factor for the evaluation of results at different temperatures and pressures, as the experimental results lie in a small range. The experimental error of cell voltage and hydrogen production rate for N-MEA and N-GDE are given in Table 4-4.

Table 4-4 Experimental errors of N-MEA and N-GDE experiments

Reproducible experiment	**Ewe (V)**	**$\dot{H}_2$ (Nm^3/hr)**	**Ewe (V)**	**$\dot{H}_2$ (Nm^3/hr)**	**Ewe (V)**	**$\dot{H}_2$ (Nm^3/hr)**
N-MEA	30°C, 0 $bar_{(g)}$		40°C, 3 $bar_{(g)}$		60°C, 6 $bar_{(g)}$	
Mean value (0.5A.cm^{-2})	1.908	0.0104	1.865	0.0108	1.801	0.0105
Standard deviation (σ)	3.6×10^{-2}	2×10^{-4}	7.7×10^{-2}	4×10^{-4}	0.8×10^{-2}	4×10^{-4}
N-GDE	30°C, 0 $bar_{(g)}$		40°C, 3 $bar_{(g)}$		60°C, 6 $bar_{(g)}$	
Mean value (0.5A.cm^{-2})	2.374	0.0101	2.408	0.0102	2.236	0.0100
Standard deviation (σ)	1.4×10^{-2}	1×10^{-4}	0.117	3×10^{-4}	2.8×10^{-2}	1×10^{-4}

The average standard deviation for the polarisation curves of N-MEA and N-GDE were calculated as 4×10^{-2} and 5.3×10^{-2} at 0.5 A.cm^{-2} respectively. Hydrogen production data for N-MEA and N-GDE showed an average standard deviation of 3×10^{-4} and 2×10^{-4} at 0.5 A.cm^{-2} respectively.

4.3.3 Influence of reaction temperature

The influence of water temperature on PEM water electrolyser performance for N-MEA and N-GDE was studied by operating at varying temperatures between 30°C and 60°C. The results obtained for N-MEA at 0bar$_{(g)}$ cathode pressure and 0.5A.cm^{-2} are summarised in Table 4-5 and Figure 4-5. The results obtained for N-GDE at 0bar$_{(g)}$ cathode pressure and 0.5A.cm^{-2} are summarised in Table 4-6 and Figure 4-6.

Table 4-5 Temperature influence on N-MEA performance [0.5 A.cm^{-2}, 0 bar$_{(g)}$]

Temperature (°C)	**Potential** (V)	**Hydrogen production** (Nm^3.hr^{-1})	**$\varepsilon_{\Delta G}$** (%)	**E_S** (kWh.Nm^{-3})
30	1.908±3.6×10^{-2}	0.0104±2×10^{-4}	65.48±1.24	4.61±0.02
40	1.865±7.7×10^{-2}	0.0108±7×10^{-4}	65.28±2.60	4.39±0.03
50	1.780	0.0107	67.91	4.14
60	1.801±8.4×10^{-3}	0.0105±4×10^{-4}	64.31±0.29	4.44±0.12

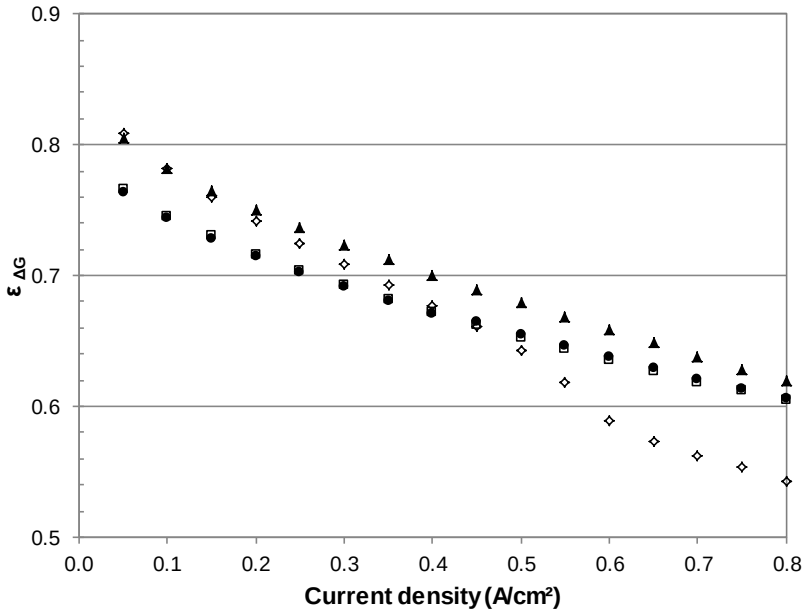

Figure 4-5 Energy efficiency of N-MEA at varying temperatures with a cathode pressure of 0 bar$_{(g)}$.
[● 30°C;□ 40°C;▲ 50°C;◊ 60°C]

The polarisation curves and cell potential values indicate that the reaction temperature had an influence on the performance of both N-MEA and N-GDE. The comparison of energy efficiencies and cell voltages for N-MEA at temperatures of 30, 40 and 50°C in Figure 4-5 and Table 4-5 clearly demonstrate the effect of increasing temperature. As the reaction temperature

increased from 30 to 50°C, the energy efficiency increased from 65.48 to 67.91% and cell voltage decreased from 1.908 to 1.780V. A similar trend was visible when comparing the specific energy consumption of N-MEA at 30, 40 and 50°C (Table 4-5). As the reaction temperature increased from 30 to 40°C, the specific energy consumption decreased by ~0.2kWh.Nm^{-3}. When the temperature was increased to 50°C the specific energy consumption was ~0.3kWh.Nm^{-3} lower than that at 40°C. The trends of energy efficiency and specific energy consumption that were observed for N-MEA was due to the effect that temperature had on the components of the PEM water electrolyser.

The results of N-MEA indicate that activation overpotential was present as the initial measured cell voltage exceeded the required cell voltage at which water electrolysis takes place (Nieminen *et al.*, 2010). The increasing reaction temperature demonstrates a reduction of cell voltage and thus also activation overpotential, in effect improving the energy efficiency and reducing specific energy consumption. According to Ni *et al.* (2008), the conductivity of the PEM and reaction kinetics of the electrocatalyst increases with temperature. The increase of electrocatalyst kinetics with temperature is visible in Figure 4-5 as the cell potential required decreased with temperature.

When the profiles of polarisation curves of N-MEA are evaluated (Figure 4-5), the curve of 60°C (◊) deviated from the curves for other temperatures. The initial current densities of the polarisation curve for N-MEA (Figure 4-5) show that a temperature of 60 °C produced a higher initial efficiency than 30 °C, but as the current density increased the efficiency of the 60 °C temperature decreased at a higher rate than the efficiencies at other temperatures. Polarisation curves of previous experiments conducted with N-MEA at temperatures lower than 60°C were viewed and it was found that this phenomenon started occurring from 50 °C and 3 $bar_{(g)}$. The decrease in energy efficiency is attributed to an increase in resistance across the electrolyser. Energy efficiency is a function of cell voltage, which is a function of cell resistance and current density based on the principles of Ohm's law. The experimental repetition of the N-MEA 60 °C, 6 $bar_{(g)}$, at a later stage, had a lower cell voltage thus indicating that the increased resistance across the electrolyser was no longer present.

The cause of the increased cell resistance may be as a result of poor contact between the internal components of the PEM water electrolyser. The poor contact of the N-MEA cathode and GDL was thought to be the main cause of the increased cell resistance. According to Barbir (2005), the overall ohmic overpotential depends on the PEM type, electrode and the contact between the PEM and electrode. GDL degradation, where changes in GDL structure and wetting behaviour have an impact on heat and electrical conductivity (Seidenberg *et al*., 2011) were considered, but

seeing that the increased resistance had declined at a later stage it ruled out the possibility of GDL degradation. GDL degradation impacts the GDL structure and wetting behaviour permanently. On closer examination the disappearance of the overpotential may have something to do with the period of time between experiments and experimental repetitions.

The influence of reaction temperature was also investigated for N-GDE and is given in Table 4-6 and Figure 4-6.

Table 4-6 Temperature influence on N-GDE performance [0.5 A.cm^{-2}, 0 bar$_{(g)}$]

Temperature (°C)	**Potential** (V)	**Hydrogen production** (Nm^3.hr^{-1})	$\varepsilon_{\Delta G}$ (%)	E_S (kWh.Nm^{-3})
30	2.374±1.4×10^{-2}	0.0101±1×10^{-4}	51.18±0.30	5.88±0.03
40	2.408±0.116	0.0104±3×10^{-4}	54.51±2.69	5.35±0.13
50	2.209	0.0104	54.68	5.32
60	2.236±2.8×10^{-2}	0.0099±1×10^{-4}	56.96±0.75	5.30±0.01

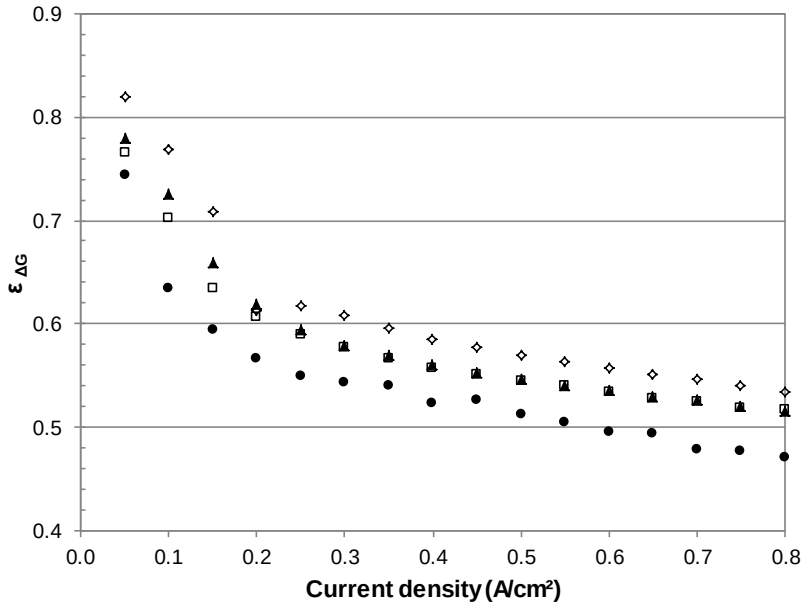

Figure 4-6 Energy efficiency of N-GDE at varying temperatures with a cathode pressure of 0 bar$_{(g)}$.
[● 30°C;□ 40°C;▲ 50°C;◊ 60°C]

The comparison of energy efficiencies for N-GDE at temperatures of 30 to 60°C in Figure 4-6 also demonstrated the effect of increasing temperature on the PEM water electrolyser. As the reaction temperature increased from 30 to 40°C, the energy efficiency increased from 51.18% to

54.51%. The comparison of energy efficiencies for 50 and 60°C showed a 2.28% increase in energy efficiency. When evaluating N-GDE performance in terms of specific energy consumption (Table 4-6), a declining trend is observed. A temperature increase from 30 to 40°C had a reduction in specific energy consumption of ~0.5kWh.Nm^{-3} whereas temperature increases from 40 to 50°C and 50 to 60°C both resulted in a slight reduction of specific energy consumption (~0.02kWh.Nm^{-3}). The trends of energy efficiency and specific energy consumption that were observed for N-GDE were due to the effect of temperature on the components of the PEM water electrolyser.

The results of N-GDE also indicate that activation overpotential was present, as with N-MEA. The increasing reaction temperature demonstrates a reduction of cell voltage and in effect improving the energy efficiency and reducing specific energy consumption. It is believed that the effect of increased PEM conductivity and electrocatalyst reaction kinetics from 30 to 60°C may also be observed at reaction temperatures exceeding 60°C, as a result of the relationship between temperature and conductivity of the electrolyser components.

Similar results were obtained by Ni *et al*. (2008) using a MEA with regard to the effect of reaction temperature on the energy efficiency of a PEM water electrolyser. Ni *et al*. (2008) found that the energy efficiency increased by ~1.3% when the reaction temperature was increased from 27 to 50°C. They also found that energy efficiency increased by ~1.5% when the reaction temperature was increased from 50 to 70°C. Ni *et al* (2008) determined that the electrodes of a PEM water electrolyser were more reactive at higher reaction temperatures and as a result, lowered the activation overpotential and reduced the electrical energy required.

It is clear from the results, polarisation curves and the comparison of Ni *et al*. (2008) that reaction temperature increases the electrode reactivity and energy efficiency of N-MEA and N-GDE. Based on the experimental results achieved it can be concluded that the desired reaction temperature for operating the PEM water electrolyser should be at 60°C.

4.3.4 Influence of cathode pressure

The influence of cathode pressure on PEM water electrolyser performance for N-MEA and N-GDE was studied by operating at varying pressures between 0 and 6 $bar_{(g)}$. A manually operated pressure regulator produced the desired cathode pressure/ polarisation curves and the hydrogen production rate was monitored throughout the experiments. The results and polarisation curves of N-MEA and N-GDE at varying cathode pressures are presented in Tables 4-7 and 4-8 and Figures 4-7 and 4-8.

Table 4-7 Pressure effect on N-MEA [0.5A.cm^{-2}, 30°C]

Pressure ($bar_{(g)}$)	**Potential** (V)	**Hydrogen production** ($Nm^3.hr^{-1}$)	$\varepsilon_{\Delta G}$ (%)	E_S ($kWh.Nm^{-3}$)
0	1.870±3.6×10^{-2}	0.0101±3×10^{-4}	65.48±1.24	4.58±0.05
1	1.894±3.6×10^{-2}	0.01051±3×10^{-4}	65.18±1.22	4.50±0.04
2	1.884±3.6×10^{-2}	0.0104±3×10^{-4}	65.82±1.23	4.53±0.04
3	1.888±3.6×10^{-2}	0.0105±3×10^{-4}	65.90±1.23	4.51±0.04
4	1.897±3.6×10^{-2}	0.0106±3×10^{-4}	65.73±1.22	4.49±0.04
5	1.908±3.6×10^{-2}	0.0102±3×10^{-4}	65.51±1.21	4.67±0.05
6	1.956±3.6×10^{-2}	0.0106±3×10^{-4}	64.01 ±1.16	4.61±0.04

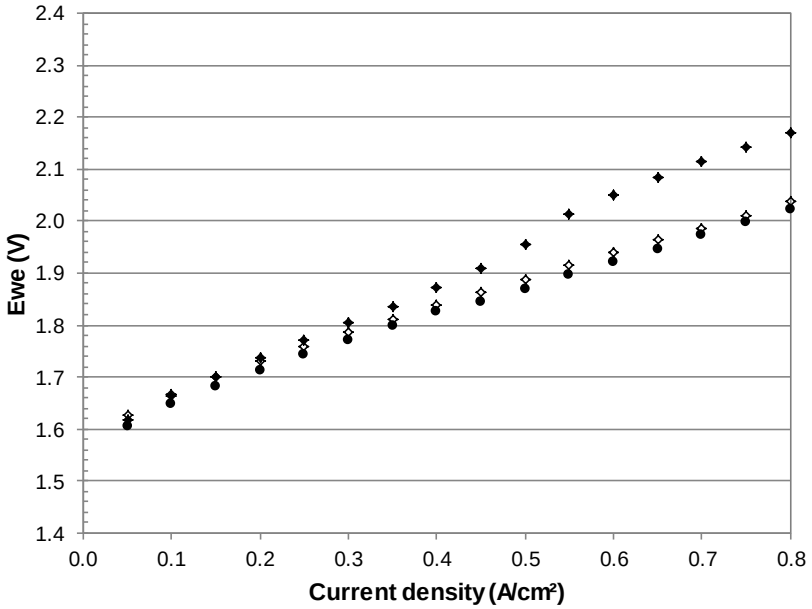

Figure 4-7 Cell voltage of N-MEA at varying cathode pressures and current densities at a water temperature of 30°C.
[● 0 $bar_{(g)}$; ◊ 3 $bar_{(g)}$; ♦ 6 $bar_{(g)}$;]

The results and polarisation curves of Table 4-7 and Figure 4-7 indicate that cathode pressure had a minor influence on the performance of N-MEA. No major changes were observed for the energy efficiencies of N-MEA and N-GDE, as the energy efficiency calculations for PEM electrolysis depended on the temperature and cathode pressure that the electrolyser was operating at. Energy efficiency calculations can be found in Appendix B.

When evaluating N-MEA at different cathode pressures (Table 4-7), an increase from 2 to 3 $bar_{(g)}$ increased the cell voltage of N-MEA by 0.004 V at a current density of 0.5A.cm^{-2}. When

the PEM water electrolyser was operated at a cathode pressure of 6 $bar_{(g)}$, the cell voltage increased by 0.068V compared to that at 3 $bar_{(g)}$.

The trend for specific energy consumption of N-MEA at increasing cathode pressures is not clear. As the cathode pressure increased from 0 $bar_{(g)}$ to 3 $bar_{(g)}$ the specific energy consumption decreased by ~0.1 $kWh.Nm^{-3}$. When the cathode pressure was increased from 3 $bar_{(g)}$ to 6 $bar_{(g)}$ the specific energy consumption increased by ~ 0.1 $kWh.Nm^{-3}$. The specific energy consumptions of 0 $bar_{(g)}$ and 6 $bar_{(g)}$ are practically the same. The specific energy consumption value is defined as the energy required producing $1Nm^3$ of hydrogen. Due to a slight variation in hydrogen production rate at different pressures, the results of specific energy consumption differed. Evaluating the effect of increased pressure solely on cell potential and current density shows increased energy requirements at increased pressure and constant current density.

When evaluating the increased cathode pressure results of N-MEA, an increase in cell voltage from 0 to 6 $bar_{(g)}$ was observed. The standard deviation for the polarisation curves of N-MEA at 30°C was calculated as 0.0356V. When the results of N-MEA were compared and standard deviation was taken into account, it was clear that the additional overpotential and the fluctuation of specific energy consumption / cell voltage deemed the results of N-MEA invalid.

On viewing the polarisation curves of N-MEA, an additional overpotential occurred at N-MEA 30°C, 5 $bar_{(g)}$, and disappeared after the experiment of N-MEA 40°C, 2 $bar_{(g)}$. The cause of this additional overpotential was discussed and covered in Section 4.3.2.

The influence of cathode pressure on PEM water electrolyser performance for N-GDE was studied and is presented in Table 4-8 and Figure 4-8.

Table 4-8 Pressure effect on N-GDE [0.5A.cm^{-2}, 50°C]

Pressure ($bar_{(g)}$)	**Potential** (V)	**Hydrogen production** ($Nm^3.hr^{-1}$)	$\varepsilon_{\Delta G}$ (%)	E_S ($kWh.Nm^{-3}$)
0	2.209	0.0104	54.68	5.32
1	2.227	0.0104	54.72	5.36
2	2.230	0.0103	54.92	5.40
3	2.235	0.0103	54.97	5.42
4	2.253	0.0103	54.69	5.44
5	2.254	0.0106	54.78	5.32
6	2.263	0.0102	54.65	5.52

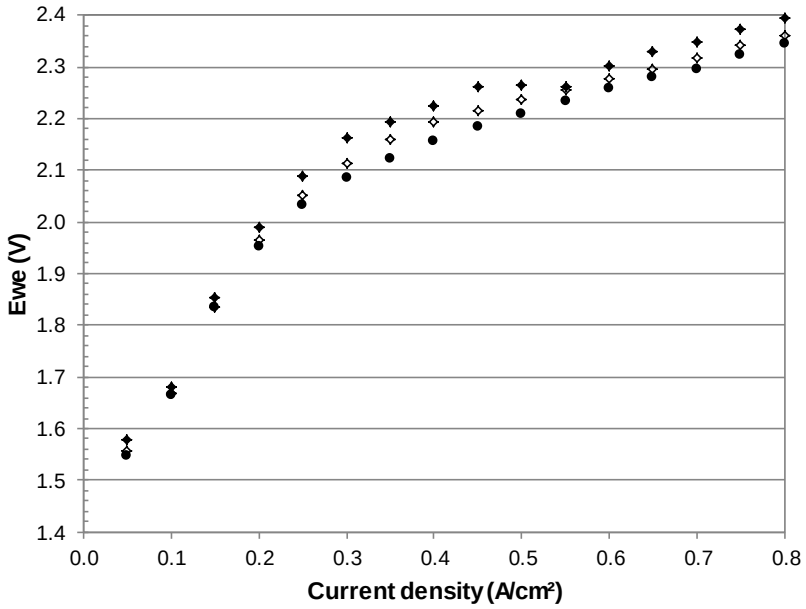

Figure 4-8 Cell voltage of N-GDE at varying cathode pressures and current densities at a water temperature of 50°C.
[● 0 $bar_{(g)}$; ◊ 3 $bar_{(g)}$; ♦ 6 $bar_{(g)}$;]

When evaluating the effect of increased cathode pressure for N-GDE in terms of cell voltage, an increase from 0 $bar_{(g)}$ to 3 $bar_{(g)}$ demonstrated an increase in cell voltage of 0.026 V. When the cathode pressure was increased from 3 $bar_{(g)}$ to 6 $bar_{(g)}$, the cell voltage exhibited an increase of 0.028 V. A trend similar to that of cell voltage was observed for specific energy consumption, as specific energy consumption is a function of cell voltage. A cathode pressure increase from 0 $bar_{(g)}$ to 3 $bar_{(g)}$ had an increase of ~0.1 $kWh.Nm^{-3}$. When the PEM water electrolyser operated at a cathode pressure of 6 $bar_{(g)}$, an increase of ~0.1 $kWh.Nm^{-3}$ was observed when compared to 3 $bar_{(g)}$. The results of N-GDE illustrate how the energy requirements to operate at a higher pressure and constant current density increased with pressure. This increased energy consumption was at a constant temperature and was regarded as isothermal compression work in which energy was used to pressurise the hydrogen gas on the cathode side of the PEM water electrolyser.

According to Millet *et al*. (2011) a higher operating cathode pressure increases the standard voltage to operate the PEM water electrolyser by +10 mV per decade of pressure (bar). In practice a slight improvement in overall cell efficiency was observed, particularly when operating at high current densities. As the pressure experiments of N-MEA and N-GDE had a maximum operating cathode pressure of 6 $bar_{(g)}$, the results of N-MEA did not exhibit the required output to exceed the standard deviation values at a current density of 0.5 $A.cm^{-2}$.

The polarisation curve of N-GDE in Figure 4-8 illustrates a decrease in cell voltage at 6 $bar_{(g)}$, in the current density range of 0.5 to 0.8 $A.cm^{-2}$. Grigoriev *et al*. (2009) also found that an increase of operating pressure resulted in an increase in thermodynamic voltage. They found that high pressure operations (50 bar) at high current densities (0.5-1.0 $A.cm^{-2}$) improved the PEM water electrolyser kinetics, due to a decrease in size of gaseous bubbles with pressure. This is thought to be the reason for the decrease in cell voltage as found in Figure 4-8 at 6 $bar_{(g)}$. At a pressure of 6 $bar_{(g)}$ the hydrogen forming on the cathode side was compressed and thus allowed more water to contact the cathode electrocatalyst. Grigoriev *et al*. (2009) found that the improved kinetics of high pressure operation, owing to gas cross-permeation phenomena, was counterbalanced by the faradaic efficiency. This phenomenon was found to be larger at low current density and at low gas production rates.

From the results it was found that with an increase of operating cathode pressure, the N-GDE performance exhibited higher cell voltages and higher specific energy consumption with an almost constant energy efficiency. Improved kinetics were also visible in Figure 4-8 (b), which agreed with findings of Grigoriev *et al*. (2009) and may imply that improved faradaic efficiencies were present at current densities of 0.5 $A.cm^{-2}$ and higher. For the PEM water electrolyser to take full advantage of high pressure operation, the current density should be larger than 0.5 $A.cm^{-2}$ and the pressure should be tested in the range of 30–50 $bar_{(g)}$.

4.3.5 Comparison of N-MEA and N-GDE performance

The key difference between N-MEA and N-GDE is that the anode and cathode electrocatalyst were deposited on different electrolyser components (as presented in Section 3.1). N-MEA and N-GDE are compared graphically in Figures 4-9 and 4-10 at varying temperatures and pressures and are discussed below.

(a) (b)

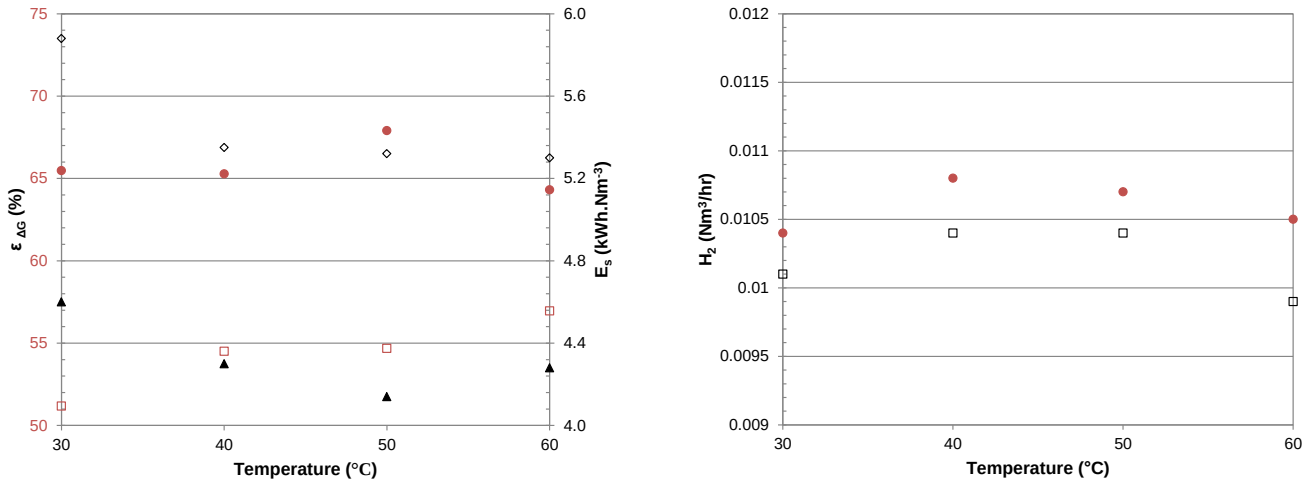

Figure 4-9 Comparison of N-MEA and N-GDE at varying temperatures,
a)Energy efficiency and specific energy consumption at a current density of 0.5A.cm^{-2} and pressure of 0 bar$_{(g)}$.
[$\varepsilon_{\Delta G}$: ● N-MEA; □ N-GDE] [E_S: ▲ N-MEA; ◊ N-GDE]
b)Hydrogen production at a current density of 0.5A.cm^{-2} and pressure of 0 bar$_{(g)}$.
[● N-MEA; □ N-GDE]

(a) (b)

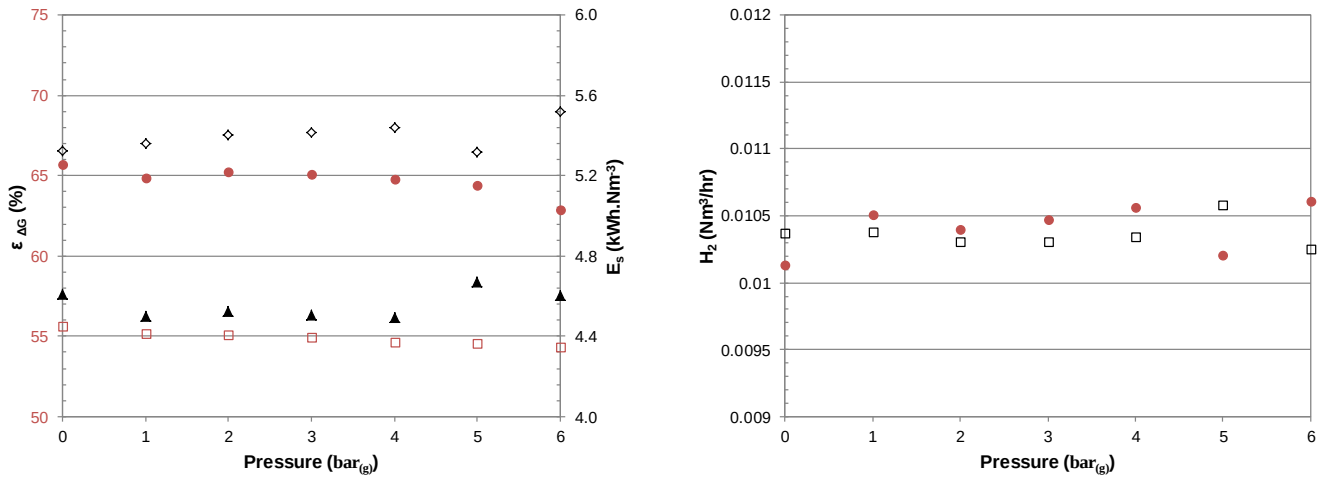

Figure 4-10 Comparison of N-MEA and N-GDE at varying pressures,
a)Energy efficiency and specific energy consumption at a current density of 0.5A.cm^{-2} and temperature of 50°C.
[$\varepsilon_{\Delta G}$: ● N-MEA; □ N-GDE] [E_S: ▲ N-MEA; ◊ N-GDE]
b)Hydrogen production at a current density of 0.5A.cm^{-2} and temperature of 50°C.
[● N-MEA; □ N-GDE]

Figures 4-9 and 4-10 illustrate the summarised results of Tables 4-5 to 4-8. Comparing N-MEA and N-GDE at varying temperature shows in Figure 4-9 (a) that the efficiency for N-MEA was at

least 8% higher than that of N-GDE at the same temperature and specific energy consumption of N-MEA was approximately 0.7kWh.Nm^{-3} less than that of N-GDE. Hydrogen production figures were found to be very similar. The energy efficiencies of N-MEA and N-GDE, as shown in Figure 4-10 (a), clearly indicate that the energy efficiency of N-MEA was ~10% higher than N-GDE across the pressure range of 0-6 bar$_{(g)}$. The slight increase of specific energy consumption for both N-MEA and N-GDE is also visible, where N-GDE used ~0.8 kWh.Nm^{-3} more than N-MEA. Figure 4-10 (b) illustrates similar hydrogen production figures for both N-MEA and N-GDE, with the slight fluctuation being attributable to standard deviation.

The performance differences of N-MEA and N-GDE are noticeable with the cause thereof explained at microscopic level. Electrocatalyst's contact with the surface of the PEM played a role in the amount of active area and might have caused the differences in performance. According to the results of Grigoriev *et al*. (2009), MEA with the electrocatalytic layers directly deposited onto the PEM surface exhibit slightly more efficient results than those with the electrocatalyst layer deposited onto the current collector. When evaluating the ohmic overpotential, Lebbal *et al.* (2009) found that PEM resistance is considered to be the main source of ohmic overpotential for conventional MEA with the electrocatalyst directly deposited onto the PEM surface. According to the work of Biaku *et al*. (2008), the overall ohmic overpotential depends on the PEM type, electrocatalyst and the contact of electrocatalyst active area with the PEM.

As the GDE of N-GDE was placed on the PEM the electrocatalyst layer did not have the same electrocatalyst contact as a MEA with the electrocatalyst directly deposited onto the PEM surface. The electrocatalyst used in comparing N-MEA with N-GDE was the same; therefore the decrease in N-GDE efficiency may be as a result of poor contact of the active area with the PEM. The difference in porous current collectors may also be contributing to the overpotential, as the N-GDE implements sintered titanium current collector and N-MEA implements carbon cloth current collector on the cathode side of the PEM water electrolyser. The root cause for the decrease in N-GDE performance was most possibly due to the reduced contact of the active area.

4.3.6 Summarised remarks about N-MEA and N-GDE

In this section the PEM water electrolyser performance was investigated at different water temperatures (30 to 60°C) and cathode pressures (0 to 6 bar$_{(g)}$). It was found that water temperature had a significant effect on water electrolysis energy efficiency and specific energy consumption, and cathode pressure a minor effect. Higher operating temperatures produced increased energy efficiencies for N-MEA and N-GDE. Higher operating cathode pressures resulted in increased cell voltages with practically constant energy efficiencies. The comparison

of N-MEA and N-GDE at the varying temperature and pressure ranges showed enhanced performance for N-MEA, and is most likely due to the superior electrocatalyst contact. It is recommended that MEA are used in PEM water electrolysers as it exhibited the best performance, and should be operated at a temperature of 30°C and cathode pressure of 6 $bar_{(g)}$. These operating conditions will be the easiest to meet when implemented in rural areas as the surrounding temperature will provide the required operating temperature, and high pressure operation energy losses will reduce compression costs associated with hydrogen storage.

4.4 PEM water electrolysis with NS-MEA and PS-MEA

4.4.1 Introduction

The synthesised MEA of NS-MEA and PS-MEA, as described in Section 4.2, were evaluated in the PEM water electrolyser to ascertain the performance results thereof. NS-MEA and PS-MEA were evaluated at a fixed temperature of 30°C and a varying cathode pressure range. The effect of cathode pressure in the PEM water electrolyser was evaluated with respect to hydrogen production rate, energy efficiency and specific energy consumption. Performance results of both NS-MEA and PS-MEA were compared to determine which of the synthesised MEA is best suited for PEM water electrolysis.

4.4.2 Experimental results and discussion

4.4.2.1 Influence of cathode pressure

The influence of cathode pressure on PEM water electrolyser performance for NS-MEA and PS-MEA was studied by operating at cathode pressures of 0, 3 and 6 $bar_{(g)}$, at a temperature of 30°C. Tables 4-9 and 4-10, and also Figures 4-11 and 4-12 summarise the performance results of the synthesised MEA of NS-MEA and PS-MEA.

Table 4-9 Pressure effect on NS-MEA [0.5A.cm^{-2}, 30°C]

Pressure ($bar_{(g)}$)	**Potential** (V)	**Hydrogen production** ($Nm^3.hr^{-1}$)	$\varepsilon_{\Delta G}$ (%)	E_S ($kWh.Nm^{-3}$)
0	$3.806\pm8.1\times10^{-2}$	$0.0109\pm3\times10^{-4}$	32.18±0.67	8.69±0.05
3	$3.820\pm3.5\times10^{-2}$	$0.0108\pm4\times10^{-4}$	32.57±0.67	8.81±0.24
6	$3.838\pm1.5\times10^{-2}$	$0.0107\pm2\times10^{-4}$	32.62±0.67	8.93±0.13

Table 4-10 Pressure effect on PS-MEA [0.5A.cm^{-2}, 30°C]

Pressure ($bar_{(g)}$)	**Potential** (V)	**Hydrogen production** ($Nm^3.hr^{-1}$)	$\varepsilon_{\Delta G}$ (%)	E_S ($kWh.Nm^{-3}$)
0	3.642±0.017	$0.0108\pm3\times10^{-4}$	33.63±0.73	8.46±0.21
3	3.656±0.012	$0.0113\pm4\times10^{-4}$	34.03±0.74	8.12±0.22
6	3.647±0.020	$0.0110\pm1\times10^{-4}$	34.32±0.75	8.28±0.03

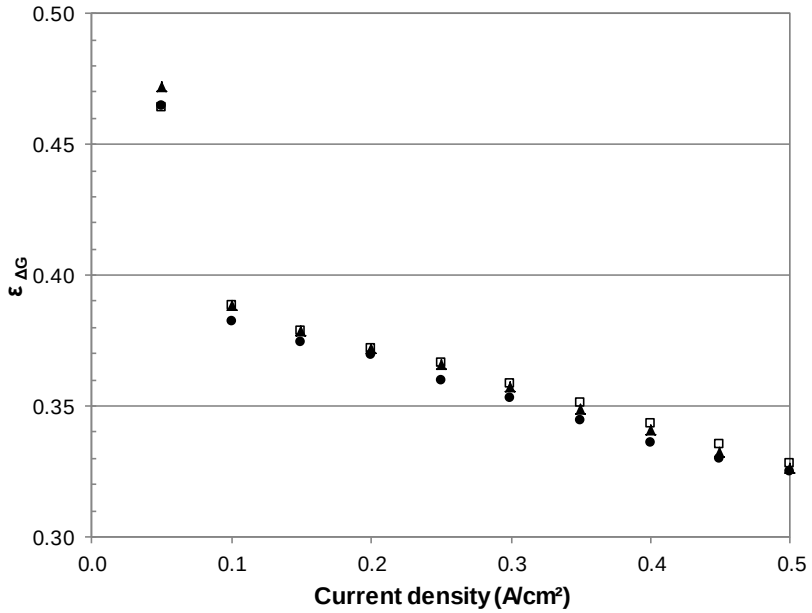

Figure 4-11 Energy efficiency of NS-MEA at varying cathode pressures at a water temperature of 30°C.
[● 0 $bar_{(g)}$;□ 3 $bar_{(g)}$;▲ 6 $bar_{(g)}$;]

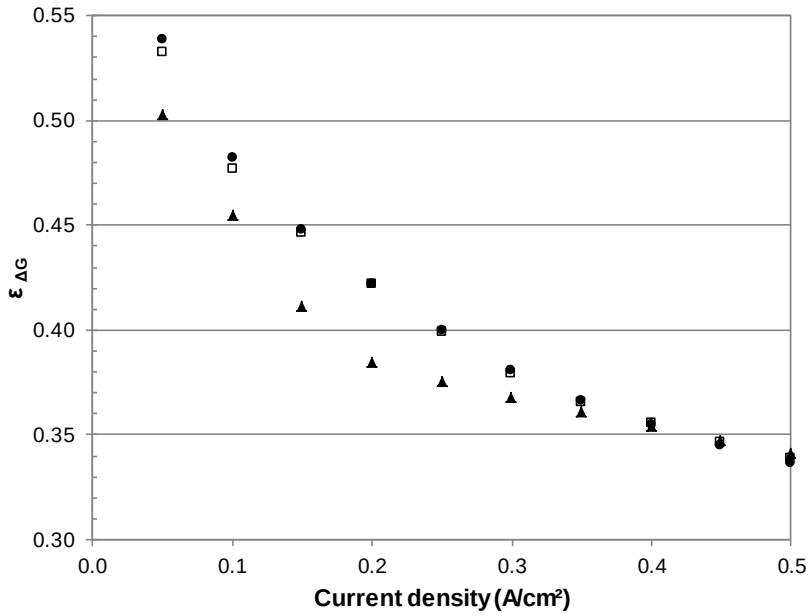

Figure 4-12 Energy efficiency of PS-MEA at varying cathode pressures at a water temperature of 30°C.
[● 0 $bar_{(g)}$;□ 3 $bar_{(g)}$;▲ 6 $bar_{(g)}$;]

The results of Tables 4-9 and 4-10, and Figures 4-11 and 4-12 indicate that cathode pressure had a minor influence on the performance of both NS-MEA and PS-MEA. The performance data of Table 4-9 shows that a pressure increase from 0 $bar_{(g)}$ to 3 $bar_{(g)}$ resulted in an increase (0.014 V) of cell voltage for NS-MEA. When the PEM water electrolyser was operated at a cathode

pressure of 6 $bar_{(g)}$ the cell voltage increased by 0.018 V, compared to that at 3 $bar_{(g)}$. As the energy efficiency calculations were adjusted for operating temperature and pressure, no major change in energy efficiency was observed for increased cathode pressure. The evaluation of NS-MEA with respect to specific energy consumption produced no visible trend at increased cathode pressures. As the cathode pressure increased from 0 $bar_{(g)}$ to 3 $bar_{(g)}$ the specific energy consumption increased by 0.12 $kWh.Nm^{-3}$. When the cathode pressure was increased from 3 $bar_{(g)}$ to 6 $bar_{(g)}$ the specific energy consumption increased by 0.16 $kWh.Nm^{-3}$. These results show that PEM electrolyser operation at higher cathode pressures required more power to produce one unit of hydrogen at standard temperature and pressure (STP). Increased cathode pressure thus influenced cell potential directly and also increased the required energy input with increased pressure.

The evaluation of PS-MEA for increased cathode pressure exhibited different tendencies for cell voltage and specific energy consumption. As the cathode pressure of PS-MEA was increased from 0 $bar_{(g)}$ to 3 $bar_{(g)}$ the cell voltage demonstrated an increase (0.014 V). When the cathode pressure was increased from 3 $bar_{(g)}$ to 6 $bar_{(g)}$ the cell voltage exhibited a decrease (0.009 V). Specific energy consumption on the other hand, had a decrease of 0.34 $kWh.Nm^{-3}$ when the cathode pressure was increased from 0 $bar_{(g)}$ to 3 $bar_{(g)}$. When the PEM water electrolyser operated at a cathode pressure of 6 $bar_{(g)}$ an increase of ~0.2 $kWh.Nm^{-3}$ was observed, compared to that at 3 $bar_{(g)}$. Figure 4-12 illustrates a reducing rate of energy efficiency from 0.1 to 0.2 $A.cm^{-2}$ when the electrolyser was operated at a cathode pressure of 6 $bar_{(g)}$. The decrease of specific energy consumption was mainly due to an increase in hydrogen production. On average, hydrogen production figures differed for experiments at all pressures. Seeing that specific energy consumption is a function of the hydrogen production rate and cell voltage, it only provides the energy required per unit of hydrogen produced. The cell voltages reported in Table 4-9 give a better indication of energy required for electrolysis and shows that cell voltage increased slightly with operating cathode pressure.

According to Millet *et al*. (2011) a higher operating cathode pressure increases the standard voltage to operate the PEM water electrolyser by +10 mV per decade of pressure (bar). In practice a slight improvement in overall cell efficiency is observed, particularly when operating at high current densities.

The increased cathode pressure results of NS-MEA and PS-MEA demonstrated an increase in cell voltage from 0 to 6 $bar_{(g)}$. The comparison of 0 and 6 $bar_{(g)}$ shows an increase of 0.032 V and 0.005 V in cell voltage, for NS-MEA and PS-MEA. A linear extrapolation of the results of NS-MEA and PS-MEA showed an increase of 53mV and 8mV per decade of pressure. The results of

NS-MEA and PS-MEA did not exceed the values of standard deviation as the change in voltage per decade of pressure was too small.

It was concluded that increased operating cathode pressures resulted in slightly higher cell voltages for NS-MEA and PS-MEA at almost constant energy efficiency. A conclusion similar to Section 4.3.3 was made - that experiments should be conducted at pressures in the range of 0-50 $bar_{(g)}$ and at higher current densities to see the effect of pressure clearly on performance of a PEM water electrolyser.

4.4.3 Comparison of NS-MEA and PS-MEA

For the comparison of NS-MEA and PS-MEA the key difference distinguishing them was the type of PEM used in synthesising the MEA. The likes of NS-MEA and PS-MEA were compared graphically in Figure 4-13 at varying pressures and constant temperature and are discussed below.

(a) (b)

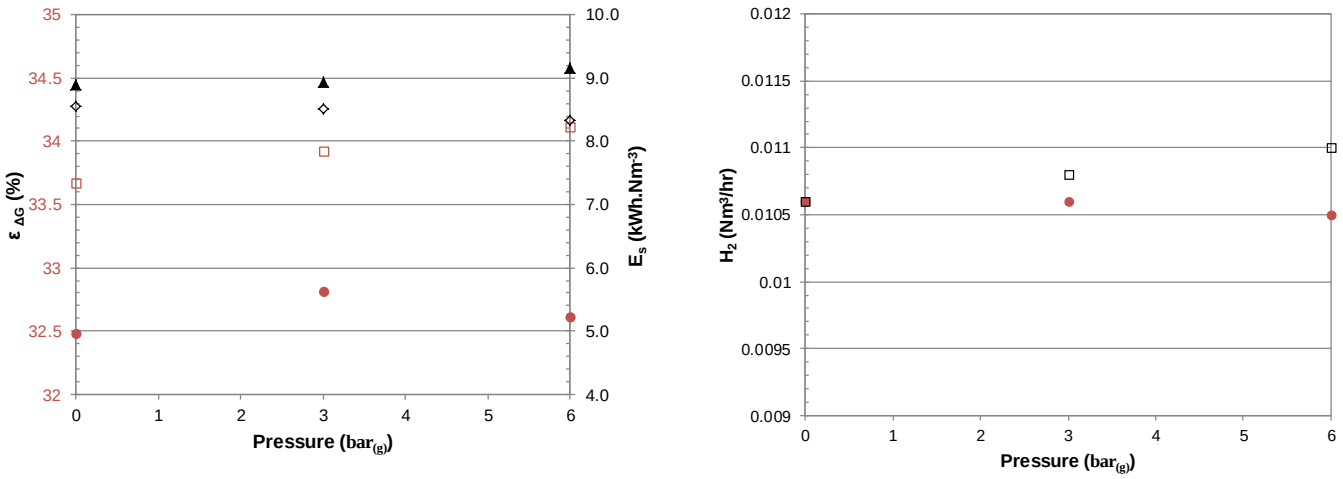

Figure 4-13 Comparison of NS-MEA and PS-MEA at varying pressures,
a)Energy efficiency and specific energy consumption at a current density of 0.5A.cm^{-2} and temperature of 30°C.
[$\varepsilon_{\Delta G}$: ● NS-MEA; □ PS-MEA] [E_S: ▲ NS-MEA; ◊ PS-MEA]
b)Hydrogen production at a current density of 0.5A.cm^{-2} and temperature of 30°C.
[● NS-MEA; □ PS-MEA]

Figure 4-13 (a) in which the energy efficiencies of NS-MEA and PS-MEA were compared clearly indicates that the efficiency of PS-MEA was ~1.6% higher than that of NS-MEA at 0.5A.cm^{-2}, 30°C and 0$bar_{(g)}$. At pressures of 3$bar_{(g)}$ and 6$bar_{(g)}$ the energy efficiency of PS-MEA was ~1.1% and ~1.5% higher than that of NS-MEA. The cause of the increased efficiency of PS-MEA was investigated in terms of electrocatalyst deposition and PEM thickness.

From the SEM elemental analysis results in Table 4-3 of Section 4.3, it was obvious that the electrocatalyst layers of NS-MEA had similar thicknesses (~10.75 μm). The cathode electrocatalyst layer of PS-MEA had an average thickness of 22.35 μm, where thickness varied significantly (~4 μm). Although the exact same procedure was followed in applying the electrocatalyst to both NS-MEA and PS-MEA, a better catalyst distribution was present on NS-MEA.

The influence of electrocatalyst on the activation overpotential was investigated by measuring the cell voltage at the initial current density of 0.05 A.cm^{-2}. The activation cell voltages were found to be 1.38 V and 1.06 V for NS-MEA and PS-MEA respectively. With the assumption that the anode electrocatalyst layer had a thickness similar to the cathode electrocatalyst layer, the active area of PS-MEA might have been higher than NS-MEA as the electrocatalyst layers for PS-MEA were much thicker than NS-MEA. The higher catalytic loading ultimately leads to reduced activation overpotential up to the point where mass transport limitations through the electrocatalyst layers set in. Song *et al*. (2008) found that platinum formed an oxide film when used as anode electrocatalyst and exhibited a high over potential due to its poor conductivity.

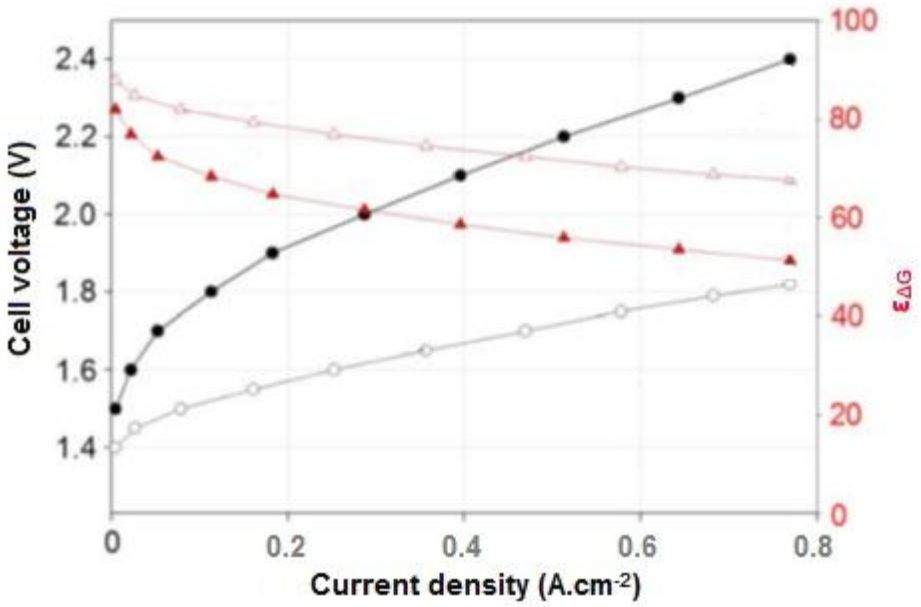

Figure 4-14 Polarisation curve relationships for PEM water electrolysis (Millet *et al.*, 2009:4974).
[● Pt for anode and cathode;○ Pt for cathode and Ir for anode]
[▲$\varepsilon_{\Delta G}$ for Pt cathode and anode;Δ $\varepsilon_{\Delta G}$ for Pt cathode and Ir anode]

When comparing experimental findings with Millet *et al*. (2009) in Figure 4-14, the cell voltage of ~1.67 V at a current density of 0.05 A.cm^{-2} is significantly higher than that of NS-MEA and PS-MEA at the same conditions. The lowered activation overpotential was most likely due to an

increased electrocatalyst loading, as Millet *et al*. (2009) mention that electrocatalyst loading is usually a few milligrams per square centimetre.

The influence of PEM thickness on the ohmic overpotential was investigated by calculating the slope of the polarisation curve (Appendix B). The average ohmic resistances for NS-MEA and PS-MEA were calculated as 0.0338 Ω and 0.0274 Ω respectively. According to Lebbal *et al*. (2009), the PEM is the main source of resistance, where total ohmic resistance is depends on PEM and electrode type, and the contact between electrocatalyst and the PEM (Biaku *et al.*, 2008:4247).

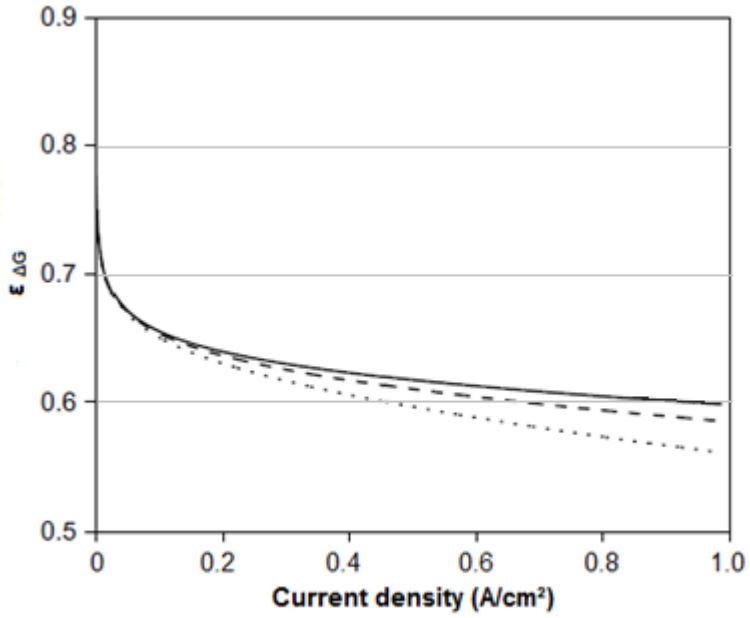

Figure 4-15 Effect of PEM thickness on PEM water electrolyser performance (Ni *et al.*, 2008:2748).
[PEM electrolyte thickness (μm): —— 50;– – – 100;- - - 200]

Results of Ni *et al*. (2008) in Figure 4-15 show that PEM thickness has a significant and constant effect on the energy efficiency of a PEM water electrolyser. On comparing the measured thickness of both the Nafion® N117 (~180μm) and PBI-sPSU (~60μm) in Table 4-3, it was found that Nafion was three times the thickness of PBI-sPSU. Based on the differences in PEM thickness the results of PS-MEA should display a polarisation curve with a gradient (ohmic resistance) smaller than that of NS-MEA. This is the case as the calculated ohmic resistance of NS-MEA is larger than that of PS-MEA. It is thought that the electrocatalyst layers of PS-MEA most probably increased the ohmic resistance, due to reduced contact between the electrocatalyst layer and PEM and that the ohmic resistance of PS-MEA would have been lower if the electrocatalyst layer had bonded properly.

4.4.4 Summarised remarks about NS-MEA and NS-GDE

In this section the PEM water electrolyser performance was investigated with different MEA at different cathode pressures (0, 3 and 6 $bar_{(g)}$). It was found that cathode pressure had an effect on water electrolyser performance, but insufficient to be significant. Increased cathode pressures had increased cell voltages and virtually consistent energy efficiencies. NS-MEA and PS-MEA at varying conditions exhibited similar ohmic overpotentials. Although the PEM of PS-MEA was approximately three times thinner than NS-MEA, the additional losses due to inferior electrocatalyst contact still showed a lower ohmic overpotential for PS-MEA. Other GDE experiments with PBI-sPSU showed that PBI-sPSU were more susceptible to damage under severe conditions when compared to Nafion®. From the results of this section it can be concluded that Nafion® is the obvious choice for PEM water electrolysis and that further studies with PBI-sPSU have to be conducted to determine whether it can take the place of the commercially known Nafion® PEM.

4.5 PEM water electrolysis with iron and magnesium salt solutions

4.5.1 Introduction

In this section the performances of $FeSO_4$-MEA and $MgSO_4$-MEA were evaluated in the PEM water electrolyser to investigate the effect of $FeSO_4$ and $MgSO_4$ concentrations in the PEM water electrolyser feed water on the MEA. MEA regeneration with sulphuric acid was evaluated in an attempt to restore the MEA to its original condition after exposure to the magnesium and iron salts. The performance results of both $FeSO_4$-MEA and $MgSO_4$-MEA were compared and discussed to determine the degradation effects of both Fe^{2+} and Mg^{2+} on the MEA.

4.5.2 Experimental results and discussion

4.5.2.1 Influence of iron (II) sulphate

The influence of iron (II) sulphate solution on the performance of $FeSO_4$-MEA was investigated by exposing the MEA to a concentration of 100 ppm solution of $FeSO_4$ continuously for 72 hours. The performance data was generated by operating the electrolyser at 30°C and a current density of 0.5 $A.cm^{-2}$, as described in Section 3.3.3. The attained results are summarised in Table 4-11 and Figure 4-16.

Table 4-11 Effect of 0.1M $FeSO_4$ solution [0.5 $A.cm^{-2}$, 30°C]

Exposure (Hours)	**Potential** (V)	**Hydrogen production** ($Nm^3.hr^{-1}$)	$\varepsilon_{\Delta G}$ (%)	E_S ($kWh.Nm^{-3}$)
0	1.741	0.0101	70.33	4.33
2	1.800	0.0102	68.06	4.42
4	2.023	0.0101	60.52	4.79
8	2.163	0.0107	56.63	5.07
12	2.223	0.0102	55.09	5.44
19	2.285	0.0099	53.60	5.75
26	2.319	0.0103	52.82	5.62
36	2.401	0.0098	51.01	6.11
46	2.434	0.0098	50.31	6.19
59	2.481	0.0103	49.35	6.01
72	2.536	0.0100	48.30	6.37

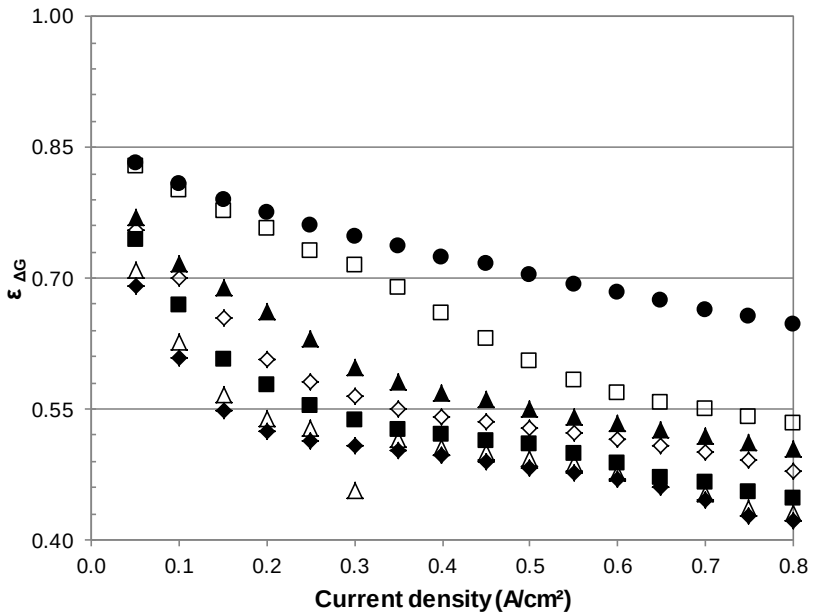

Figure 4-16 Energy efficiency of $FeSO_4$-MEA with exposure to 100ppm $FeSO_4$ solution over a period of 72 hours.
[● 0 hours;□ 4 hours;▲ 12 hours;◊ 26 hours; ■ 36 hours; Δ 59 hours; ♦ 72 hours]

From the results in Table 4-11 and Figure 4-16 it is clear that exposure to Fe^{2+} ions has a considerable effect on the performance of the PEM water electrolyser over time, as decreases in energy efficiency are observed over time. The initial condition of the experiment with exposure time 0 hours, represents electrolyser operation with deionised water. Exposure of $FeSO_4$-MEA to 100ppm $FeSO_4$ solution, showed a decreasing trend of energy efficiency, as in Figure 4-16. An exposure time of 4 hours for $FeSO_4$-MEA, shows a decrease in energy efficiency of ~10%. When the exposure time of 8 hours is compared to 4hours, a further decrease in energy efficiency of ~5% is observed. The comparison of 26 hours to 12hours of exposure shows additional ~2% decrease in energy efficiency. The exposure time of 72 hours had a further decrease of ~2% in energy efficiency when compared to 46 hours of exposure. A similar trend can be observed for specific energy consumption of $FeSO_4$-MEA over time. The exposure of $FeSO_4$-MEA to 100ppm Fe^{2+} ions for a period of 72 hours has a large increase of specific energy consumption (~3kWh.Nm^{-3}) in effect.

According to Collier *et al*. (2006), most metal cations have higher affinities for sulfonic acid than hydrogen. It was also found that hydrogen displacement by metal cation exchange decreases water content, ionic conductivity and transference numbers.

The presence of Fe^{2+} had a negative impact on the efficiency and specific energy consumption of the electrolyser. It is thought that the Fe^{+2} ions that were present in the water reservoir exchanged with the protons on the surface of the PEM, in turn contaminating the PEM and reducing the

proton transfer through the MEA. The resistance of the PEM increased over time, due to the Fe^{+2} ions on the surface of the PEM thereby reducing proton exchange through the PEM. The reduced conductivity together with MEA contamination may be the foremost reason for the decrease of electrolyser performance when in contact with Fe^{2+} cations for extended periods.

Bas *et al*. (2010) found that the performance of the PEM did not depend on cation concentration alone, but on the number of cations in contact with the PEM. Results gathered by Bas *et al*. (2010) of Nafion® with different counterions, showed that ionic conductivity of H^+ was 90.2 (mS cm). The ionic conductivity of Fe^{2+} was found to be 8.2 mS cm. They also found that cationic contamination of the MEA influenced MEA performance negatively, due to kinetic losses that arose at both electrodes, particularly at the anode.

The experimental results showed that the presence of Fe^{2+} cations in the electrolyser water supply reservoir decreased energy efficiency and increased specific energy consumption. From the work of Collier *et al*. (2006) and Bas *et al*. (2010) it is clear that the displacement of hydrogen ions with Fe^{2+} may reduce water content of the PEM, and so may lower the ionic conductivity.

The comparison of experimental findings with those of Bas *et al.* (2010) and Collier *et al.* (2006) showed that the energy efficiency of the electrolyser decreased with time. The resistance over the electrolyser thus had increased, more specifically, the resistance of the MEA. Literature findings show that metal ions exchange with hydrogen ions of the PEM and cause kinetic losses at the electrodes. This in turn increases the activation overpotential and the PEM resistance, and is clearly illustrated in Figure 4-16.

4.5.2.2 Influence of magnesium salt

The influence of magnesium sulphate solution on the performance of $MgSO_4$-MEA was investigated by exposing the MEA to a concentration of 100ppm solution of $MgSO_4$ continuously for 72 hours. The performance data was generated by operating the electrolyser, as described in Section 3.3.3. The attained results are summarised in Table 4-12 and Figure 4-17.

Table 4-12 Effect of 0.1M $MgSO_4$ solution [0.5A.cm^{-2}, 30°C]

Exposure (hours)	**Potential** (V)	**Hydrogen production** ($Nm^3.hr^{-1}$)	$\varepsilon_{\Delta G}$ (%)	E_S ($kWh.Nm^{-3}$)
0	1.712	0.0110	71.55	3.88
2	2.208	0.0097	55.46	5.72
4	2.208	0.0100	55.47	5.54
8	2.238	0.0095	54.72	5.91
12	2.419	0.0097	50.62	6.26
19	2.362	0.0101	51.86	5.87
26	2.407	0.0101	50.88	5.94
36	2.486	0.0097	49.25	6.44
46	2.496	0.0100	49.07	6.22
59	2.524	0.0097	48.53	6.52
72	2.616	0.0098	46.82	6.68

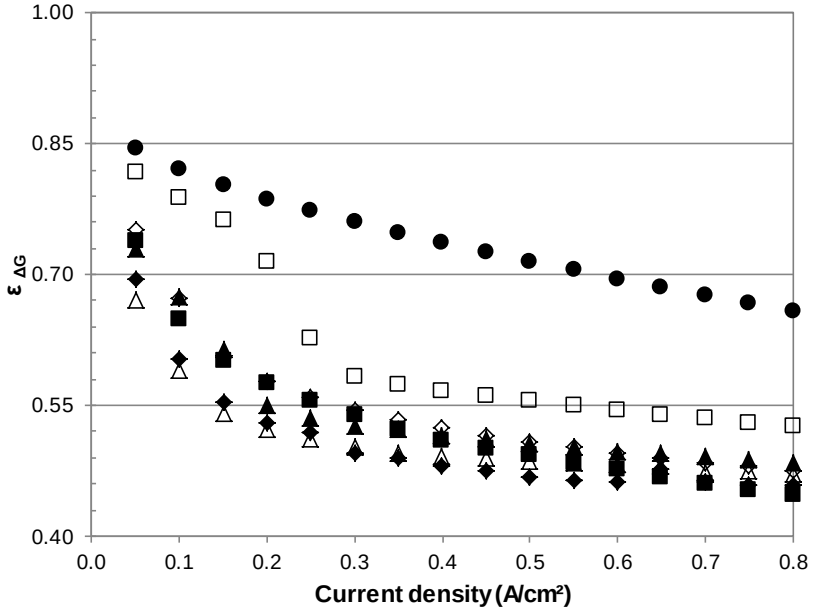

Figure 4-17 Energy efficiency of $MgSO_4$-MEA with exposure to 100ppm $FeSO_4$ solution over a period of 72 hours.
[● 0 hours;□ 4 hours;▲ 12 hours;◊ 26 hours; ■ 36 hours; Δ 59 hours; ♦ 72 hours]

From the results in Table 4-12 and Figure 4-17 it is clear that exposure to Mg^{2+} ions has a considerable effect on the performance of the PEM water electrolyser, as the energy efficiency decreases over time. The initial condition of the experiment with exposure time 0 hours, represents electrolyser operation with deionised water. Figure 4-17 illustrates the decrease in

energy efficiency as $MgSO_4$-MEA was exposed to the 100ppm $MgSO_4$ solution for increased periods of time. An exposure time of 4 hours for $MgSO_4$-MEA shows a decrease in energy efficiency of ~15%. The comparison of 8 hours to 4 hours of exposure showed a decrease of ~5% in energy efficiency. Comparing 26 hours to 8 hours of exposure time shows a further decrease in energy efficiency of ~2%. The comparison of 72 hours and 46 hours of exposure shows a decrease in energy efficiency of an additional ~2%. The same trend was observed for specific energy consumption. A total increase of ~2.9kWh.Nm^{-3} in specific energy consumption is observed when $MgSO_4$-MEA was exposed to a 100ppm Mg^{2+} solution for a period of 72 hours.

The results of Section 4.5.2.1 are applicable when explaining decreasing electrolyser performance due to Mg^{2+} contamination of the water reservoir. Bas *et al*. (2010) found the ionic conductivity of Mg^{2+} to be 8.9 mS cm. It was found that the presence of Mg^{2+} cations in the electrolyser water supply reservoir decreased energy efficiency and increased specific energy consumption. The resistance over the electrolyser had thus increased, more specifically, the resistance of the $MgSO_4$-MEA. Literature findings show that metal ions exchange with hydrogen ions of the PEM and cause kinetic losses at the electrodes. This in turn increases the activation overpotential and the PEM resistance, like that of $FeSO_4$-MEA and was clearly observed as illustrated in Figure 4-17. Reduced conductivity together with MEA contamination may be the foremost reason for electrolyser performance decrease when contacted with Mg^{2+} cations for extended periods.

4.5.3 Influence of sulphuric acid regeneration

Sulphuric acid regeneration was investigated with the contaminated MEA of $FeSO_4$-MEA and $MgSO_4$-MEA by submerging each MEA separately in sulphuric acid for 16 hours under magnetic agitation. The MEA were then tested in the PEM water electrolyser and performance data of Tables 4-13 and 4-14, and Figures 4-18 and 4-19 were generated by the protocol as described in Section 3.3.2. Once the performances of the MEA were tested SEM analysis was completed to determine the extent of contamination.

Table 4-13 Regeneration of 0.1M $FeSO_4$ MEA [0.5A.cm^{-2}, 30°C]

Exposure (hours)	**Potential** (V)	**Hydrogen production** ($Nm^3.hr^{-1}$)	$\varepsilon_{\Delta G}$ (%)	E_S (kWh.Nm^{-3})
72	2.536	0.0100	48.30	6.37
Regen1	2.029	0.0103	60.36	4.94
Regen2	2.077	0.0102	58.95	5.08
Regen3	2.066	0.0105	59.27	4.91

Table 4-14 Regeneration of 0.1M $MgSO_4$ MEA [0.5A.cm^{-2}, 30°C]

Exposure (hours)	**Potential** (V)	**Hydrogen production** ($Nm^3.hr^{-1}$)	$\varepsilon_{\Delta G}$ (%)	E_S ($kWh.Nm^{-3}$)
72	2.616	0.0098	46.82	6.68
Regen1	1.880	0.0104	65.13	4.50
Regen2	1.926	0.0106	63.58	4.56
Regen3	1.964	0.0105	62.36	4.67

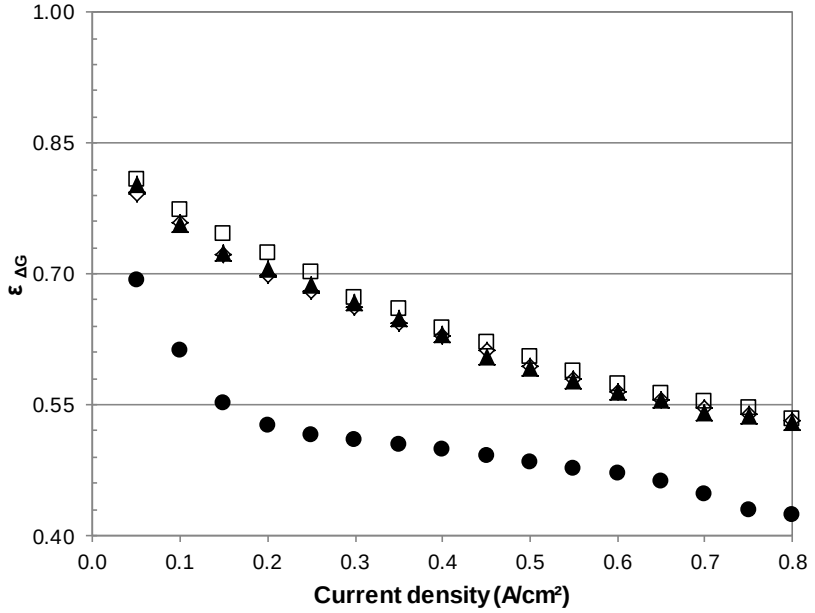

Figure 4-18 Energy efficiency of $FeSO_4$-MEA after 16 hours of 0.1M sulphuric acid regeneration. [● 72 hours;□ Regen1;▲ Regen2;◊ Regen3]

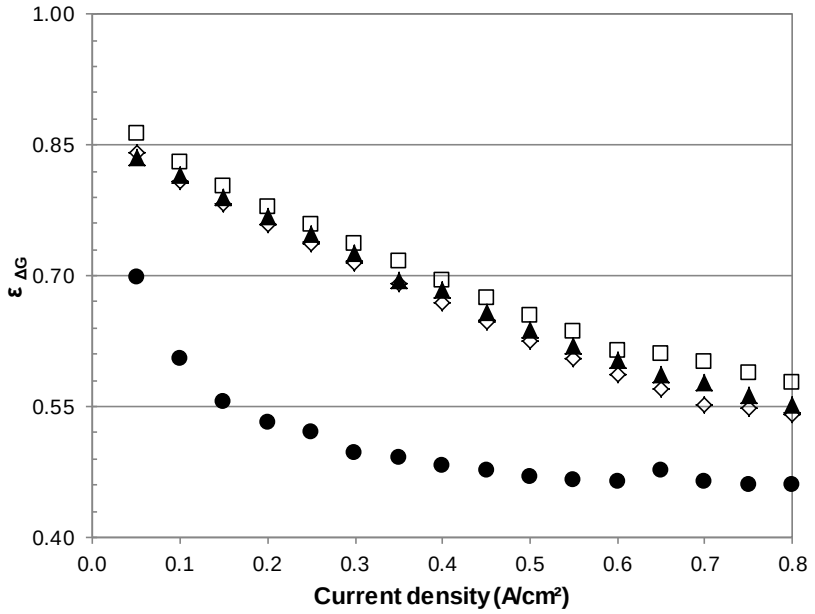

Figure 4-19 Energy efficiency of $MgSO_4$-MEA after 16 hours of 0.1M sulphuric acid regeneration.
[● 72 hours;□ Regen1;▲ Regen2;◊ Regen3]

The regeneration results of $FeSO_4$-MEA and $MgSO_4$-MEA with sulphuric acid had a clear improvement on electrolyser performance, as illustrated in Tables 4-13 and 4-14, and Figures 4-18 and 4-19. On comparing the energy efficiency of $FeSO_4$-MEA after 72 hours of exposure (Table 4-13) to the first regeneration experiment, an increase in energy efficiency of ~12% is observed. After completing two additional electrolyser performance evaluations, a decrease of ~1% is observed, compared with the first regeneration performance evaluation. A similar trend was noticed for specific energy consumption. After sulphuric acid regeneration of $FeSO_4$-MEA, a decrease of ~1.5 $kWh.Nm^{-3}$ in specific energy consumption was observed. The comparison of 0 hours exposure (Table 4-11) with the regeneration results shows a decrease in energy efficiency of ~10% and an increase in specific energy consumption of ~0.6 $kWh.Nm^{-3}$ for $FeSO_4$-MEA.

Sulphuric acid regeneration of $MgSO_4$-MEA followed a similar trend to that of $FeSO_4$ as an increase in energy efficiency of ~15% is observed when compared to 72 hours of exposure (Table 4-14). The comparison of the third regeneration experiment with the first of $MgSO_4$-MEA, shows a decrease in energy efficiency of ~3%. The specific energy consumption exhibited similar results. Regeneration results of $MgSO_4$-MEA exhibit a decrease of ~2 $kWh.Nm^{-3}$ in specific energy consumption, compared to 72 hours of exposure (Table 4-14). When the reference 0 hours of exposure (Table 4-12) is compared with regeneration results, a decrease of

~8% in energy efficiency and increase in specific energy consumption of ~0.8 kWh.Nm^{-3} is observed for $MgSO_4$-MEA.

The regeneration results clearly illustrated the effect of sulphuric acid regeneration on $FeSO_4$-MEA and $MgSO_4$-MEA, as their energy efficiency and specific energy consumption values improved. A vital observation was made on the extent of regeneration, where the energy efficiency of $FeSO_4$-MEA and $MgSO_4$-MEA were restored to 90% and 92% of their original performance values. According to the results of Nasef and Yahaya (2009), pure Nafion® 117 can be completely regenerated when soaked in 0.1M HNO_3 for 16 hours. They also found that the Nafion® 117 PEM adsorbed nearly the same amount of metal ions after five cycles of adsorption and desorption. Metal ions tested were Cu^{2+}, Ni^{2+}, Co^{2+}, Pb^{2+} and Ag^{+}. The results of Nasef and Yahaya (2009) were solely based on PEM, and not on MEA.

From the results there is reason to believe that the electrocatalyst of $FeSO_4$-MEA and $MgSO_4$-MEA were permanently damaged, as Nasef and Yahaya (2009) proved in their work that a Nafion® 117 could be restored completely. The results of Bas *et al*. (2010) found that cationic contamination of the MEA had a negative influence on MEA performance due to kinetic losses at both electrodes. The energy efficiencies of $FeSO_4$-MEA and $MgSO_4$-MEA after sulphuric acid regeneration indicated that degradation of the MEA had occurred.

SEM analyses of the MEA were completed after sulphuric acid regeneration and are given in Table 4-15.

Table 4-15 SEM elemental analysis results of inner PEM.

Elemental analysis	$FeSO_4$-MEA	$MgSO_4$-MEA
C	25.61	20.21
O	-	1.02
F	73.60	78.20
Mg	-	0.11
S	0.77	0.45
Total (weight%)	100	100

SEM results show traces of magnesium in $MgSO_4$-MEA after regeneration. No traces of iron are for $FeSO_4$-MEA SEM results. Bas *et al*. (2010) found that cationic contamination of the MEA influenced MEA performance negatively, due to kinetic losses that arose at both electrodes, particularly at the anode. The decreased energy efficiency of both $FeSO_4$-MEA and $MgSO_4$-

MEA after sulphuric acid regeneration was most likely due to electrocatalyst degradation of the MEA.

4.5.4 Comparison of $FeSO_4$-MEA and $MgSO_4$-MEA

As the experiments with Fe^{2+} and Mg^{2+} contaminants conducted on commercially available MEA were very similar, the effect of the different ions could be compared. A thorough description can be found in Sections 3.3.3 and 3.3.5. Figures 4-20 and 4-21 illustrate the summarised results of Tables 4-11, 4-12, 4-13 and 4-14.

(a) (b)

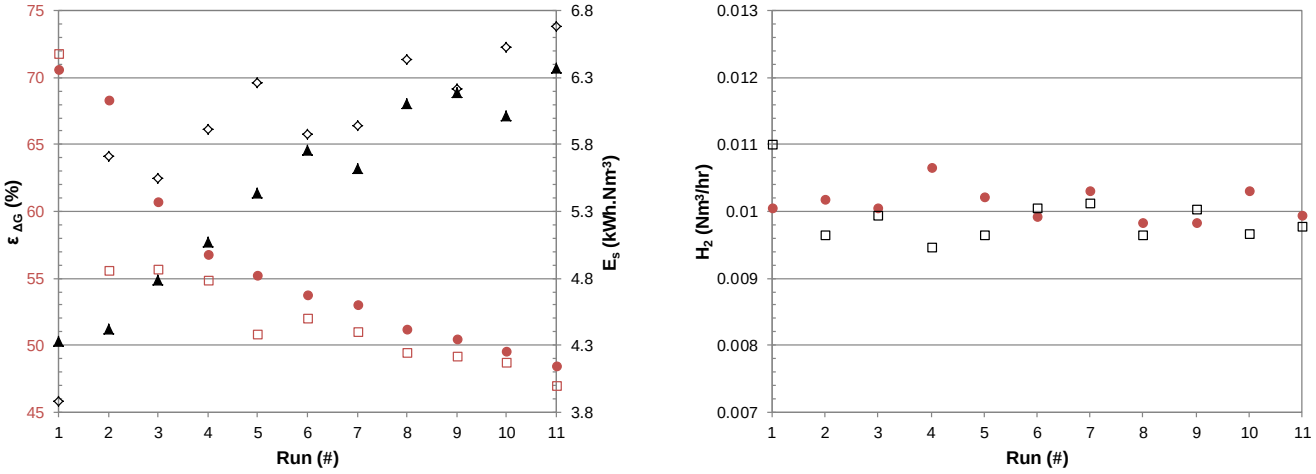

Figure 4-20 Comparison of $FeSO_4$-MEA and $MgSO_4$-MEA,
a)Energy efficiency and specific energy consumption at a current density of 0.5A.cm^{-2} and temperature of 30°C.
[$\varepsilon_{\Delta G}$: ● $FeSO_4$-MEA; □ $MgSO_4$-MEA] [E_S: ▲ $FeSO_4$-MEA; ◊ $MgSO_4$-MEA]
b)Hydrogen production at a current density of 0.5A.cm^{-2} and temperature of 30°C.
[●$FeSO_4$-MEA; □ $MgSO_4$-MEA]

(a) (b)

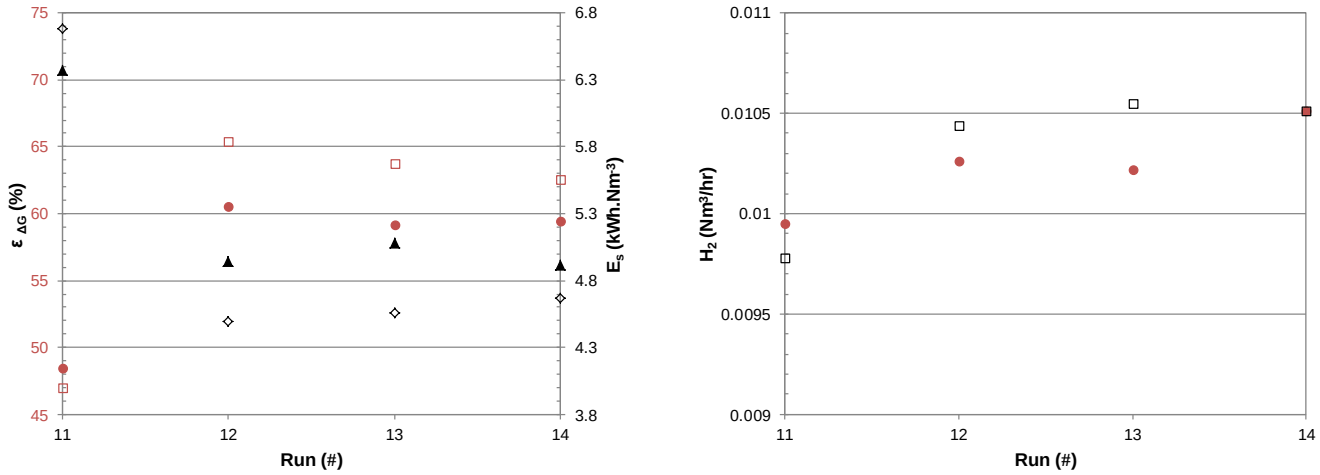

Figure 4-21 Regeneration of $FeSO_4$-MEA and $MgSO_4$-MEA,
a)Energy efficiency and specific energy consumption at a current density of 0.5A.cm^{-2} and temperature of 30°C.
[$\varepsilon_{\Delta G}$: ● $FeSO_4$-MEA; □ $MgSO_4$-MEA] [E_S: ▲ $FeSO_4$-MEA; ◊ $MgSO_4$-MEA]
b)Hydrogen production at a current density of 0.5A.cm^{-2} and temperature of 30°C.
[●$FeSO_4$-MEA; □ $MgSO_4$-MEA]

When comparing the energy efficiencies of both $FeSO_4$-MEA and $MgSO_4$-MEA in Figure 4-20 (a), the energy efficiency of the Nafion® 117 MEA is lower for Fe^{2+} than for Mg^{2+} at the same exposure times. Specific energy consumption of $MgSO_4$-MEA is also lower than $FeSO_4$-MEA at corresponding times of exposure. SEM analysis showed that Mg^{2+} was still present in the $MgSO_4$-MEA after regeneration, while no traces of iron were found in $FeSO_4$-MEA. Figure 4-20 shows that Mg^{2+} and Fe^{2+} exhibit similar decreases in electrolyser performance, with the performance of Mg^{2+} being better than that of Fe^{2+}. When the energy efficiencies of both MEA were compared to their uncontaminated energy efficiencies it was found that Mg^{2+} had a greater effect on performance reduction than Fe^{2+}.

From the comparison there was reason to believe that Mg^{2+} reduced the performance of the standard Nafion® 117 MEA more than that of Fe^{2+}.

4.5.5 Summarised remarks about iron and magnesium salt solutions

In this section the PEM water electrolyser performance was investigated with two commercial MEA from GES that were exposed to 100ppm concentrations of Fe^{2+} and Mg^{2+}. The results of Fe^{2+} and Mg^{2+} exhibited a decrease of energy efficiency and increase of specific energy consumption with exposure time to the metal ion solutions. SEM analysis showed the presence of Mg^{2+} in the PEM after sulphuric acid regeneration, but no traces of Fe^{2+} were found for $FeSO_4$-

MEA after sulphuric acid regeneration. From these results it was found that both Fe^{2+} and Mg^{2+} influenced PEM water electrolyser performance negatively and that permanent damage was inflicted on the electrocatalyst. From the results it is recommended that any water electrolyser system have a contaminant free water supply, as results showed that partial MEA regeneration was possible, but permanent damage was inflicted on the electrocatalyst of the MEA. In the event of water supply contamination for future applications it is recommended that a sulphuric acid wash regeneration cycle be made available to consumers to regenerate their MEA to an extent. This will reduce the additional costs associated with electrolyser maintenance.

4.6 PEM water electrolysis with aqueous methanol solutions

4.6.1 Introduction

The operation of PEM water electrolysers require a high purity of deionised water to prevent MEA contamination and maintain an adequate efficiency. In this section it was attempted to increase the efficiency and specific energy consumption by adding different concentrations of methanol to the feed water reservoir of the PEM electrolyser. MEA regeneration with sulphuric acid was evaluated in the attempt to restore the MEA to its original condition after the exposure to methanol. The performance results of both 1MeOH-MEA and 4MeOH-MEA are compared and discussed to reveal any degradation or performance enhancing effects for both 1M and 4M methanol concentrations on the MEA.

4.6.2 Experimental results and discussion

4.6.2.1 Influence of methanol concentration on electrolyser performance

The influence of methanol concentration on the performance of 1MeOH-MEA and 4MeOH-MEA was investigated by exposing the MEA to methanol solutions of 1M and 4M for a period of 46 hours. The performance data was generated by operating the electrolyser, as described in Section 3.3.4. The results are summarised in Tables 4-16 and 4-17.

Table 4-16 Effect of 1M Methanol solution [0.5A.cm^{-2}, 30°C]

Exposure (hours)	**Potential** (V)	**Hydrogen production** ($Nm^3.hr^{-1}$)	$\varepsilon_{\Delta G}$ (%)	E_S ($kWh.Nm^{-3}$)
0	1.815	0.0103	67.46	4.39
2	1.840	0.0106	66.57	4.34
4	2.010	0.0106	60.92	4.76
8	2.076	0.0108	59.00	4.81
12	2.073	0.0102	59.09	5.07
19	2.100	0.0101	58.32	5.20
26	2.150	0.0106	56.96	5.08
36	2.185	0.0098	56.05	5.59
46	2.220	0.0097	55.17	5.71

Table 4-17 Effect of 4M Methanol solution [0.5A.cm^{-2}, 30°C]

Exposure (hours)	**Potential** (V)	**Hydrogen production** ($Nm^3.hr^{-1}$)	$\varepsilon_{\Delta G}$ (%)	E_S ($kWh.Nm^{-3}$)
0	2.374	0.0105	51.58	5.66
2	1.549	0.0117	79.08	3.30
4	1.521	0.0119	80.52	3.20
8	1.590	0.0113	77.01	3.51
12	1.674	0.0112	73.16	3.73
19	1.532	0.0112	79.97	3.41
26	1.544	0.0119	79.30	3.23
36	1.858	0.0110	65.90	4.23
46	1.786	0.0113	68.56	3.95

The results of Table 4-16 illustrates the increase in cell voltage with the MEA exposed to a 1M methanol concentration. At 0 hours of methanol exposure and 0.5A.cm^{-2} current density the cell voltage was 1.815V relating to an energy efficiency of 67.46% and specific energy consumption 4.387 kWh.Nm^{-3}. After 12hours of methanol exposure the cell voltage increased to 2.073V, relating to an energy efficiency of 59.09% and specific energy consumption 5.07kWh.Nm^{-3}. After 12hours of methanol exposure the energy efficiency decreased by 8.37% and the specific energy consumption increased with 0.68kWh.Nm^{-3}. When comparing MEA methanol exposure of 46 hours to 12hours a decrease in energy efficiency and increase in specific energy consumption of 3.92% and 0.63kWh.Nm^{-3} are observed. The overall trend shows a decrease in PEM electrolyser performance over time.

A similar trend was observed with the results of Table 4-17, where the MEA was exposed to a 4M methanol concentration. At zero hours of methanol exposure and 0.5A.cm^{-2} current density the cell voltage of 2.374V was considered an error as the MEA had just been in contact with the methanol solution. At 2 hours of methanol exposure a cell voltage of 1.549V, which relates to an energy efficiency and specific energy consumption of 79.08% and 3.30kWh.Nm^{-3}, is observed. After 12hours of methanol exposure the cell voltage increases to 1.674V, relating to an energy efficiency of 73.16% and specific energy consumption 3.734kWh.Nm^{-3}. After 26hours of methanol exposure a cell voltage of 1.544V, which relates to an energy efficiency of 79.30% and specific energy consumption of 3.23kWh.Nm^{-3} is observed. Methanol exposure times of 36 and 46hours shows cell voltages of 1.858 and 1.786V which relate to energy efficiencies of 65.90 and 68.56% respectively. The specific energy consumption for 36 and 46 hours of exposure are 4.230 and 3.94kWh.Nm^{-3}respectively. The trend for Table 4-17 shows oscillating cell voltages but had

an overall increase in cell voltage and specific energy consumption and a decrease in energy efficiency.

The polarisation curves of the aqueous methanol experiments illustrate a point of crossover and also an increasing activation voltage in Figures 4-22 and 4-23.

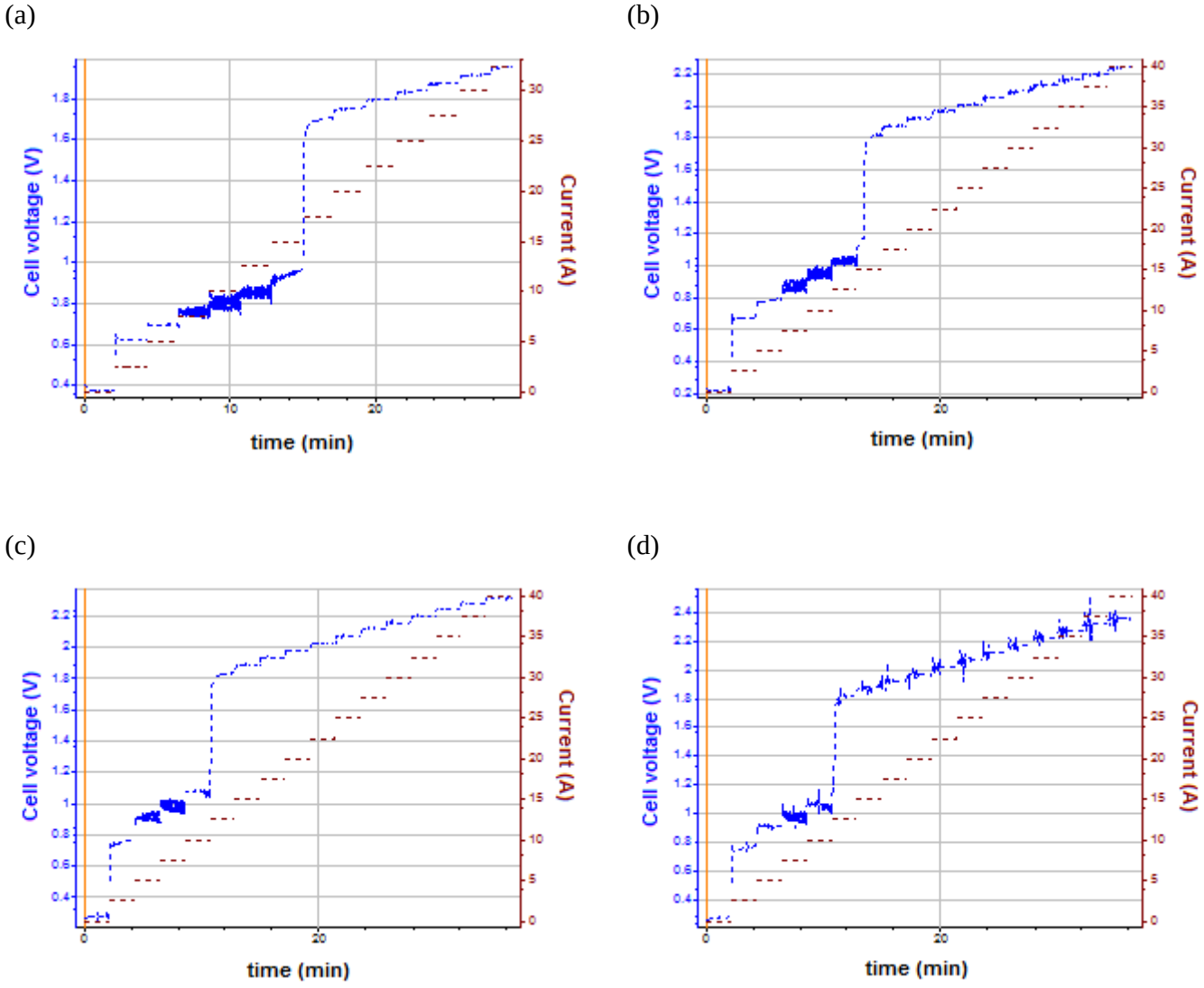

Figure 4-22 Cell voltage and current vs. time for 1MeOH-MEA, a) 2 hours exposure (0M methanol), b) 4 hours exposure, c) 8 hours exposure, d) 12 hours exposure.

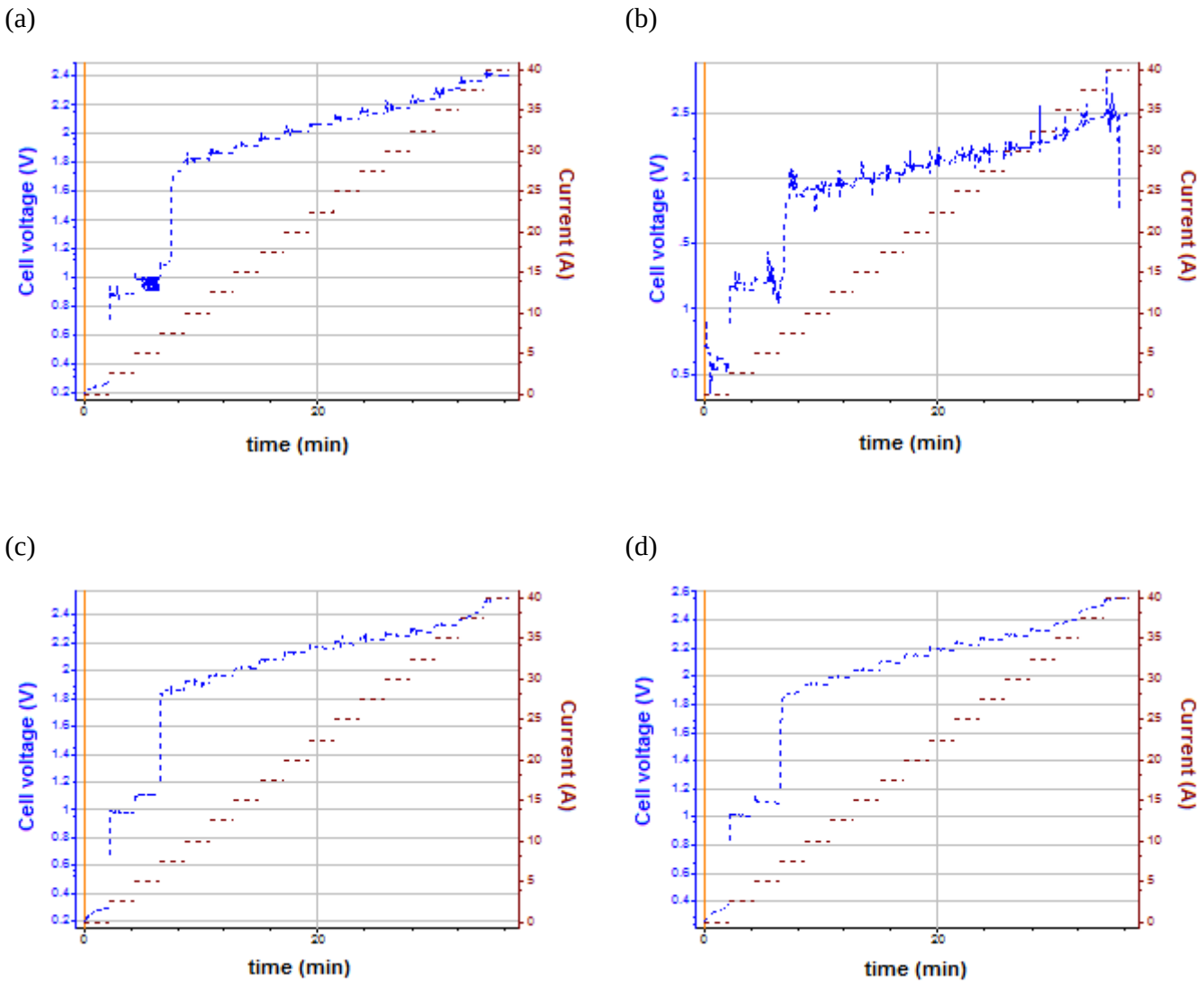

Figure 4-23 Cell voltage and current vs. time for 1MeOH-MEA, a) 19 hours exposure, b) 26 hours exposure, c) 36 hours exposure, d) 46 hours exposure.

Figures 4-22 and 4-23 show that 1M methanol solution has a substantial effect on the measured cell voltage. Figure 4-22 (a) illustrates that a cell voltage of ~0.62 V was required for operation at a current density of 0.05 $A.cm^{-2}$. When the current density reaches 0.35 $A.cm^{-2}$ an increase of cell voltage is observed (~0.7 V). Thereafter a constant increase of cell voltage is observed. Figure 4-22 (b) illustrates similar results, but the activation cell voltage required at 0.05 $A.cm^{-2}$ increases (~0.68 V) and the increase (~0.8 V) took place at a lower current density (0.3 $A.cm^{-2}$). Figures 4-22 (c) and (d) also exhibited similar results, where the increase of cell voltage took place at lower current densities than that observed in Figure 4-22-b and the activation voltage required at 0.05 $A.cm^{-2}$ also increases. Figure 4-23 (a), (b), (c) and (d) required activation voltages of 0.9 V, 1.2 V, 1.0 V and 1.0 V.

From the results of Figure 4-22 and Figure 4-23 it can be observed that the activation voltage for the reaction to commence at 0.05 A.cm^{-2} increases from ~ 0.62 V to ~1.0 V. The increase in cell voltage started to occur at lower current densities, with the initial increase taking place at 0.35 A.cm^{-2} and the last two experiments at a current density of 0.1 A.cm^{-2}.

The results of Figures 4-22 and 4-23 show that a reaction was taking place at a cell voltage below that of standard water electrolysis. With aqueous methanol electrolysis starting to occur at 0.016V and water electrolysis at 1.229, it was clear that aqueous methanol electrolysis was occurring at lower current densities. Once the current density of the cell reached a value between 0.15 and 0.35 A.cm^{-2} the cell voltage increased to a value above that of standard water electrolysis. The results indicate that aqueous methanol electrolysis alone could not be sustained at higher current densities. At this point it is believed that a combination of aqueous methanol and standard water electrolysis took place.

With the increase in cell voltage initially taking place at 0.35 A.cm^{-2} and at a later stage at 0.15 A.cm^{-2} it was decided to investigate the ohmic resistance of 1MeOH-MEA at the different times of exposure.

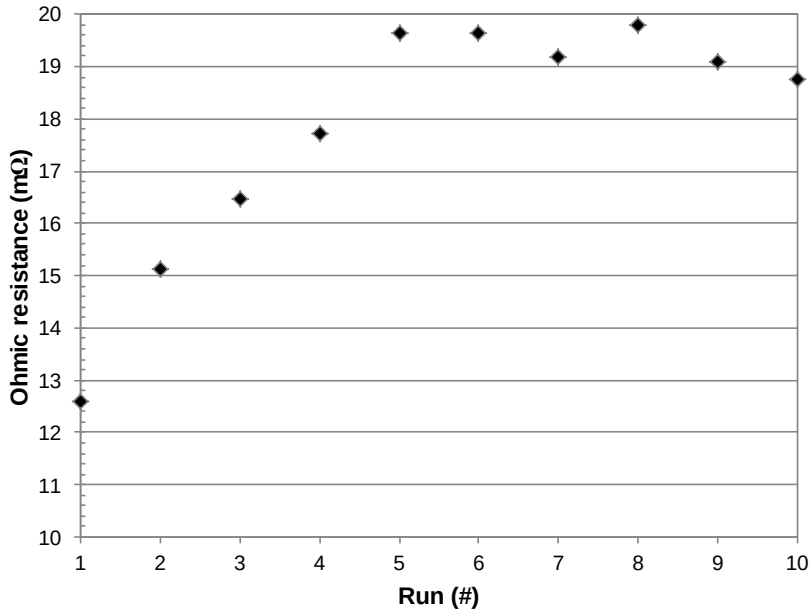

Figure 4-24 Calculated ohmic resistance of 1MeOH-MEA during 1M methanol solution experiments.

Figure 4-24 shows the calculated ohmic overpotential of the 1M methanol experiments. The results of Figure 4-24 demonstrates how the ohmic resistance of 1MeOH-MEA increases over time and stabilises at ~19.5 mΩ. Run 10 of Figure 4-24 illustrates the ohmic resistance of regeneration 1 and this will be discussed in Section 4.6.2.2.

The polarisation curves of the 4M aqueous methanol experiments also illustrate a point of crossover and also an increasing activation voltage in Figures 4-25 and 4-26.

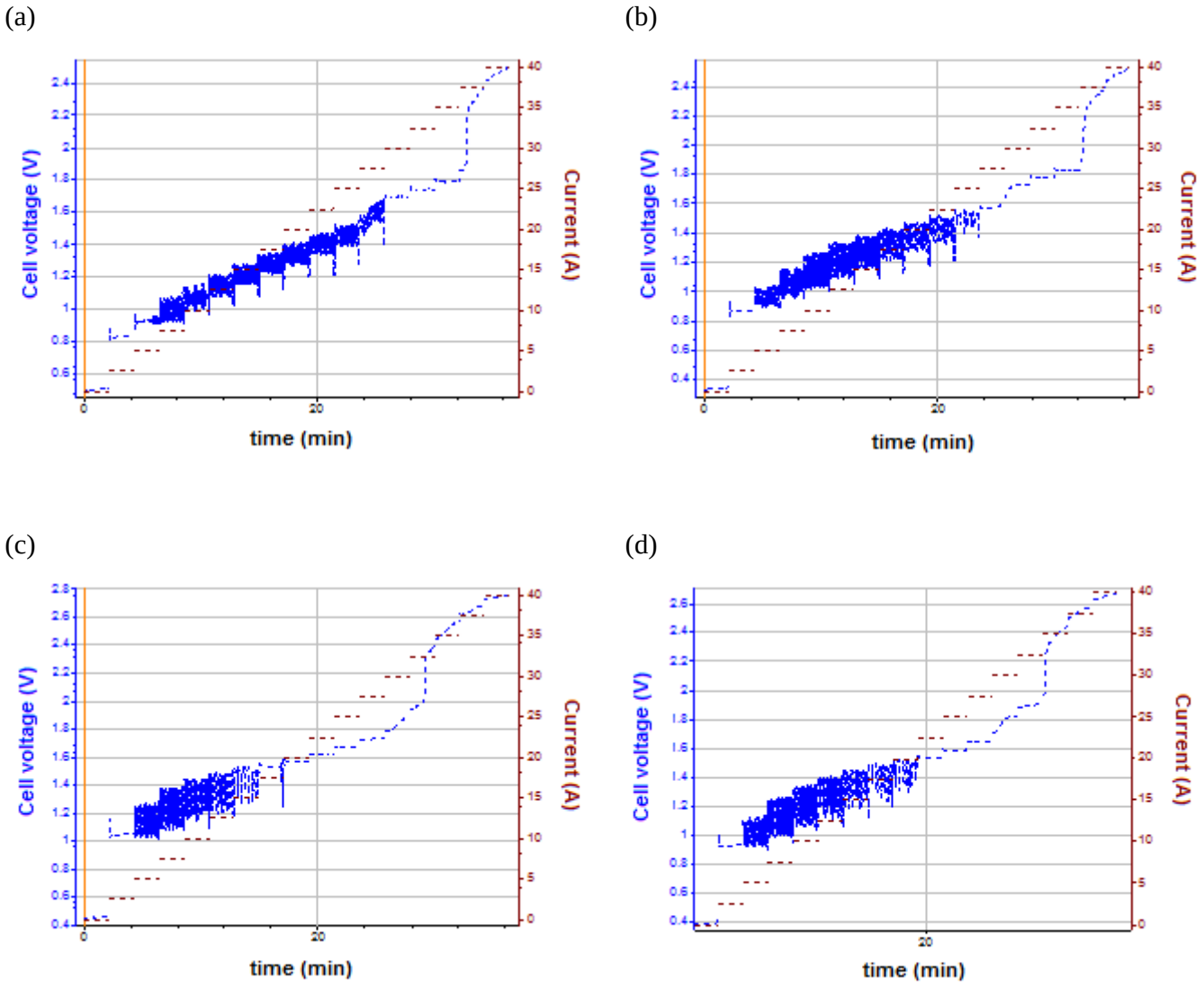

Figure 4-25 Cell voltage and current vs. time for 4MeOH-MEA, a) 2 hours exposure (0M methanol), b) 4 hours exposure, c) 8 hours exposure, d) 12 hours exposure.

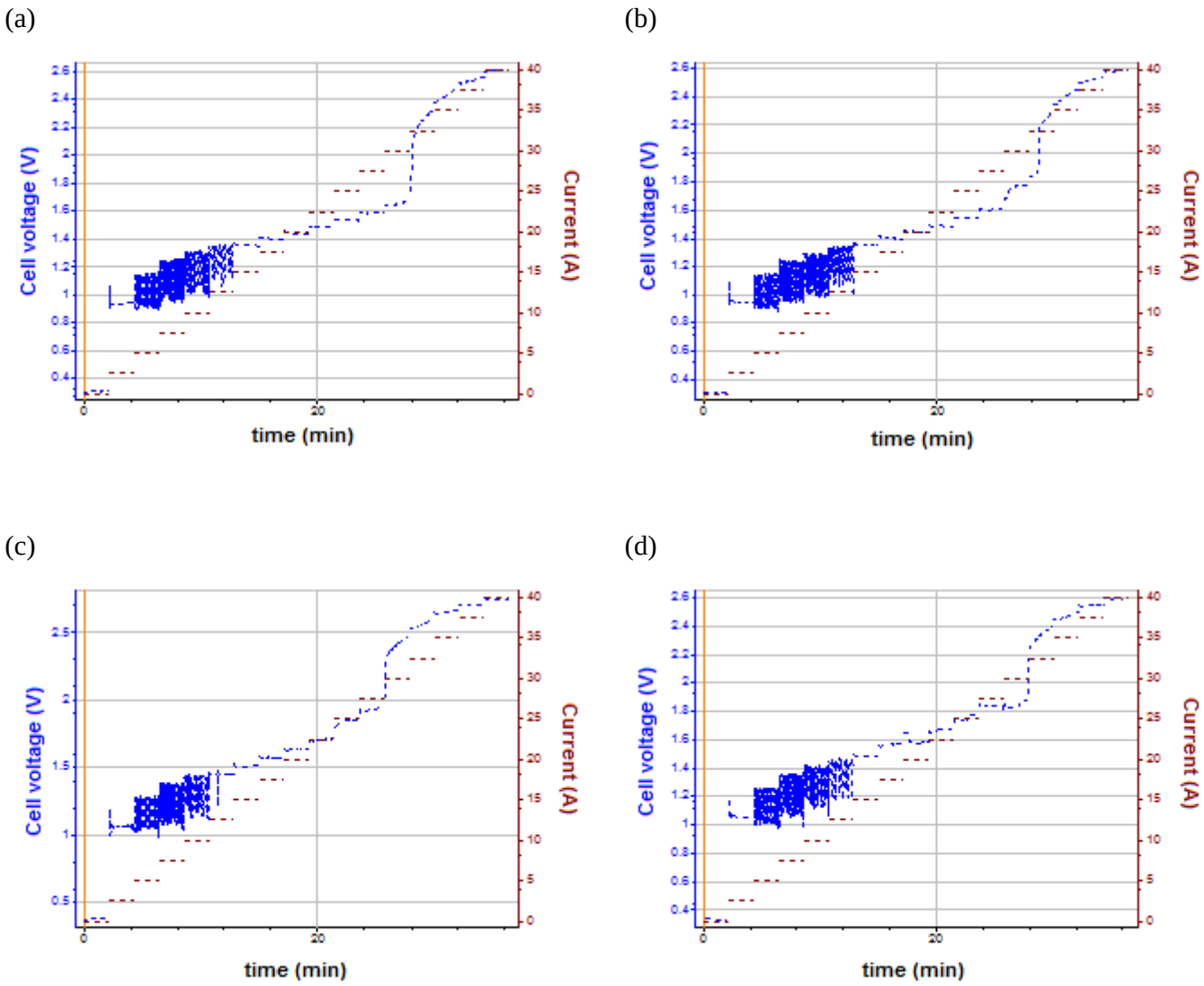

Figure 4-26 Cell voltage and current vs. time for 1MeOH-MEA, a) 19 hours exposure, b) 26 hours exposure, c) 36 hours exposure, d) 46 hours exposure.

Figures 4-25 and 4-26 show that 4M aqueous methanol solution has a substantial effect on the measured cell voltage. Figure 4-25 (a) illustrates that a cell voltage of ~0.82 V is required for operation at a current density of 0.05 A.cm^{-2}. When the current density reaches 0.75 A.cm^{-2} a sudden increase of cell voltage is observed (~0.45 V). Figure 4-25 (b) illustrates similar results, but the cell voltage required at 0.05 A.cm^{-2} increases (~0.87 V), and the increase of cell voltage takes place at a current density of 0.75 A.cm^{-2}. Figures 4-25 (c) and (d) also exhibit similar results with the first increase of cell voltage taking place at a lower current density of 0.55 and 0.70 A.cm^{-2} and the activation voltage required at 0.05 A.cm^{-2} increases to ~1.0 V. Figures 4-26 (a) and (b) required activation voltages of ~ 0.95 V and the increase in cell voltage occurred at 0.65 A.cm^{-2}. Figures 4-26 (c) and (d) required activation voltages of ~1.1 V and the increase in cell voltage occurs at 0.6 A.cm^{-2}. Figures 4-25 and 4-26 show that the activation voltage for the

reaction at 0.05 A.cm^{-2} increased from ~ 0.82 V to ~1.1 V. This increase in cell voltage started to occur at lower current densities over time, with the initial increase taking place at 0.75 A.cm^{-2} and the last two experiments at a current density of 0.60 A.cm^{-2}.

The results of Figures 4-25 and 4-26 exhibited results similar to those of 1MeOH-MEA in Figures 4-22 and 4-23. A reaction was also taking place at a cell voltage below that of standard water electrolysis. The results show that aqueous methanol electrolysis was present at cell voltages below 1.229V. After this point it is believed that a combination of aqueous methanol and standard water electrolysis took place. Once the current density of the cell reached a value between 0.60 and 0.75 A.cm^{-2} the cell voltage increased substantially, where it is believed that in the majority, water electrolysis was taking place.

The effect of ohmic resistance for 4MeOH-MEA was also investigated relative to exposure time and is illustrated in Figure 4-27.

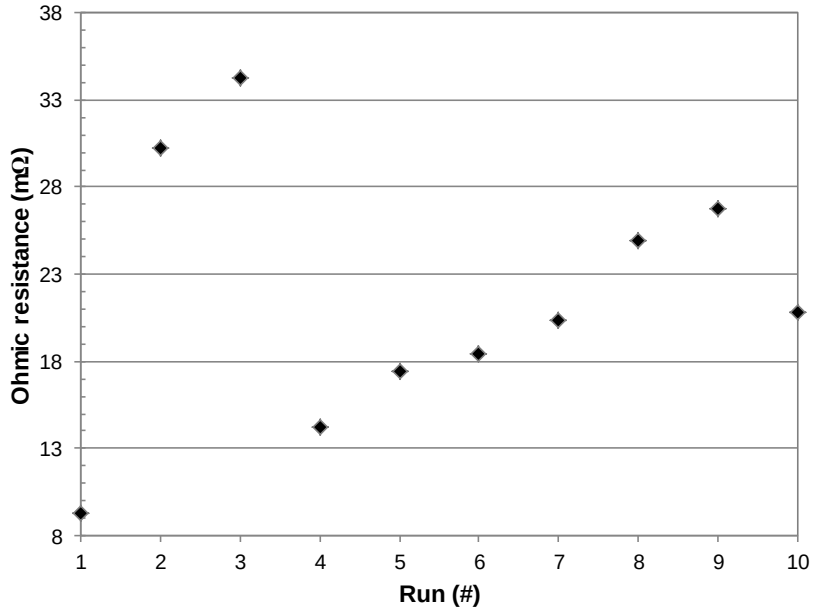

Figure 4-27 Calculated ohmic resistance of 4MeOH-MEA during 4M methanol solution experiments.

The ohmic resistance of 4MeOH-MEA increases and decreases drastically. A fairly constant increase of ohmic resistance occurred from run 4 (8 hour exposure time) to run 9 (46 hour exposure time). Run 10 in Figure 4-26 illustrates the ohmic resistance of the second regeneration of 4MeOH-MEA and shows a decrease in ohmic resistance. The regeneration of 4MeOH-MEA will be discussed in Section4.6.2.2.

Similar results with regard to aqueous methanol electrolysis, have been reported by Take *et al*. (2007) and Cloutier and Wilkinson (2010). Take *et al*. (2007) found that a current density lower

than 0.35 A.cm^{-2} produced a constant voltage, but as soon as the current density reached 0.39 A.cm^{-2} the voltage increased. After 40 minutes, a rapid increase in cell voltage took place, to a value equivalent to that of water electrolysis at 0.43 A.cm^{-2}. Take *et al*. (2007) believes that the applied current could not be maintained with methanol oxidation alone, which led to a voltage increase at which the oxygen evolution reaction could also take place. Cloutier and Wilkinson (2010) also found that lower current densities allowed for stable oxidation of methanol and high current densities, could not be sustained solely by methanol oxidation resulting in increased cell voltage and other undesirable side-reactions. Cloutier and Wilkinson (2010) also confirmed that the MEA resistance (ohmic overpotential) increased with increasing methanol concentration. Cloutier and Wilkinson (2010) also found that higher methanol concentrations could sustain higher current densities at steady voltages.

The hydrogen production rate of aqueous methanol electrolysis, compared to standard water electrolysis, is illustrated in Figure 4-28.

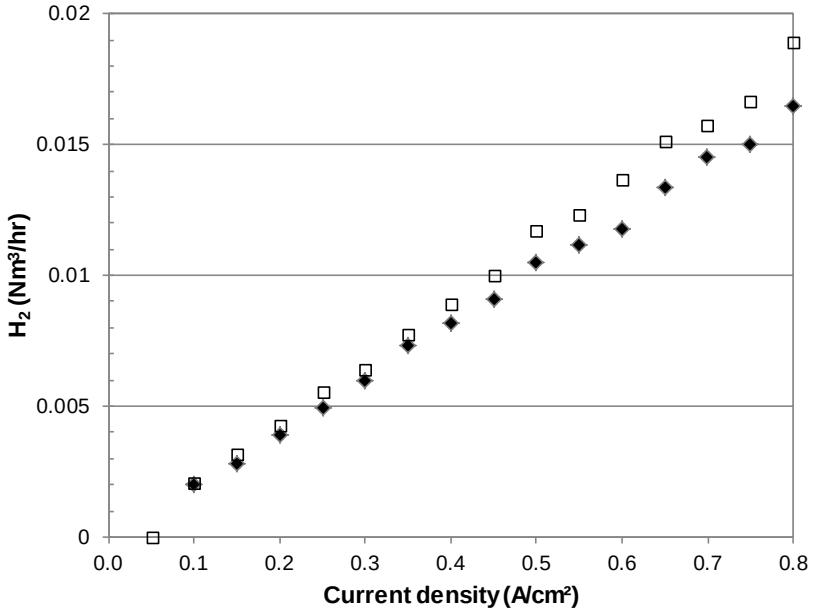

Figure 4-28 Hydrogen production rate at 30°C and 0 bar$_{(g)}$.
[● water electrolysis; □ 4M aqueous methanol electrolysis]

From Figure 4-28 it is clear that aqueous methanol electrolysis did exhibit improved hydrogen generation. From Figures 4-22, 4-23, 4-25 and 4-26 it was found that the reaction taking place at low current densities was in fact aqueous methanol electrolysis and that water electrolysis started occurring at higher current densities, depending on the methanol concentration. Methanol concentrations influenced the current densities at which the methanol oxidation took place and it was concluded that higher methanol concentrations allow for methanol oxidation at higher

current densities. When comparing the calculated ohmic resistances of 1M and 4M methanol solutions, the MEA resistance increased with increasing methanol concentration. These results correspond to the end result of Cloutier and Wilkinson (2010).

4.6.2.2 Influence of sulphuric acid regeneration

The influences of sulphuric acid regeneration of 1MeOH-MEA and 4MeOH-MEA were investigated by submerging the MEA separately in sulphuric acid for 16 hours under magnetic agitation. The MEA were then tested in the PEM water electrolyser and generated the performance data of Tables 4-18 and 4-19, and Figure 4-29.

Table 4-18 Regeneration of 1M methanol MEA [0.5A.cm^{-2}, 30°C]

Exposure (hours)	**Potential** (V)	**Hydrogen production** ($Nm^3.hr^{-1}$)	$\varepsilon_{\Delta G}$ (%)	E_S ($kWh.Nm^{-3}$)
46	2.220	0.00972	55.17	5.71
Regen1	2.219	0.01002	55.19	5.53
Regen2	2.485	0.01025	49.28	6.06
Regen3	2.653	0.01078	46.16	6.15

Table 4-19 Regeneration of 4M methanol MEA [0.5A.cm^{-2}, 30°C]

Exposure (hours)	**Potential** (V)	**Hydrogen production** ($Nm^3.hr^{-1}$)	$\varepsilon_{\Delta G}$ (%)	E_S ($kWh.Nm^{-3}$)
46	1.786	0.01131	68.56	3.95
Regen1	2.138	0.00991	57.29	5.39
Regen2	1.848	0.01074	66.26	4.30
Regen3	1.891	0.01040	64.77	4.54

(a) (b)

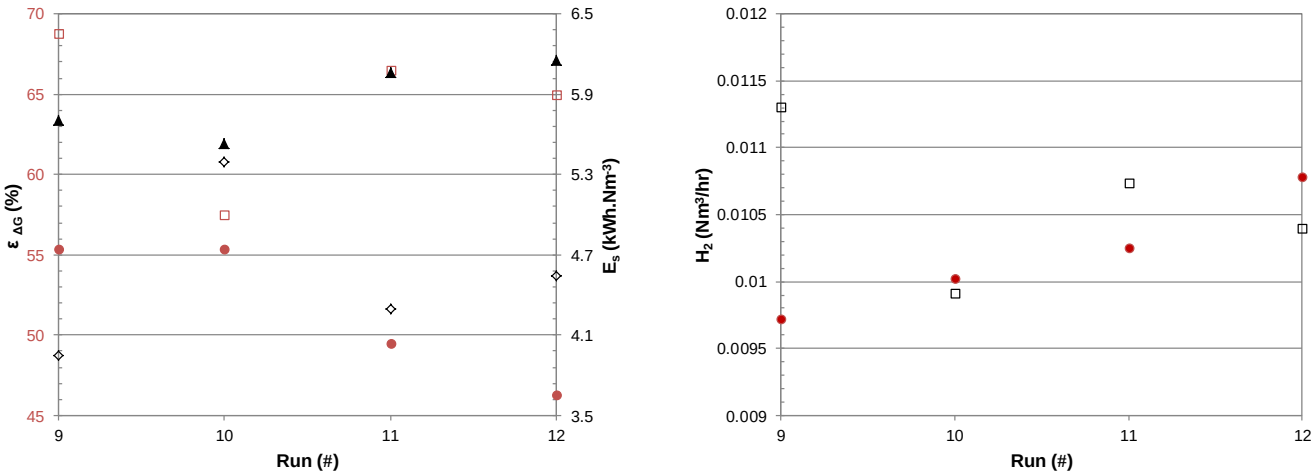

Figure 4-29 Comparison of 1MeOH-MEA and 4MeOH-MEA
a)Energy efficiency and specific energy consumption at a current density of 0.5A.cm^{-2} and temperature of 30°C.
[$\varepsilon_{\Delta G}$: ● 1MeOH-MEA; □ 4MeOH-MEA] [E_S: ▲ 1MeOH -MEA; ◊ 4MeOH-MEA]
b)Hydrogen production at a current density of 0.5A.cm^{-2} and temperature of 30°C.
[● 1MeOH -MEA; □ 4MeOH -GDE]

The regeneration results of 1MeOH-MEA and 4MeOH-MEA with sulphuric acid had an overall decrease on electrolyser performance. When the energy efficiency of 1MeOH-MEA with an exposure time of 46 hours (Table 4-18) is compared to the third regeneration experiment, a clear decrease in energy efficiency (~9%) is observed. When the energy efficiency of 4MeOH-MEA with an exposure time of 46 hours (Table 4-19) is compared to the third regeneration experiment, a decrease (~4%) is observed. The effect of MEA regeneration on the specific energy consumption of both 1MeOH-MEA (Table 4-18) and 4MeOH-MEA (Table 4-19) shows an increase of ~0.45 and ~0.6 kWh.Nm^{-3} when compared to the 46 hour exposure time of each of the experiments. Comparison of the initial experiments (0 M methanol) with the third regeneration experiment for both 1MeOH-MEA and 4MeOH-MEA, showed a 0.838 V increase of cell voltage for 1MeOH-MEA and a 0.483 V decrease of cell voltage for 4MeOH-MEA. It should be noted that the initial experiment of 1MeOH-MEA with water, had a high overpotential present when compared to 1.879 V at 30°C and 0 bar$_{(g)}$ (Table 4-5). As both the MEA were the same, one can assume that an unforeseen overpotential of experimental error occurred, related to a higher cell voltage. The comparison of the third regeneration experiment of 4MeOH-MEA with the initial water experiment at 30°C and 0 bar$_{(g)}$ (Table4-5), shows that a thorough regeneration of 4MeOH-MEA took place.

4.6.3 Summarised remarks about methanol solutions

In this section the PEM water electrolyser performance was investigated with two aqueous solutions of methanol, 1M and 4M concentrations poured into the water supply reservoir. It was found that methanol oxidation took place at low current densities. For the case where current densities reached higher values, a jump from methanol oxidation to normal water electrolysis took place. Results showed that the concentration of the aqueous methanol solution had an influence on the current density at which the water electrolysis commenced. It was found that higher concentrations of methanol increased transition current density at which water electrolysis started to occur. It is recommended that aqueous methanol electrolysis be conducted at current densities below those at which water electrolysis takes place. Further recommendations involve testing the effect of aqueous methanol oxidation at very high concentrations (16M and higher) and investigating different electrocatalysts to optimise aqueous methanol oxidation performance.

4.7 References

BARBIR, F. 2005. PEM electrolysis for production of hydrogen from renewable energy sources. *Solar energy,* 78(5):661-669.

BAS, C., ALBÉROLA, N.D. & FLANDIN, L. 2010. Effects of contaminant on thermal properties in perfluorinated sulfonic acid membranes. *Journal of membrane science,* 363(1-2):67-71.

BIAKU, C.Y., DALE, N.V., MANN, M.D., SALEHFAR, H., PETERS, A.J. & HAN, T. 2008. A semiempirical study of the temperature dependence of the anode charge transfer coefficient of a 6 kW PEM electrolyzer. *International journal of hydrogen energy,* 33(16):4247-4254.

CLOUTIER, C.R. & WILKINSON, D.P. 2010. Electrolytic production of hydrogen from aqueous acidic methanol solutions. *International journal of hydrogen energy,* 35(9):3967-3984.

COLLIER, A., WANG, H., ZI YUAN, X., ZHANG, J. & WILKINSON, D.P. 2006. Degradation of polymer electrolyte membranes. *International journal of hydrogen energy,* 31(13):1838-1854.

GRIGORIEV, S.A., MILLET, P., VOLOBUEV, S.A. & FATEEV, V.N. 2009. Optimization of porous current collectors for PEM water electrolysers. *International journal of hydrogen energy,* 34(11):4968-4973.

ITO, H., MAEDA, T., NAKANO, A., HASEGAWA, Y., YOKOI, N., HWANG, C.M., ISHIDA, M., KATO, A. & YOSHIDA, T. 2010. Effect of flow regime of circulating water on a proton exchange membrane electrolyzer. *International journal of hydrogen energy,* 35(18):9550-9560.

LEBBAL, M.E. & LECŒUCHE, S. 2009. Identification and monitoring of a PEM electrolyser based on dynamical modelling. *International journal of hydrogen energy,* 34(14):5992-5999.

MILLET, P., MBEMBA, N., GRIGORIEV, S.A., FATEEV, V.N., AUKAULOO, A. & ETIÉVANT, C. 2011. Electrochemical performances of PEM water electrolysis cells and perspectives. *International journal of hydrogen energy,* In Press, Corrected Proof.

MILLET, P., DRAGOE, D., GRIGORIEV, S., FATEEV, V. & ETIEVANT, C. 2009. GenHyPEM: A research program on PEM water electrolysis supported by the european commission. *International journal of hydrogen energy,* 34(11):4974-4982.

MILLET, P., NGAMENI, R., GRIGORIEV, S.A., MBEMBA, N., BRISSET, F., RANJBARI, A. & ETIÉVANT, C. 2010. PEM water electrolyzers: From electrocatalysis to stack development. *International journal of hydrogen energy,* 35(10):5043-5052.

NASEF, M.M. & YAHAYA, A.H. 2009. Adsorption of some heavy metal ions from aqueous solutions on nafion 117 membrane. *Desalination,* 249(2):677-681.

NI, M., LEUNG, M.K.H. & LEUNG, D.Y.C. 2008. Energy and exergy analysis of hydrogen production by a proton exchange membrane (PEM) electrolyzer plant. *Energy conversion and management,* 49(10):2748-2756.

NIEMINEN, J., DINCER, I. & NATERER, G. 2010. Comparative performance analysis of PEM and solid oxide steam electrolysers. *International journal of hydrogen energy,* In Press, Corrected Proof.

SEIDENBERGER, K., WILHELM, F., SCHMITT, T., LEHNERT, W. & SCHOLTA, J. 2011. Estimation of water distribution and degradation mechanisms in polymer electrolyte membrane fuel cell gas diffusion layers using a 3D monte carlo model. *Journal of power sources,* 196(12):5317-5324.

SONG, S., ZHANG, H., MA, X., SHAO, Z., BAKER, R.T. & YI, B. 2008. Electrochemical investigation of electrocatalysts for the oxygen evolution reaction in PEM water electrolyzers. *International journal of hydrogen energy,* 33(19):4955-4961.

TAKE, T., TSURUTANI, K. & UMEDA, M. 2007. Hydrogen production by methanol–water solution electrolysis. *Journal of power sources,* 164(1):9-16.

THANASILP, S. & HUNSOM, M. 2010. Effect of MEA fabrication techniques on the cell performance of Pt–Pd/C electrocatalyst for oxygen reduction in PEM fuel cell. *Fuel,* 89(12):3847-3852.

Conclusions and Recommendations

Contents

5.1 Conclusions

5.1.1 Objectives

In this dissertation it was shown that PEM water electrolysis can operate with both Gas Diffusion Electrodes (GDE) and Membrane Electrode Assemblies (MEA) and that the presence of cations and methanol alter subsequent electrolyser performance.

5.1.2 Synthesis of NS-MEA and PS-MEA

This research showed that a MEA can be synthesised on Proton Exchange Membranes (PEM) with platinum black by means of the Catalyst-Coated Membrane Direct Spray (CCM-DS) method. The synthesis plan was carried out with the MEA of NS-MEA and PS-MEA. NS-MEA was synthesised correctly and displayed adequate performance.

In terms of PEM selection, Nafion® exhibited good overall results when compared to PBI-sPSU, as the electrocatalyst layer did not bond with PBI-sPSU and the PBI-sPSU was found to be more fragile.

5.1.3 Performance of N-MEA and N-GDE

The performance data of a PEM water electrolyser was evaluated with both MEA and GDE components.

In terms of water temperature, it was found that activation overpotential was lower for both N-MEA and N-GDE at increasing temperatures. Both the MEA and GDE exhibited lower cell voltages at increased water temperature and demonstrated that the energy efficiency was dependent on water temperature.

In terms of cathode pressure, it was found that the energy efficiency was higher at increased cathode pressure and that the cell voltage increased slightly as pressure increased. Both the MEA and GDE exhibited comparable results at increased cathode pressure and demonstrated that increased pressure affected both components in the same way.

In terms of component type, N-MEA exhibited lower overall cell voltages at increasing current densities when compared to N-GDE. This is most likely due to the superior electrocatalyst contact of N-MEA between the PEM and electrocatalyst.

5.1.4 Performance of $FeSO_4$-MEA and $MgSO_4$-MEA

The performance of a PEM water electrolyser was evaluated with Fe^{2+} and Mg^{2+} concentrations in the process water.

In terms of cation concentrations, both Fe^{2+} and Mg^{2+} had a significant effect on performance with increasing exposure time. Both Fe^{2+} and Mg^{2+} demonstrated comparable results in terms of energy efficiency and specific energy consumption.

In terms of sulphuric acid regeneration, it was found that the performance of $FeSO_4$-MEA and $MgSO_4$-MEA had increased, but not to its original condition. Both Fe^{2+} and Mg^{2+} demonstrated signs of PEM and electrocatalyst degradation.

5.1.5 Performance of 1MeOH-MEA and 4MeOH-MEA

The performance data of a PEM water electrolyser was evaluated with 1M and 4M aqueous methanol concentrations in the electrolyser water reservoir.

In terms of activation cell voltage, lower current densities produced low cell voltage values as aqueous methanol electrolysis took place. Increased current densities resulted in a substantial increase in cell voltage as both aqueous methanol and water electrolysis took place.

In terms of aqueous methanol concentration, it was found that higher concentrations increased the transition current density at which water electrolysis started to occur.

5.2 Recommendations

Future work following the work of this dissertation would be to create a PBI-sPSU MEA by implementing a PBI solution in the catalyst ink and to compare it with a Nafion® MEA of similar thickness. The electrocatalyst suggested to be used should be Pt/Ir as anode catalyst and Pt as cathode catalyst. It is recommended that the water supply of PEM water electrolysers be free from contaminants. For the event where contamination of the MEA has taken place, further studies of sulphuric acid wash should be completed to quantify and qualify the process conditions. This will reduce the additional costs of new MEA and installation costs. Further recommendations are to test the effect of aqueous methanol oxidation at very high concentrations (16M and higher) and to test different electrocatalyst to optimise aqueous methanol oxidation performance.

Appendix A: Experimental Error

Standard Deviation

As with all experiments it is essential to know the accuracy at which the experiments are conducted. For the case of PEM water electrolysis the results are in the form of hydrogen flow rate and polarisation curves.

The polarisation curves are measurements of potential (V) at varying current densities ($A.cm^{-2}$) which are stepped in a timely fashion every two minutes. EC-lab measures and stores both the values of potential and current density every second. Results are copied into the Microsoft Excel spread sheet where the filters are setup to convert the current (mA) values to current density ($A.cm^{-2}$) and voltages (mV→V). Microsoft Visual basic for applications then copies the voltage values just before the step change in current density takes place. These values are copied into a table above the raw data and are used for the purpose of polarisation curves.

To find the confidence level for the populations (polarisations curves) at hand the standard deviation (σ) has to be known for the z-curve which is approximately standard to normal to be calculated.

$$z = \frac{\bar{x} - \mu}{\sigma/\sqrt{n}}$$

where $\bar{x}$ is the sample distribution, μ the population mean and n the number of populations.

The population standard deviation for the experimental results is not known and for that reason it is replaced with sample standard deviation (s).

$$z = \frac{\bar{x} - \mu}{s/\sqrt{n}}$$

For a large enough value of n the new distribution will also approximately have a standard to normal distribution. The z curve with an area of 0.95 and critical values of 1.96 and -1.96 can be manipulated to produce the following:

$$\bar{x} - 1.96\frac{s}{\sqrt{n}} < \mu < \bar{x} + 1.96\frac{s}{\sqrt{n}}$$

The upper and lower confidence levels for the approximate 95% confidence level can be written as:

$$\bar{x} - 1.96\frac{s}{\sqrt{n}} \; and \; \bar{x} + 1.96\frac{s}{\sqrt{n}}$$

Polarisation curve results are processed by, firstly, calculating average values of the populations for each current density under the column named Average. Secondly, the standard deviation of the populations for each current density is calculated with the STDEV function embedded in Excel and these values appear in the column named SD. Thirdly, the upper/lower limit is calculated by multiplying the upper critical value of the 95% confidence level z curve with the standard deviation (s) (as calculated in the previous step) and is divided by the square root of the number of populations (n). This is also done for every current density and appears in the column named 95% Cl. Lastly, the upper/lower limit (as calculated in the previous step) is divided by the average value as calculated in the first step and this is also done for every current density and these values are listed in Ave. 95% Cl. The average of these values appears in the cell directly under the heading of Ave. 95% Cl is calculated by taking the average of the values calculated previously (Devore *et al.*, 2005:605).

References

DEVORE, J. & FARNUM, N., eds. 2005. Applied statistics for engineers and scientists . 2nd ed. Belmont, CA: Thomson Brooks/Cole. 605.

Appendix B: Experimental Calculations

Calculations of Gibbs free energy, enthalpy and entropy:

The Shomate equation was used to calculate the specific values of enthalpy, entropy and finally the Gibbs free energy for water formation (The National Institute of Standards and Technology (NIST)., 2011.).

$$H°_T - H°_{298.15} = A(t) + B\left(\frac{t^2}{2}\right) + C\left(\frac{t^3}{3}\right) + D\left(\frac{t^4}{4}\right) - \frac{E}{t} + F - H \quad \text{B.1}$$

$$S° = A(\ln(t)) + B(t) + C\left(\frac{t^2}{2}\right) + D\left(\frac{t^3}{3}\right) - \frac{E}{2t^2} + G \quad \text{B.2}$$

$$G°_T = H°_T - T \times S° \quad \text{B.3}$$

H° = standard enthalpy (kJ.mol^{-1})

S° = standard entropy (J.mol^{-1}.K^{-1})

t = temperature (K) / 1000.

Standard cell voltage calculations:

The standard cell voltage (V°) is commonly used in calculating the energy efficiency of an electrochemical reaction. The total Gibbs free energy of formation for the electrochemical reaction is divided by the number of electrons transferred and the Faraday constant (F = 96485 C.mol^{-1}).

$$V° = \frac{\Delta \boldsymbol{G_f^\circ}}{\boldsymbol{zF}} \quad \text{B.4}$$

The Gibbs free energy of formation for the reaction is calculated by subtracting the product's Gibbs free energy of formation from the reagent's Gibbs free energy of formation.

$$\Delta \boldsymbol{G_{f\,total}^\circ} = \sum_{products} \Delta \boldsymbol{G_f^\circ} - \sum_{reagents} \Delta \boldsymbol{G_f^\circ}$$

The reactions of water electrolysis and water/methanol electrolysis take place in the PEM water electrolyser according to Eq. B.2 and B.3.

$$H_2O_{(l)} \xrightarrow[\Delta]{} H_{2(g)} + \frac{1}{2}\, O_{2(g)} \quad \text{B.5}$$

$$CH_3OH + H_2O_{(l)} \xrightarrow[\Delta]{} 3H_{2(g)} + CO_2 \qquad \text{B.6}$$

The standard cell voltage for water and water/methanol electrolysis can be calculated as

$$V°_{H_2O,298.15} = \frac{(-38962.1 - 61164.9\,J.mol^{-1}) - (-237150\,J.mol^{-1})}{2 \times 96485\,C.mol^{-1}}$$

$$= 1.229\,V$$

$$V°_{MeOH,303.15} = \frac{(-458334 + 3(-39616.7)\,J.mol^{-1}) - (-276958 - 307038\,J.mol^{-1})}{6 \times 96485\,C.mol^{-1}}$$

$$= 0.011766\,V$$

These calculated voltages are used in determining the energy efficiencies of water and water/methanol electrolysis.

Temperature (°C/K)	Standard cell potential: Water electrolysis (V)	Standard cell potential: Methanol electrolysis (V)
25/298.15	1.229	0.0153
30/303.15	1.225	0.0118
40/313.15	1.216	0.0047
50/323.15	1.208	-0.0024
60/333.15	1.200	-0.0096

Standard cell voltage for varying cathode pressure

The standard cell voltage for increased pressure is given in theory as (Millet *et al.*, 2009:4974):

$$V°(P) = \frac{\Delta G}{nF} = \frac{\Delta G°}{nF} + \frac{RT}{nF} ln\left(P_{H_2} P_{O_2}^{0.5}\right) = E° + \frac{RT}{nF} ln\left(P_{H_2} P_{O_2}^{0.5}\right) \qquad \text{B.7}$$

As the anode pressure of the PEM water electrolyser is not monitored, and the pressure is given as ~1.8 bar at a current density of 0 A.cm^{-2}, and ~2 bar at a current density of 0.8 A.cm^{-2}. The pressure increase of oxygen is thus minimal and is disregarded for calculating the adjusted standard voltage (V°(P)).

$$V°(P) = V° + \frac{RT}{nF} ln\left(P_{H_2}\right)$$

Calculation of ohmic overpotential

The calculation of ohmic overpotential requires the polarisation curve to be linear after the initial overpotential caused by the activation overpotential. The calculation is based on Ohm's law:

$$Resistance\ (\Omega) = \frac{Voltage\ (V)}{Current\ (A)}$$

The slope of the polarisation curve provides the ohmic resistance of the electrolyser components. Figure B.1 illustrates the calculation of ohmic resistance for NS-MEA and PS-MEA. The value of R^2 indicates the precision of the linear fit and the values of ~1 indicate that the fit for both NS-MEA and PS-MEA are exact.

(a) (b)

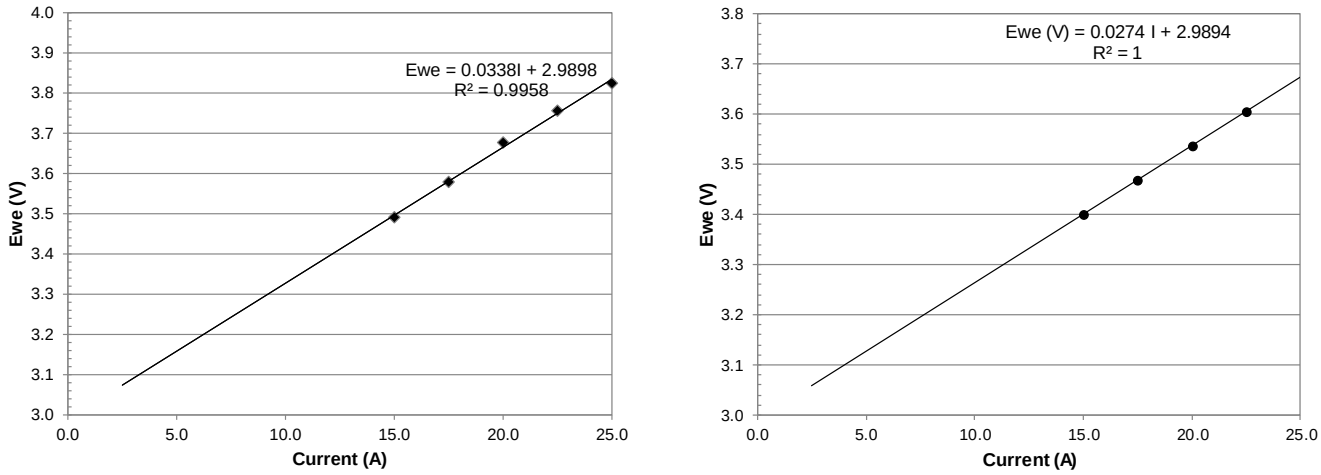

Figure B.1 Comparison of ohmic overpotential at a temperature of 30°C and a pressure of 6 $bar_{(g)}$.
a) Sectional polarisation curve of NS-MEA.
b) Sectional polarisation curve of PS-MEA.

References

MILLET, P., DRAGOE, D., GRIGORIEV, S., FATEEV, V. & ETIEVANT, C. 2009. GenHyPEM: A research program on PEM water electrolysis supported by the european commission. *International journal of hydrogen energy*, 34(11):4974-4982.

THE NATIONAL INSTITUTE OF STANDARDS AND TECHNOLOGY (NIST). 2011. http://webbook.nist.gov/chemistry/.

Appendix C: Experimental Results

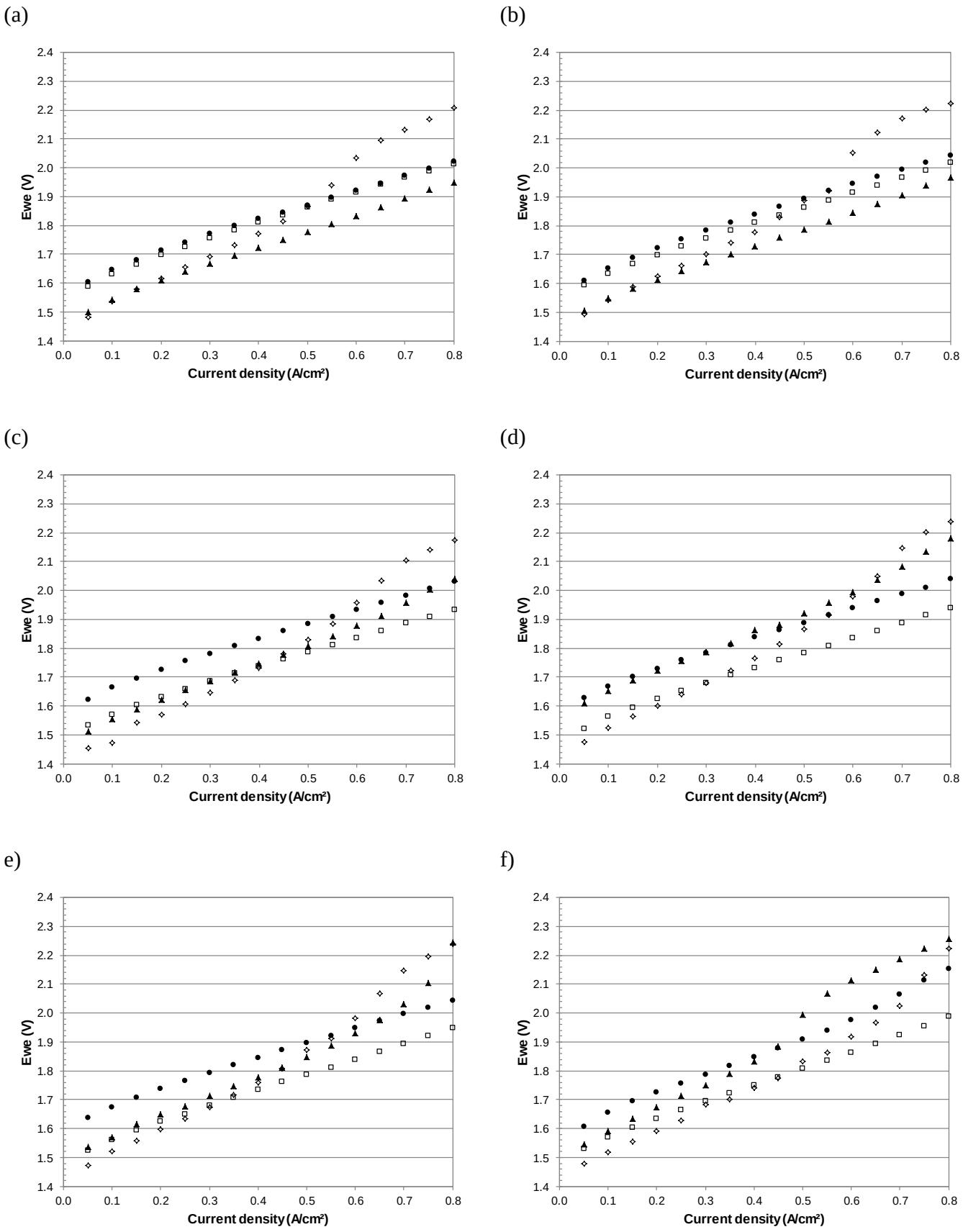

Figure C.1 Cell voltage of N-MEA. Cathode pressure a) of 0 $bar_{(g)}$, b) 1 $bar_{(g)}$, c) 2 $bar_{(g)}$, d) 3 $bar_{(g)}$, e) 4 $bar_{(g)}$, f) 5 $bar_{(g)}$; [● 30°C;□ 40°C;▲ 50°C;◊ 60°C]

(a)

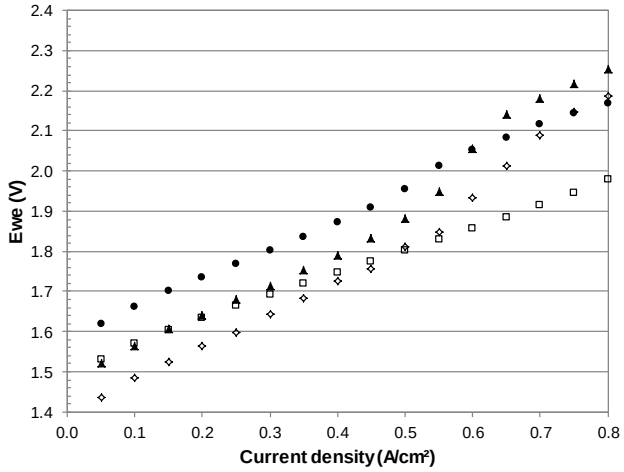

Figure C.2 Cell voltage of N-MEA. Cathode pressure a) 6 $bar_{(g)}$;
[● 30°C;□ 40°C;▲ 50°C;◊ 60°C]

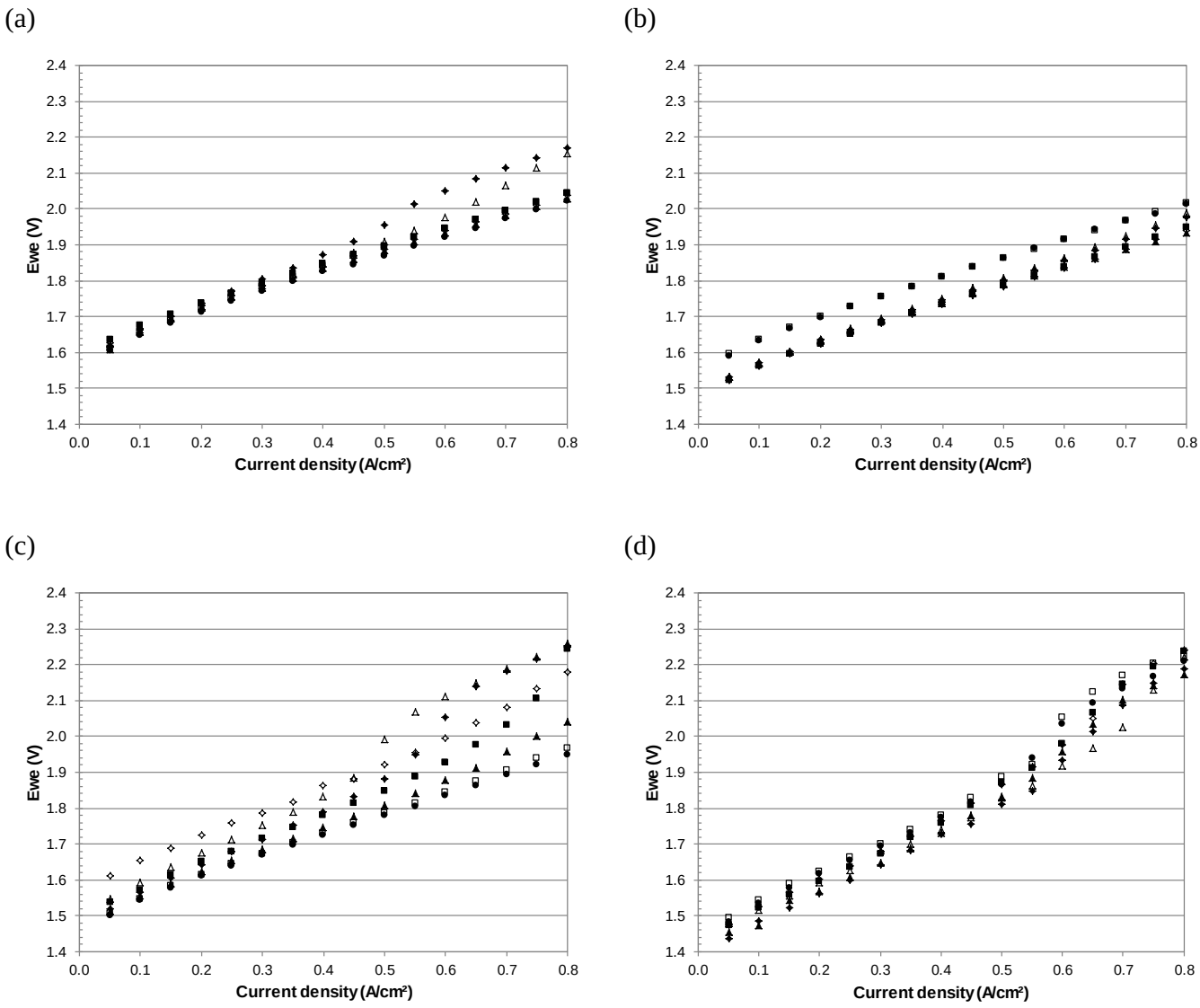

Figure C.3 Cell voltage of N-MEA. Cell temperature a) of 30°C, b) 40°C, c) 50°C, d) 60°C; [●0 $bar_{(g)}$;□ 1 $bar_{(g)}$;▲ 2 $bar_{(g)}$;◊ 3 $bar_{(g)}$; ■ 4 $bar_{(g)}$; Δ 5 $bar_{(g)}$;♦ 6 $bar_{(g)}$;]

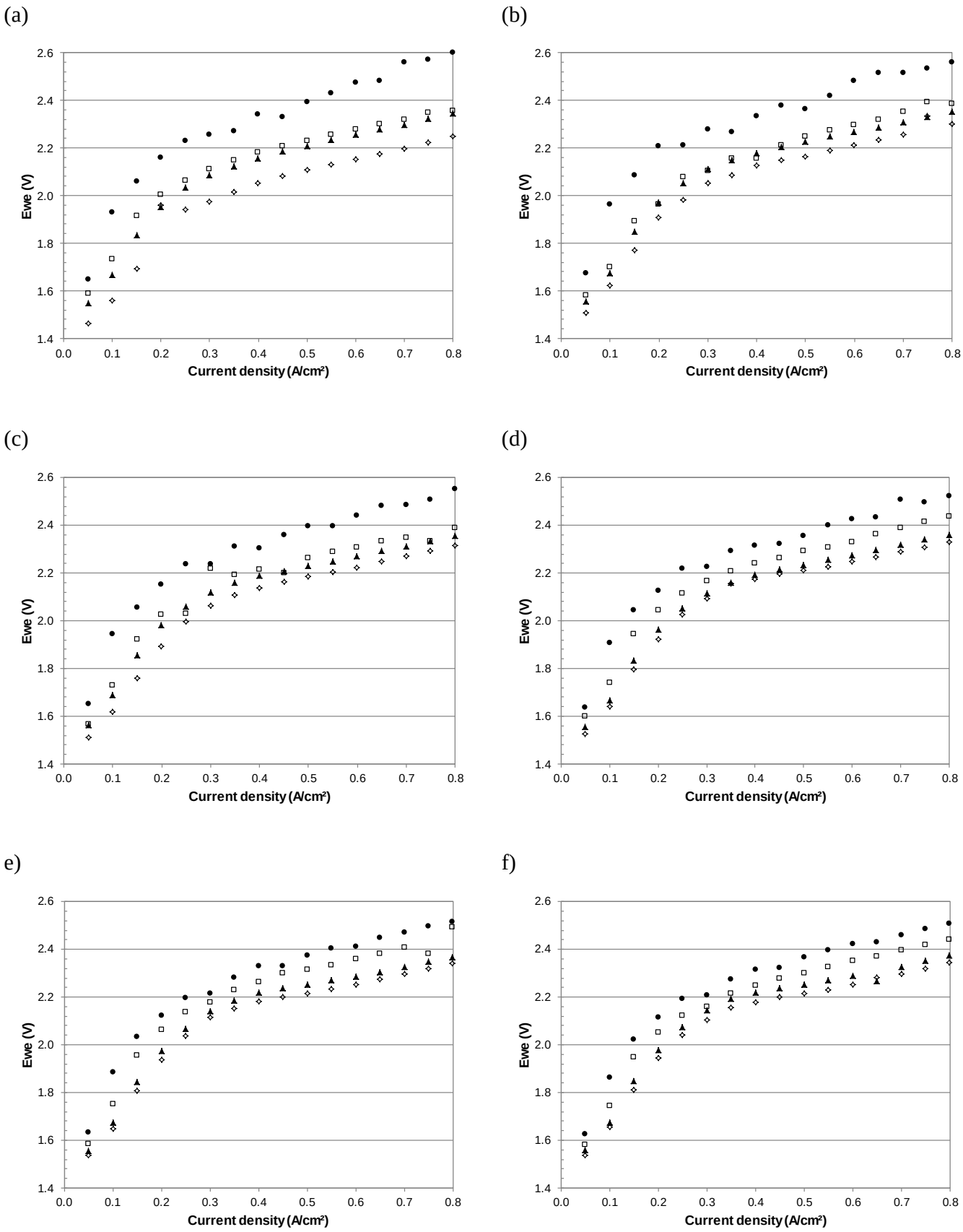

Figure C.4 Cell voltage of N-GDE. Cathode pressure a) of 0 $bar_{(g)}$, b) 1 $bar_{(g)}$, c) 2 $bar_{(g)}$, d) 3 $bar_{(g)}$, e) 4 $bar_{(g)}$, f) 5 $bar_{(g)}$; [● 30°C;□ 40°C;▲ 50°C;◊ 60°C]

(a)

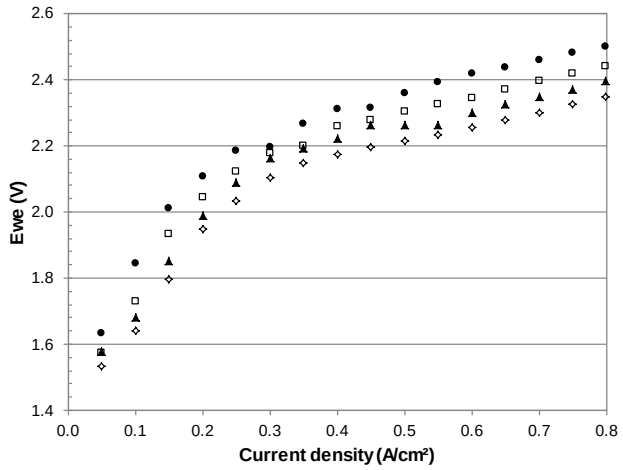

Figure C.5 Cell voltage of N-GDE. Cathode pressure, a) 6 $bar_{(g)}$;
[● 30°C;□ 40°C;▲ 50°C;◊ 60°C]

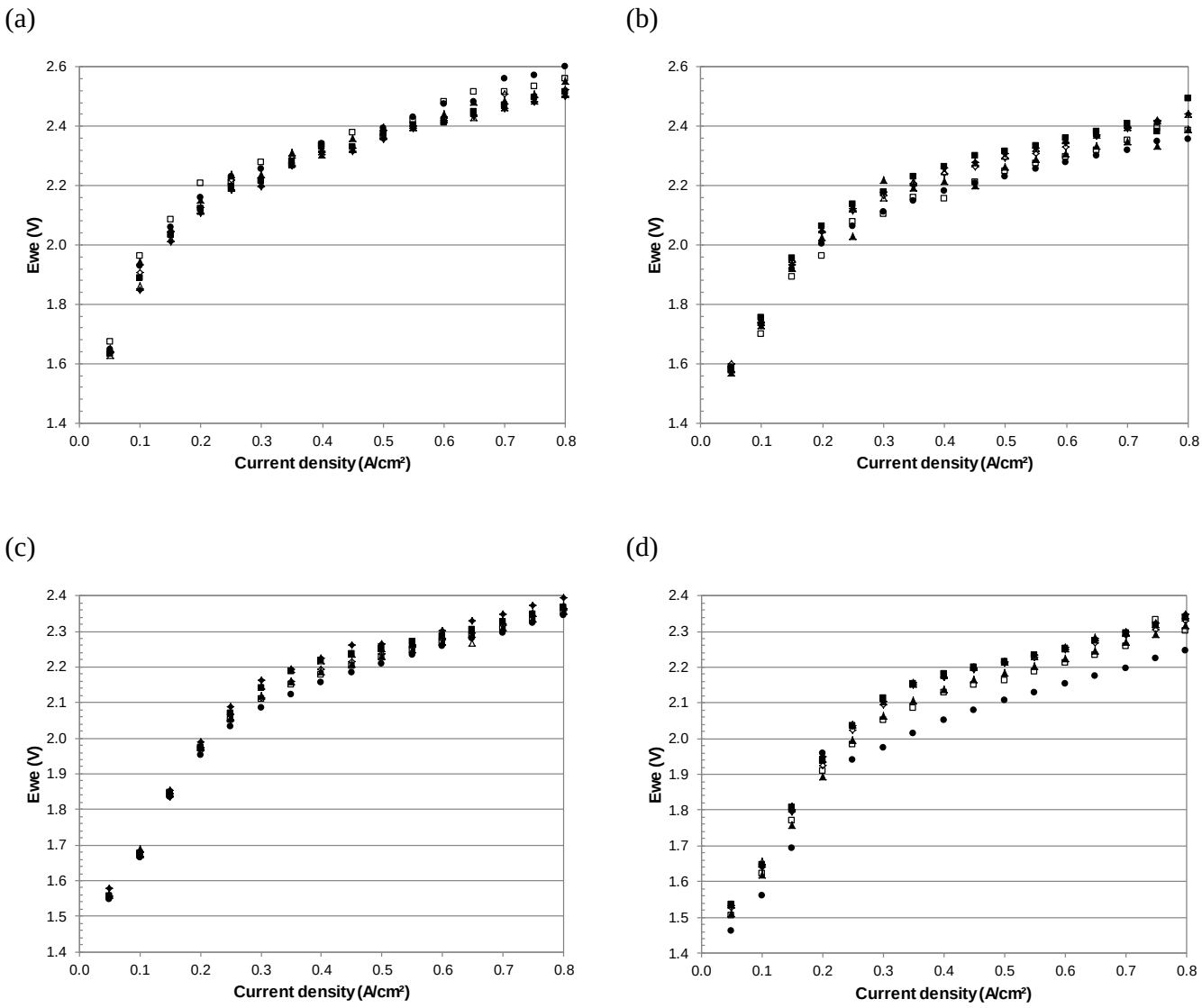

Figure C.6 Cell voltage of N-GDE. Cell temperature a) of 30°C, b) 40°C, c) 50°C, d) 60°C; [●0 $bar_{(g)}$;□ 1 $bar_{(g)}$;▲ 2 $bar_{(g)}$;◊ 3 $bar_{(g)}$; ■ 4 $bar_{(g)}$; Δ 5 $bar_{(g)}$;♦ 6 $bar_{(g)}$;]

(a) (b)

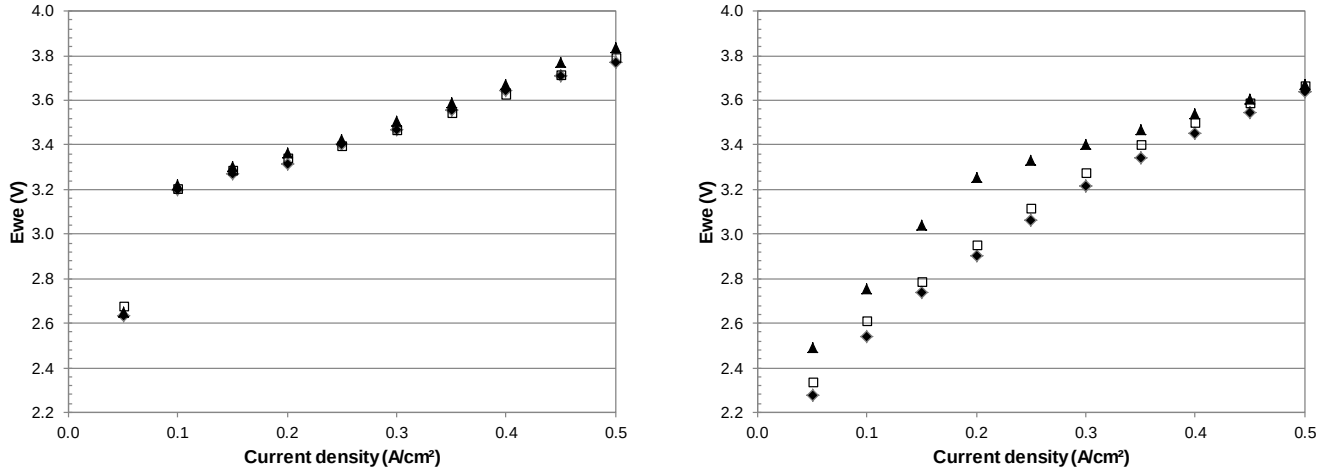

Figure C.7 Cell voltage at 30°C, a) NS-MEA, b) PS-MEA;
[●0 $bar_{(g)}$;□ 3 $bar_{(g)}$;▲ 6 $bar_{(g)}$]

(a) (b)

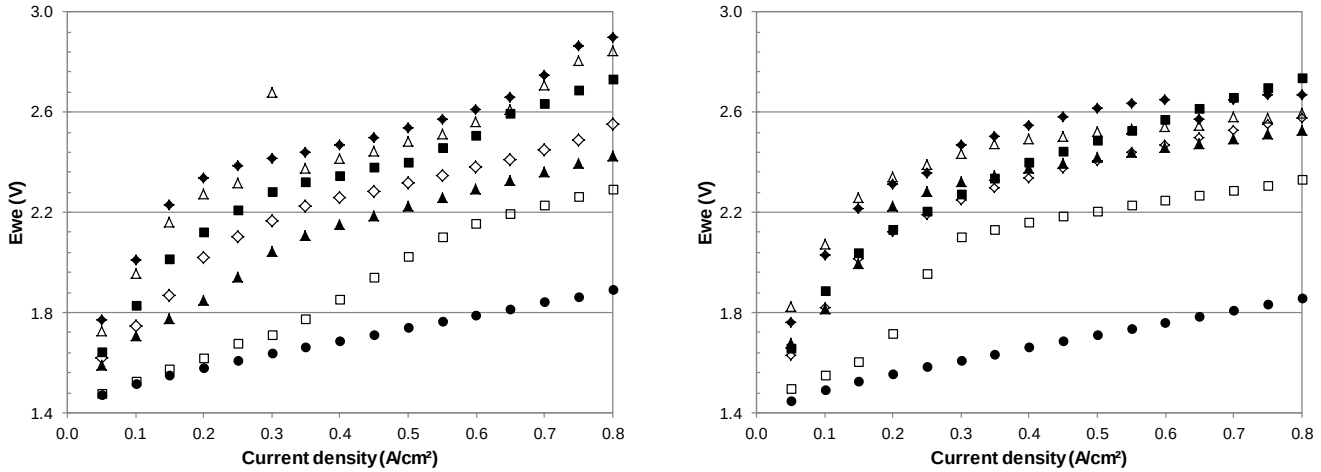

Figure C.8 Cell voltage at 30°C and 0 $bar_{(g)}$ a) $FeSO_4$-MEA, b) $MgSO_4$-MEA;
[● Run 1;□ Run 3;▲ Run 5;◊ Run 7; ■ Run 8; Δ Run 10; ♦ Run 11;]

(a) (b)

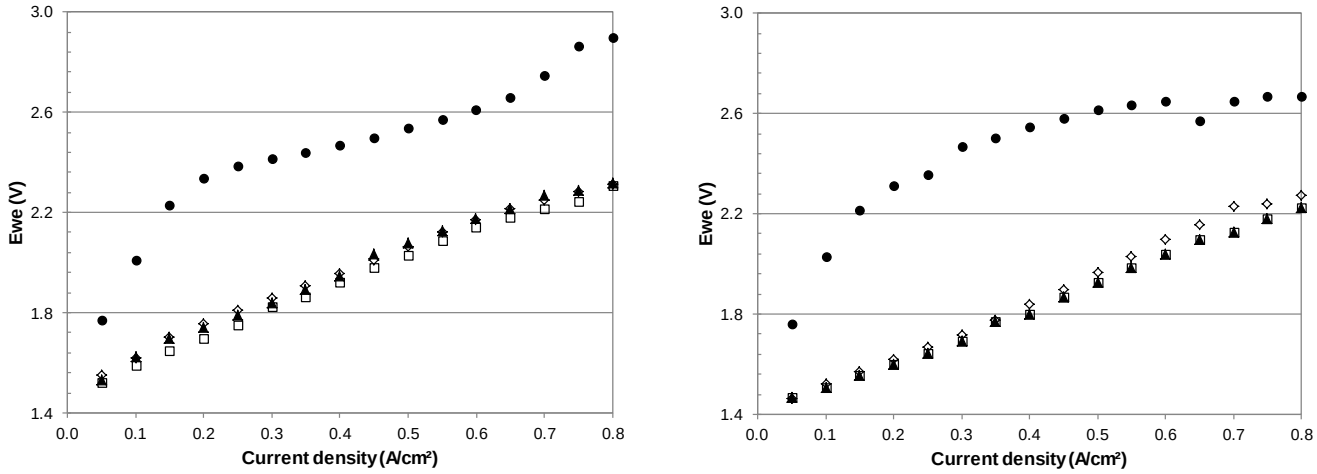

Figure C.9 Cell voltage at 30°C and 0 $bar_{(g)}$ with 0.1M sulphuric acid regeneration a) $FeSO_4$-MEA, b) $MgSO_4$-MEA;
[● Run 11;□ Regen1;▲ Regen2;◊ Regen3]

Appendix D :
Equipment and additional protocol

Experimental Equipment

GES PEM Water Electrolyser

A laboratory scale single cell PEM water electrolyser from GES was used to conduct all relevant performance and degradation experiments. The maximum hydrogen production of the unit is 300mL/min at 40 Ampere and the maximum operating cathode pressure is 8.6 $bar_{(g)}$.

HCP-803 - Potentiostat/galvanostat

A potentiostat was acquired for the purpose of supplying and monitoring the cell voltage and current to the electrolyser. The HCP-803 (Bio-logic Science instruments) potentiostat was selected and operated together with the power booster unit. This makes it possible to supply the electrolyser with ± 3 V at 80 Ampere.

Figure D.1 HCP-803 potentiostat (www.bio-logic.info)

Additional experimental protocol

Electrolyser conditioning

The purchased PEM water electrolysers from GES are prepared using hydrated PEM materials and are kept hydrated to ensure proper proton exchange. On delivery the electrolysers can be tested to ensure proper hydration of the membrane. The tests include checking for shorts (DC resistance) and cell resistance (AC impedance).

DC Resistance test

The test is conducted with a multimeter which is set to measure resistance. Once the multimeter is connected to the electrolyser the measured resistance will increase from ~ 10 Ω to infinity, indicating that there is no electrical short. Generally if the resistance surpasses 30 Ω it is sufficient proof that there is no short.

AC Impedance test

The test can be conducted by connecting the electrolyser to either a potentiostat or impedance meter. Measurements of impedance at 1kHz ought to be in the range of 0 – 15 mΩ. Should the electrolyser resistance be higher it may be due to a dehydrated membrane or low contact resistance between the catalyst and membrane. Dehydrated membrane treatment consists of recycling deionised hot water (80^{o}C) through the electrolyser for 30min or to remove the membrane from the electrolyser and boil it in deionised water (80^{o}C) for 30min.

MEA hydration

After the heat pressing of the synthesised MEAs the heat pressed Nafion® MEA was hydrated for 24 hours at 40°C in a plastic bag filled with deionised water. The Nafion® MEA was removed and placed in a glass beaker filled with deionised water at a temperature of 65°C for 1 hour. The Nafion® MEA was then placed in the PEM water electrolyser and broken in. The PBI MEA was removed from the Teflon platens and placed in an empty plastic bag. The PBI MEA was then placed in the PEM water electrolyser where deionised water (50°C) was circulated over the MEA for a period of 6 hours.

Breaking in of synthesised MEA

The break-in procedure for NS-MEA and PS-MEA required a day each. The MEAs were operated at a cell voltage of 1.8 V for a period of 25 minutes and then operated at OCV (Open Circuit Voltage) for a period of 5 minutes. As the protocol was repeated it was observed that the

operating current to the PEM water electrolyser increased over time. The protocol was repeated until no escalating values of current were observed.

Breaking in of GDE

As the catalyst decals are not directly bonded to the PEM the catalyst on the support films will gradually become more active during cell operation. GDE manufacturers Giner Electrochemical Systems recommend that the breaking in takes place at a cell voltage of 1.8V where the power setpoint should not exceed 60A. It is recommended to operate the cell with 50-80°C deionised water until the current density has exceeded 1A.cm^{-2}, where the occasional cycling to low current or open circuit voltage may assist this process. If stock membranes from Giner are being used (i.e., Nafion® 1110), the current should be limited to 50A. Thinner membranes can probably take up to 60-75A, but keeping the cell voltage below 2.2V is probably a good guideline.

References

http://www.bio-logic.info/potentiostat/products.html. Date of access: 29 Nov. 2011.